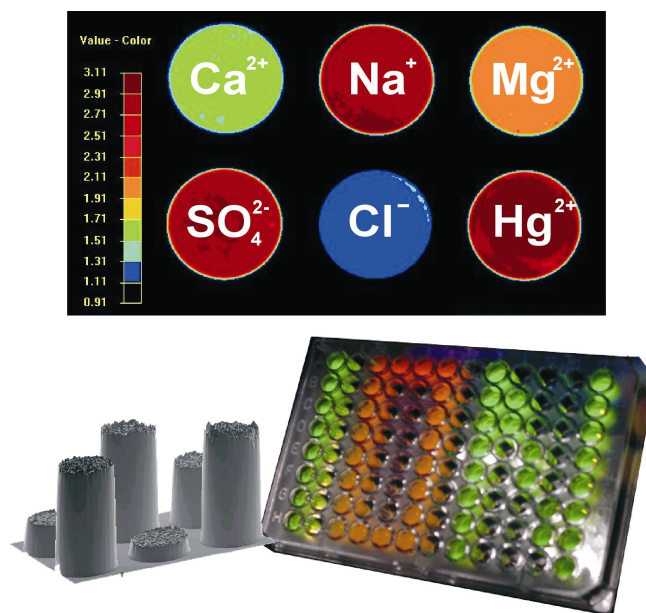# *Optical Sensors for the Determination of Heavy Metal Ions*

Dissertation zur Erlangung des Doktorgrades der Naturwissenschaften

(Dr. rer. nat.)

der Fakultät Chemie und Pharmazie

der Universität Regensburg

vorgelegt von

Torsten Mayr

im März 2002

Optical Sensors for the Determination of Heavy Metal Ions

Doctoral Thesis

by

Torsten Mayr

Für Melanie und meine Eltern

Diese Doktorarbeit entstand in der Zeit von Juni 1999 bis März 2002 am Institut für Analytische Chemie, Chemo- und Biosensorik an der Universität Regensburg.

Die Arbeit wurde angeleitet von Prof. Dr. Otto S. Wolfbeis.

Promotionsgesuch eingereicht am 28.3.2002

Kolloquiumstermin: 13.5.2002

Prüfungsausschauß:	Vorsitzender:	Prof. Dr. Claudia Steinem
	Erstgutachter:	Prof. Dr. Otto S. Wolfbeis
	Zweitgutachter:	Prof. Dr. Ingo Klimant
	Drittprüfer:	Prof. Dr. Nikolaus Korber

Table of Contents

Abbreviations and Symbols

Φ	Phase shift or phase angle of the modulated light
Θ	Quantum yield
λ_{em}	Position of the emission maximum
λ_{ex}	Position of the excitation maximum
μM	μmol per liter
AAS	Atomic absorption spectroscopy
A_{em}	Image recorded in the emission period
A_{ex}	Image recorded in the excitation period
ANN	Artificial neural network
BAPTA	2-(bis)-2-aminophenoxyethane-N-N-N´-N´-tetraacetic acid)
$c_{1/2}(Me^{2+})$	Point of inflection of a Boltzmann fit for a certain cation
CCD	Charge Coupled Device
CT	Charge transfer
D4	Hydrogel based on polyurethane
DLR	Dual Lifetime Referencing
EDTA	1,2-diaminoethane-N,N,N',N'-tetraacetic acid
EGTA	ethylene glycol-bis(2-aminoethyl)-N,N,N',N'-tetraacetic acid
EU	European Union
F	Fluorescence intensity
F_0	Fluorescence intensity in absence of analyte
F_{530}	Fluorescence intensity measured at 530 nm
F_{620}	Fluorescence intensity measured at 620 nm
HTS	High throughput screening
I	Ionic strength
i. d.	In diameter
ICC	Indian Childhood Cirrhosis
ISE	Ion selective electrode
K_D	Quenching constant
K_S	Complex formation constant
LED	Light emitting diode
LOD	Limit of detection

$logK_{Me(II)}$	selectivtiy coefficient
LY	Lucifer Yellow Carbohydrazide
LY-VS	Lucifer Yellow Vinylsulfonyl
MLP	Multi layer perceptron
MOPS	3-[N-Morpholino]propanesulfonic acid
NICC	Non-Indian Childhood Cirrhosis
nm	nanometer
nM	Nanomol per liter
ns	nanosecond
PAN	1-(2-pyridylazo)-2-naphtol
PAN	Poly(acrylonitril)
pCO_2	Carbon dioxide partial pressure
PD	Reference beads (particles) containing Ru(dpp)
PEG	Poly(ethylene glycol)
PET	Photoinduced electron transfer
PMT	Photomultiplier tube
pO_2	Oxygen partial pressure
ppm	Parts per million
PS100	Reference particles containing Ru(dpp) incorporated in PAN
PVC	Poly(vinyl chlorid)
R	Fraction of the intensity of the excitation and the emission window
Ru(dpp)	ruthenium(II)-tris-4,7-diphenyl-1,10-phenantroline
SSM	Separate solution method
t	Tons
t_{90}	Time to reach 90% of the equilibrium signal
t-DLR	Time resolved Dual Lifetime Referencing
WHO	World Health Organization

Chapter 1

1. Introduction

A few decades ago, there was a general feeling that nature could effectively handle hazardous substances. Although, nowadays human beings are more concerned of their sensitive natural environment, pollution is still a problem. Experts estimate that industrial processes introduce up to a million different pollutants into the atmosphere and the aquatic ecosystem [1]. Heavy metals are one group of these substances, although not all of them are considered harmful to humans.

1.1. Heavy Metals in the Environment

Heavy metals are defined as metals of a density higher than 5 g/cm^3 [2]. They occur as pure elements, as ions and complexes. Heavy metals were brought into the environment by human activities, which has influenced and modified natural cycles. Human activities started more than 4000 years ago with metal mining. Unprecedented pollution came up with the industrialization and its consumption of energy. The combustion of fossil fuels introduces a large amount of heavy metals into the atmosphere and the aquatic environment. Crude oil, for example, contains 3.4 ppm mercury and the firing of coal causes the worldwide emission of 2.4 x 10^4 t of lead per year [3]. Additionally, heavy metals are released to the ecosystem with the exponential growth of metal mining, the following processes and their industrial use.

Heavy metals show a large tendency to form complexes, especially with nitrogen, sulphur and oxygen containing ligands of biological matter [4]. Toxicological effects can be explained by this interaction. As a result, changes in the molecular structure of proteins, breaking of hydrogen bonds or inhibition of enzymes can appear. Acute poisoning is rarely observed and usually the result of suicide attempts or accidents [3]. Chronic toxicity is much more relevant and caused by repeated exposure over long periods of time. Mutagenic, carcinogenic or teratogenic effect have been described for some heavy metals [3].

Besides the fact that mercury, cadmium or arsenic are highly toxic, some heavy metals such as iron, copper, zinc, manganese, cobalt, nickel, tin, and selenium are essential to many organisms. These elements, along with amino and fatty acids and vitamins are required for normal biochemical processes such as respiration, biosynthesis and metabolism [5]. An undersupply of these so called trace metals leads to deficiency, while oversupply results in

toxic effects [1]. Copper is one of the heavy metals which is, on the one side, essential for life but on the other, highly toxic to organism like certain algea, funghi and many bacteria or viruses. In recent years copper is suspected to cause infant liver damages. This so called Non-Indian Childhood Cirrhosis (NICC) as well as the former known Indian Childhood Cirrhosis (ICC) are connected with an excessive intake of copper and genetic disorders [6,7]. Drinking water can be a source for an intense copper exposition due to the common practice using copper pipes in domestic water distribution systems, especially in regions with soft water at below pH 7.3. Copper is also widely used in the electroplating and electronics industries, in cooking utensils, in fertilizers, bactericides, fungicides, algicides, and anti-fouling paints, and in animal feed additives and growth promoters. Industrial applications include use in the production of wood preservatives, and in the manufacturing of azo-dyes [5].

In accordance with toxicity data and scientific studies, the WHO (World Health Organization) as well as the European Water Quality Directive recommends standards and guidelines for heavy metals in drinking water. These are summarized in Table 1.1.

Table 1.1. *Standards and guidelines for heavy metals in drinking water [8,9]*

Metal	WHO mg/l	European Water Quality Directive [1] mg/l
Cd	0.003	0.005
Cu	2	2
Pb	0.01	0.01
Hg	0.001	0.001
Ni	0.02	0.02

[1] guidelines for drinking water in countries of the European Union are based on these data

1.2. Conventional Methods for the Determination of Heavy Metals

The determination of heavy metals is a challenging subject for analytical chemists regarding concentration ranges set by standards and guidelines for reasons of toxicity. In addition, similar chemistry of these metals is fastidious with respect to selectivity of the determination method.

A variety of analytical methods fulfilling these demands are available. However, only some of them have found application in routine analysis. Recommended procedures for the detection of heavy metals in watery samples include photometric methods, flame or graphite

furnance atomic absorption spectroscopy (AAS), inductively coupled plasma emission or mass spectrometry (ICP-ES, ICP-MS), total reflection X-Ray fluorimetry (TXRF) and anodic stripping voltammetry (ASV) [1,3,10,11]. While AAS and photometry are single element methods, ICP-ES, ICP-MS and TXRF are used for multi-element analysis, and voltammetry is an oligo-element approach.

These methods offer good limits of detection and wide linear ranges, but require high cost analytical instruments developed for the use in the laboratories. The necessary collection transportation and pretreatment of a sample is time consuming and a potential source of error [12]. However, in the last years smaller and portable and less expensive devices have been brought to the market. On the other hand, the last years have seen a growing development of chemical sensors for a variety of applications. The toxicity of heavy metals makes a continuos supervision of drinking or ground water and lentic or lotic watercourses necessary. Chemical sensors enable on-line and field monitoring and therefore can be an useful alternative tool [13].

1.3. Optical Ion Sensors

A chemical sensor can be defined as "*a portable miniaturized analytical device, which can deliver real-time and on-line information in presence of specific compounds or ions in complex samples*" [14]. Chemical sensors can be categorized into electrochemical, optical, mass-sensitive and heat-sensitive, according to the types of transducer [15].

An optical sensor device consists of the following components. (a) the recognition element, where specific interaction and identification of the analyte takes place; (b) the transducer element that converts the recognition process into a measurable optical signal; (c) an optical device (process unit) which consists of at least a light source (in the simplest form a LED) and finally (d) a detector (in the simplest form a photodiode), which detects and converts the change of optical properties, after amplification of the primary signal, into a unit readout. The optical properties measured can be absorbance, reflectance, luminescence, light polarization, Raman and other.

Ideally, a sensor provides adequate sensitivity or dynamic range, high selectivity towards the species of interest, a proportional (or other mathematical relationship) signal output to the amount of analyte, fast response time, good signal-to-noise ratio, no hysteresis and excellent long-term stability [16]. Further demands on an ideal sensor are being robust, simple, reliable, economical in terms of fabrication, size and with self-calibrating capabilities. Fulfilling all

these demands is hardly possible. Existing sensors have their limitations in insufficient long-term stability, interference of other species than the target and inadequate limits of detection. Notwithstanding and motivated by this, the field of optical sensing is still of increasing interest, which is reflected by a continuous increase in publications and reviews [13,15-23].

Optical sensors have found many applications in various fields, including biomedical [24,25], clinical [26-28], environmental monitoring [29,30] and process controlling [31]. They are an attractive analytical tool, whenever continuos monitoring and real-time information is desired. They can track sources of contamination in an industrial process, follow the formation and movement of environmental pollutants and can raise the alarm when a toxic species exceed an expected level of exposure. Thus optical ion sensing plays an important role in clinical diagnostics. The simultaneous determination of blood electrolyte/gas parameters (pH, pCO_2, pO_2, Na^+, K^+, Ca^{2+} and Cl^-), e. g. is enabled by the Critical Care Analyzer "AVL OPTI R". A small portable instrument employing disposable optical sensor membranes for the respective parameters [32].

For environmental analysis, single use test-stripes for various ions, including heavy metals, are commercially available [33], which have their limitations in accuracy and reversibility. In recent years, activities applying optical sensors for the determination of heavy metals increased [34]. Mainly two concepts were applied: The first employs lipophilic neutral ionphores, while the second makes use of immobilized indicator dyes. Due to the nature of heavy metals, their similar chemistry, nearly all sensors lack selectivity. Overcoming the problem of selectivity has lead to the development of so called artificial noses and tongues that rely on cross-reactive sensor arrays [35]. These schemes consist of a number of unselective sensors grouped to an array format, which delivers a characteristics response pattern, that can be evaluated with chemometric tools.

1.3.1. The Principle of Molecular Recognition

Molecular recognition signifies the processes of specific, non-covalent binding of a guest species by an organic host molecule. Molecular recognition has its origin in the discovery of macrocyclic compounds, which are capable of selective binding of alkali ions, and is a field in supramolecular chemistry [36]. Usually, in ion sensors the recognition process is generated by synthetic or natural receptors, so called ionophores or carriers [37,38]. Application of these molecular cavities, basket or similar hosts in which ions can fit and bind selectively and reversible, was a step forward to improve the selectivity of chemical sensors. Metal chelators and crown ethers are the forerunner of these types of selective host molecules. Further

development lead to more sophisticated organic molecules like podants, cryptands, spherands or calix(4)arenes [39]. Ionophores for heavy metals take advantage of the high affinity of oxygen, nitrogen and sulfur donor atoms towards these ions. An effect that goes back to the principles of hard and soft bases and acids (HSAB) by Pearson [40]. Hence, Ag^+, Cu^+, Cd^{2+}, Hg^{2+} and Pb^{2+} classified as soft acid, bind favorably to ligands containing sulfur; while the border line acids Ni^{2+}, Cu^{2+}, Co^{2+} and Zn^{2+} prefer binding to nitrogen. Figure 1.1 shows a selection of carriers bearing heteroatomic groups for the recognition of heavy metal ions.

R = OCH$_2$C(S)N(CH$_3$)$_2$

1   **2**   **3**   **4**
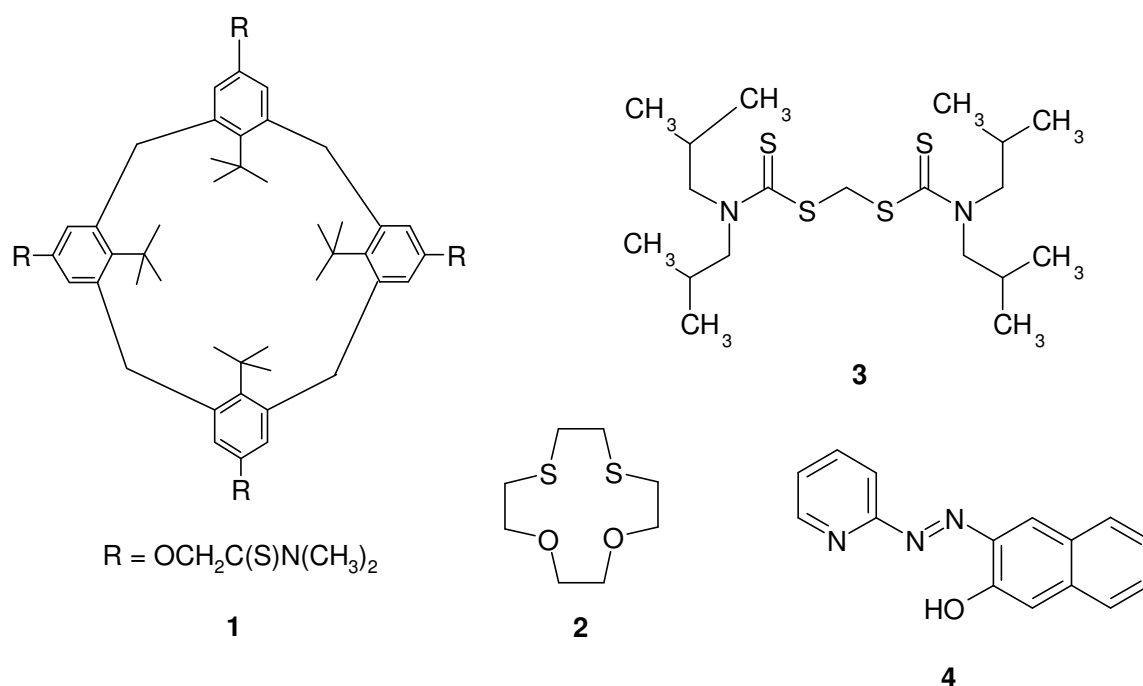
Fig. 1.1. *Various examples of ionophores and chelators for heavy metals utilized in optical sensors or ISEs.* **1**: *a calix(4)arene based ionophore for* Pb^{2+} *[41],* **2**: *1,4-dithia-12crown-4 ionophore for* Hg^{2+} *[42]* **3**: *a dithiocarbamate derivative with high selectivity for* Ag^+ *and* Hg^{2+} *[30],* **4**: *1-(2-pyridylazo)-2-napthol (PAN) responds in decreasing order to* Ni^{2+}, Cu^{2+}, Zn^{2+}, Hg^{2+}, Pb^{2+} *and* Cd^{2+} *[43].*

Another important receptor in ion recognition, especially in biological and clinical research, is the chelating compound BAPTA (2-(bis)-2-aminophenoxyethane-N-N-N´-N´-tetraacetic acid). This Ca^{2+}-selective chelator was introduced by Tsien [44], and is essentially an aromatic version of the widely used chelator EGTA (ethylene glycol-bis(2-aminoethyl)-N,N,N',N'-tetraacetic acid), see Figure 1.2), which is once more related to very well known complexing agent EDTA (1,2-diaminoethane-N,N,N',N'-tetraacetic acid). Replacing two alkyl bonds of EGTA by aromatic rings lowers the pK_a of the ion-binding amine and makes Ca^{2+}-binding insensitive to changes in pH over the physiological range. In addition, the affinity for

Ca^{2+} can be altered by substitution of electron withdrawing or donating groups in the aromatic rings, due to their electronically conjugation to the binding site.

However, selectivity of BAPTA for Ca^{2+} is achieved over the monovalent metal ions and mainly Mg^{2+}, while other polyvalent metal ions strongly interfere [45]. On the other hand this opens the door for the determination of heavy metal ions, when this receptor molecule is covalently linked with chromophoric or fluorophoric moieties (see chapter 1.3.2.4).
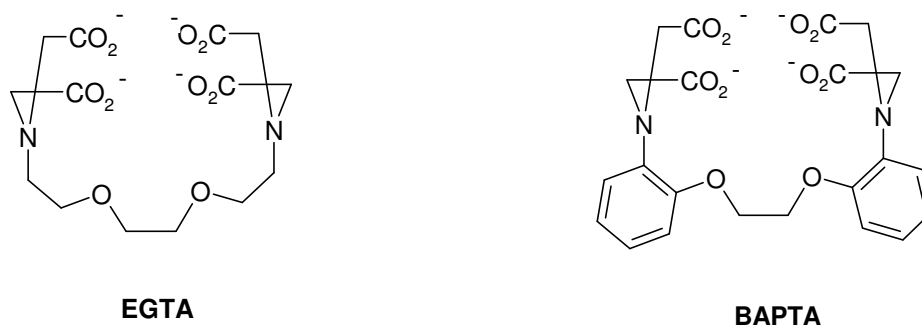
Fig. 1.2. *Chemical structures of the chelators EGTA and BAPTA*

1.3.2.   Schemes Applied in Optical Ion Sensing

1.3.2.1. Intrinsic Ion Sensing

Sensing methods, employing optical fibres, were established that rely on the intrinsic optical properties of various ionic species. Some metal ions show absorption (ranging from the UV to the near infrared) or luminescence. Examples are the detection of copper(II) [46] or the uranyl ion [47,48].

In fibre optic devices the light is guided by a fibre (or a fibre boundle) directly into the sample in order to observe the spectral properties of the analyte. Such sensors lack specificity due to interference of other species absorbing at the same wavelength or sample turbidity. Applications based on absorbance are limited because the molar absorptivities are low, typically around 10 to 1000 l mol^{-1} cm^{-1} [49].

1.3.2.2. Biosensors

Biosensors make use of biomolecules in the recognition or transduction process. The interaction of heavy metal ions with proteins such as enzymes offers remarkable possibilities in terms of selectivity and limits of detection. Heavy metals ions can act as catalysts (cofactors) or inhibitors. The quantity of inhibition or acceleration can be correlated to the concentration of

heavy metal ions. The activity of the enzyme is determined with the help of low-molecular weight species, which are consumed or produced during the enzymatic action. Such species include oxygen, ammonia and carbon dioxide. The most prominent example is the inhibition of urease by mercury, silver and copper ions, which is transduced via pH or ammonia measurements [50,51].

1.3.2.3. Carrier Based Optical Sensors

Optical ion sensors applying neutral ionophores were introduced about one decade ago and benefit from over 30 years development on ion selective electrodes (ISE) based on bulk membranes. Lipophilic ionophores are dissolved in a solvent polymeric membrane, which is physically a water-immiscible liquid of high viscosity [21]. The analyte is extracted from the aqueous into the lipophilic phase driven by the host/guest interaction with the neutral ionophore. Since electro-neutrality must hold for the bulk phase, either a counter ion is extracted into the membrane, which was introduced by Charlton 1982 [52], or an ion of equal charge is released from it. Frequently, protons are involved within this process and pH indicators were integrated into the membrane as transducers. The scope of co-extraction and ion-exchange sensing has been widely enlarged by the work of Simon and co-workers [53-58]. An obvious drawback of this sensing scheme is its pH cross-sensitivity, which can be overcome by measuring the pH of the sample simultaneously, but requires larger efforts in instrumentation. More recently pH-independent sensing schemes based on co-extraction of a coloured counter ion were developed [59,60]. The application of potential sensitive dyes was also described as possible sensing mechanism, where protons are not involved in the recognition process [61,62].

1.3.2.4. Sensors Based on Chromo- or Fluoroionophores

Colorimetric reagents for the determination of cations based on complexation have gained popularity long time ago. A large number of metal indicators exists containing various groups with electron donating atoms for binding [63]. A prominent examples is Xylenol Orange. The EDTA-type complexing agent undergoes different color changes on binding metal ions. The fluorescent counterpart calcein increases or decreases its fluorescence, besides its changes in color.

Nowadays, the field of supramolecular chemistry has brought to light new binding sites with improved selectivity. Logically, the idea of coupling these ionophores to *chromophores* or

fluorophores emerged some years later, leading to so-called *chromoionophores* and *fluoroionophores* [64]. Within these conjugates the receptor part recognizes the ion and the the chromo- or fluorophore signals the binding event by a change in its optical properties. These indicator substances are often referred to as probes and a variety is commercial available [65, 66]. Because this thesis focus on the development of fluorescent sensors only fluoroionophores are considered. The complexation of a metal ion results in either enhanced fluorescence of the probe – an event that is also termed chelation-enhanced fluorescence or **CHEF** – or in decreased fluorescence of the probe – chelation-enhanced quenching or **CHEQ** [67]. For heavy metals chelation of non-redox active, closed shell ions, e. g . Zn^{2+} or Cd^{2+} results in **CHEF,** while **CHEQ** usually is observed on inherently quenching , e. g. Cu^{2+}, Ni^{2+} or Hg^{2+}, due to open shell electron configuration or the heavy atom effect.

The most important mechanism, signaling a recognition event of a fluorionophore, include *charge transfer* (**CT**), *photoinduced electron transfer* (**PET**), *energy transfer* and *excimer* or *exciplex* formation or disappearance among others [64, 67-69]. Within intramolecular *charge transfer* probes, the analyte interacts directly with a ligand that is part of the fluorophore π-system. In the simplest form, the fluorophore contains an electron donating group conjugated to an eletron-withdrawing group able to undergo an intramolecular charge transfer on excitation by light. This results in changes of intensity in fluorescence and absorbance and simultaneously in spectral shifts of absorbance or fluorescence. Probes based on the **PET**-mechanism involves interaction with analyte electronically isolated from the fluorophore π-system. The electron density of the free binding site quenches the fluorescence of the covalently linked fluorophores. In the bound state the electron density is reduced by the bound species and the quenching effect is released. Unlike **CT** probes, only fluorescence intensity is affected. Therefore, a **PET** system can be regarded as a switch, where luminescence is switched on or off depending on the occupation of the host moieties. Photoinduced *energy transfer* is observed for complexing bifluorophores consisting of a donor (D) and an acceptor (A) fluorophore, with overlapping emission (D) and absorption (A) spectrum, linked by a flexible spacer. Binding ions heteroatoms of the spacer results in a decrease in distance of the two fluorophores and consequently in an increase in efficiency of energy transfer. The transfer efficiency depends on the distance according to Förster´s theory [70]. *Excimer* and *exciplex* formation were also investigated in form of fluoroionophores containing two identical fluorophores in spatial vicinity. On binding the analyte, the molecular structure is changed and the excimers band disappears.

Optical sensors are obtained by the immobilization of these fluoroionophores or chromoionophores to a ion permeable matrix. Three general methods are widely applied, namely physical, electrostatic and covalent immobilization [13]. The proper choice of a polymer matrix is crucial and governed by parameters like suitability for dye immobilization, mechanical stability, and permeability for the analyte [71]. Furthermore, immobilization may shift spectra, pK_a values, luminescence lifetimes and dynamic ranges, as well as binding or quenching constants of the indicators. Figure 1.3 gives a schematic representation of a fluorescent optical sensor based on an immobilized fluoroionophore.
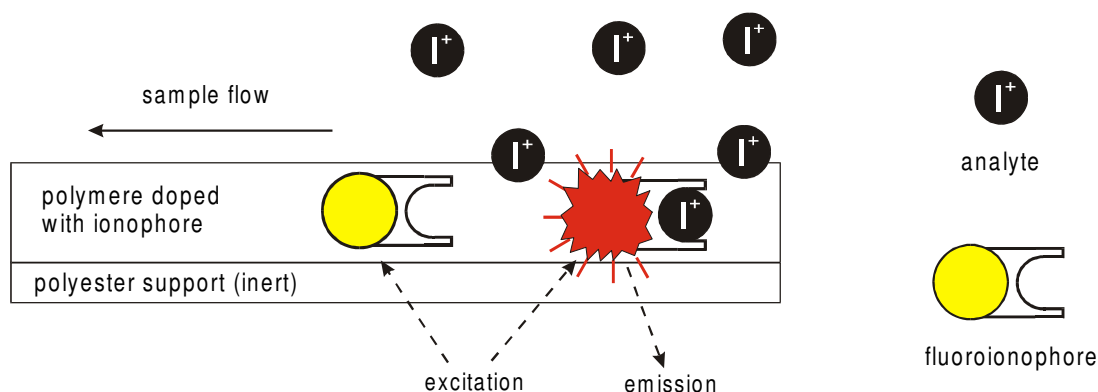
Fig. 1.3. Cross-section of a fluorescent sensing membrane containing an immobilized fluoroionophore to a polymer spread on an inert polyester support. The analyte penetrates the membrane and is selectively bound by the recognition elements of the fluoroionophore, which causes either decrease or increase of fluorescence. The latter is shown here.

1.3.2.5. *Sensors Based on Dynamic Quenching of Luminescence*

The principle of dynamic fluorescence quenching has been widely studied. A theoretical description of fluorescence quenching is given in chapter 2.2. One of the most investigated collisional (dynamic) fluorescence quencher is molecular oxygen [72]. Various sensoric applications are described in literature [73, 13]. In the field of ion analysis, the dynamic quenching effect of halides on quinolinum and acridinium compounds is well-studied [74-76]. Recently, approaches for the determination of chloride in blood [77] and the salinity of seawater [29] based on the effective quenching of immobilized lucigenin are published.

1.3.3. **Optical sensors for the Determination of Heavy Metal Ions**

A large number of optical sensors or test strips for heavy metals were developed in the past years and extensively reviewed by Oehme and Wolfbeis in 1997 [34]. The most significant

methods are the application of quenchable fluorophores or indicator dyes, which undergo a binding reaction, biosensor assays or the combination of an ionophore with a pH-indicator. More recent publications deal with metal indicators dissolved in plasticized poly(vinyl chloride) (PVC) [78,79] or immobilized to ion exchange resins [80-82], and with ion exchange membranes [83]. Although extensive work has been performed, sensing heavy metals still suffers from poor selectivity and reversibility in most cases. New approaches take advantage of combinatorial methods [84] or chemometric tools [85], e. g. regression models or artificial neuronal networks, and gain selectivity from a response pattern of unselective sensors. This parallels developments in ion-selective electrodes, where chemometry was employed for the determination of heavy metals ions [86].

1.4. Chemical imaging

Fluorescence spectroscopy and its applications to the physical and live science have rapidly evolved during the past 20 years [86, 87]. Recently, a trend has become apparent towards two-dimensional measurements of the distribution of physical and chemical parameters in heterogeneous systems [88, 89]. Examples include studies of tumor oxygenation [90] or the evaluation of pH [91] and calcium(II) [92] distribution in cells. These approaches benefit from mapping an area and visualizing the results as an image.

Since the past years have seen enormous advances in the development in the technology of Charged Coupled Devices (CCD) with respect to sensitivity, resolution, size and cost, digital cameras have become detectors of high potential for imaging purposes. CCD-Cameras together with modern imaging processing software enable two-dimensional measurements and real-time monitoring with spatially high resolution. Moreover, CCD-based imaging allows the measurement of several samples in parallel, summed up in one image. This extremely fast kind of data acquisition can not be achieved by sequential methods. Therefore CCD-based imaging can be useful, whenever a large number of samples is to be analyzed, e. g. in high-throughput screening (HTS) [93].

The combination of luminescent optical sensor technology and CCD-technology was recently presented by Liebsch who mapped gradients of pO_2, pCO_2 and pH [94,95], while Holst visualized the oxygen distribution in various biological systems [96]. The high potential of these approaches can be attributed to the basic structures of sensor membranes and CCD-chips. Both consist of an array of complementary independent elements, namely indicator and pixels.

1.5. Aim of the Thesis

The goal of this thesis was the development of optical sensors for the determination of heavy metal ions in aqueous samples. Heavy metal ions can be either essential or toxic to human beings and their determination is therefore of tremendous interest. Conventional methods require high cost analytical instruments which are insufficient for online or field monitoring. This thesis presents the applications of several sensing strategies for the determination of heavy metal ions based on fluorescent optical sensing. The sensors need to respond in concentration ranges recommended by the WHO and the EU. In the beginning, various dyes have to be investigated towards the influence of heavy metal ions on their fluorescence. The excitation wavelength of the indicators has to be in the visible range in order to use inexpensive LEDs as light source. Once found new indicators fulfilling these demands, sensing membranes have to be prepared and characterized, with regards to selectivity and sensitivity. In addition, the sensing scheme has to be extended by an existing referencing method in order to overcome adverse effects such as coloration or turbidity of the sample.

Furthermore, a new concept has been introduced for the simultaneous determination of various ions by an sensor array in microtiterplates. The analytical information has to be collected by the fasted method at present, namely time-resolved imaging. After showing the feasibility by an array of selective sensors, a cross-reactive array has to be developed employing a collection of unselective sensors. Data has to be evaluated by pattern recognition using artificial neural networks.

1.6. References

[1] U. Förstner, G. T. Wittmann, *Metal Pollution in the Aquatic Environment*, Springer, Berlin (1981).

[2] *Römpps Chemie Lexikon*, Thieme, Stuttgart (1995).

[3] E. Merian, *Metals and their Compounds in the Environment*, VCH, Weinheim (1991).

[4] L. Sigg, W. Stumm, *Aquatische Chemie*, Teubner, Stuttgart (1996).

[5] *Environmental Health Criteria*, No. 200, World Health Organization (1998).

[6] H. H. Dieter, W. Schimmelpfennig, E. Meyer, M. Tabert, *Early Childhood Cirrhoses (ECC) in Germany between 1982 and 1994 with special consideration of copper etiology*, Eur. J. Med. Res., **4**, 233 (1999).

[7] T. Müller, B. van de Sluis, W. Müller, P. Pearson, C. Wijmenga, *Non-Indian Childhood Cirrhosis*, Eur. J. Med. Res., **4**, 293 (1999).

[8] World Health Organization, *Guidelines for drinking water quality*, 2nd ed. ,Genova (1998).

[9] European Commission, *Water Quality Directive* 98/83/EU (1998).

[10] W. Fresenius, K. E. Quentin, W. Schneider, *Water Analysis*, Springer, Berlin (1988).

[11] R. Klockenkämpfer, *Total-Reflection X-ray Fluorescence Analysis,* Wiley, New York (1997).

[12] U. E. Spichiger-Keller, *Chemical Sensors and Biosensors for Medical and Biological Applications*, Wiley-VHC, Weinheim (1998).

[13] O. S. Wolfbeis (Ed.), *Fiber Optic Chemical Sensors and Biosensors*, **Vol. 1&2**, CRC, Boca Raton (1991).

[14] K. Camman, G. Guibault, E. Hall, R. Kellner, H. L. Schmidt, O. S. Wolfbeis, *The Cambridge Definition of Chemical Sensors* (1996).

[15] R. W. Cattrall, *Chemical Sensors*, Oxford University Press Inc., New York (1997).

[16] D. Diamond, *Principles of Chemical and Biological Sensors*, Wiley & Sons, New York (1998).

[17] J. Janata, *Principles of Chemical Sensors*, Plenum Press, London **(**1989**)**.

[18] G.C. Rhigini, A. G. Magnini, *Optical Metrology and Sensing*, in *Perspectives in Optoelectronics*, Jha S.S (ed.), World Scientific, Singapore, 781 (1995).

[19] J. Dakin, B. Culshaw, (eds)., *Optical Fiber Sensors. Applications Analysis and Future Trends*, Artech House, Norwood, MA (1997).

[20]   U. E. Spichiger-Keller**,** *Chemical Sensors and Biosensors for Medical and Biological Applications*, Wiley-VCH, Weinheim (1998).

[21] E. Bakker, P. Bühlmann, E. Pretsch, *Carrier Based Ion-Selective Electrodes and Bulk Optodes, 1. General Characteristics*, Chem. Rev., **97**, 3083 (1997).

[22] J. Janata, M. Josowicz, P. Vanysek, D. M. DeVaney, *Chemical Sensors,* Anal. Chem., **70,** 179R (1998).

[23] O. S. Wolfbeis, *Fiber-Optic Chemical Sensors and Biosensors*, Anal. Chem., **72**, 81R (2000).

[24] W. C. Mignani, F. Baldini, *Fiber-Optic Sensors in Health Care*, Phys. Med. Biol., **42**, 967 (1997).

[25] W. C. Mahoney, A. A. Luderer, R. A. Brier, J-N Lin, in *Immunosassay Automation: An Update Guide to Systems*, Chan. D. W. (ed.), Academic Press, San Diego, CA, 231 (1996).

[26] O. S. Wolfbeis, I. Klimant, T. Werner, C. Huber, U. Kosch, C. Krause, G. Neurauter, A. Dürkop. *A set of Luminescence Decay Time Based Chemical Sensors for Clinical Applications*, Sensors and Actuators, **B51**, 17 (1998).

[27] C. Huber, I. Klimant, C. Krause, O. S. Wolfbeis, *Dual Lifetime Referencing as Applied to a Chloride Optical Sensor*, Anal. Chem., **73**, 2097 (2001).

[28] C. Krause, T. Werner, C. Huber, O. S. Wolfbeis, *Emulsion-Based Fluorosensors for Potassium Featuring Improved Stability and Signal Change,* Anal. Chem., **71**, 5304 (1999).

[29] C. Huber, I. Klimant, C. Krause, T. Werner, T. Mayr, O. S. Wolfbeis, *Optical Sensor for Seawater Salinity*, Fresenius J. Anal. Chem., **368**, 196 (2000).

[30] M. Lerchi, E. Reitter, W. Simon, E. Pretsch, D. A. Chowdhury, S. Kamata, *Bulk Optodes Based on Neutral Dithiocarbamate Ionophores with High Selectivity and Sensitivity for Silver and Mercury Cations*, Anal. Chem., **66**, 1713 (1994).

[31] L. W. Burges, *Review of Progress in Quantitative Nondestructive Evaluation,* in D. O. Thompson, D. E. Chimenti, Plenum Press, New York, NY, **Vol. 15,** 9 (1996).

[32] http://www.roche.com/diagnostics/products/c_prodlist.htm#pc.

[33] Merck, *Reflectoquant Datasheets*, Merck, Darmstadt (1996).

[34] I. Oehme, O. S. Wolfbeis, *Fundamental Review – Optical Sensors for Determination of Heavy Metal Ions*, Microchim. Acta, **126**, 177 (1997).

[35] K. J. Albert, N. S. Lewis, C. L. Schauer, G. A. Sotzing, S. E. Stitzel, T. P. Vaid, D. R. Walt, *Cross-Reactive Chemical Sensor Arrays*, Chem. Rev., **100**, 2595 (2000).

[36] J. M. Lehn, *Supramolecular Chemisty – Concepts and Perspectives*, VCA, Weinheim (1995).

[37] P. Bühlmann, E. Pretsch, E. Bakker, *Carrier-Based Ion-Selective Electrodes and Bulk Optodes. 2. Ionophores for Potentiometric and Optical Sensors*, Chem. Rev., **98**, 1593 (1998).

[38] F. P. Schmidtchen, M.Berger, *Artificial Organic Host Molecules for Anions*, Chem. Rev., **97**, 1609 (1997).

[39] D. J . Cram, *Präorganisation – von Solventien zu Sphäranden*, Angew. Chem., **98**, 1041-1140 (1996).

[40] Pearson, *Hard and Soft Acids and Bases,* J. Am. Chem. Soc., 3533 (1963).

[41] E. Malinowska, Z. Brózka, K. Kasiura, R. J. M Egberink, D. N. Reinhoudt, *Lead selective elctrodes based on thioamide functionalized calix[4]arenes as ionophore*, Anal. Chim. Acta, **298**, 953 (1994).

[42]　M. T. Lai, J.- S. Shih, *Mercury(II) and silver(I) ion-selective electrodes based on dithia crown ethers*, Analyst, **111**, 891 (1986).

[43]　J. E. Madden, T. J. Cardwell, R. W. Cattral, L. W. Deady, *Nafion-based optode for the detection of metal ions in flow analysis*, Anal. Chim. Acta, **319**, 129 (1996).

[44]　R. Y. Tsien, *New calcium indicators and buffers with high selectivity against magnesium and protons: design, synthesis, and properties of prototype structures*, Biochemistry, **19**, 2396-2404 (1980).

[45]　K. A. McCall, C. A. Fierke, *Colorimetric and fluorimetric assays to quantitate micromolar concentrations of transition metals*, Anal Biochem, **284**, 307-315 (2000).

[46]　J. E. Freeman, A. G. Childers, A. W. Steele, G. M. Hieftje, *A Fiber-optic Absorption Cell for Remote Dtermination of Copper in Industrial Electroplating Baths*, Anal. Chim. Acta, **177**, 122 (**1995**).

[47]　R. A. Malstrom, T. Hirschfeld, *Analytical Spectroscopy*, Elsevier, Amsterdam (1983).

[48]　R. A. Malstrom, *Uranium Analysis by Remote Fiber Fluorimetry*, Rep. DP-1737, U.S Dept. Of Energy, contract DE-AC09-76SR00001 (1988).

[49]　W. R. Seitz, in: *Fiber Optic Chemical Sensors and Biosensors*, O.S. Wolfbeis (ed.), Volume **2**, Chapter. 1, Boca Raton, Florida. (1991).

[50]　C. Preininger, O. S. Wolfbeis, *Disposable cuvette test with integrated sensor layer for enzymatic determination of heavy metals*, Biosensors Bioelectronics, **11**, 981 (1996).

[51]　R. T. Andres, R. Narayanaswamy, *Effect of the coupling reagent on the metal inhibition of immobilized urease in an optical biosensor*, Analyst, **120**, 1549 (1995).

[52]　S. C. Charlton, R. L. Fleming, A. Zipp, *Solid-Phase Colorimetric Determination of Potassium,* Clin. Chem., **28**, 1857 (1982).

[53]　W. E. Morf, K. Seiler, B. Rusterholz, W. Simon, Design of a novel calcium-selective optode membrane based on neutral ionophores, Anal. Chem., 62, 738 (1990).

[54]　K. Seiler, K. Wang, E. Bakker, W. E. Morf, B. Rusterholz, W. Simon, U. E. Spichiger, *Characterization of sodium-selective optode membranes based on neutral ionophores and assay of sodium in plasma*, Clin. Chem.*,* **37**, 1350 (1991).

[55]　K. Seiler, R. Eugster, W. E. Morf, K. Wang, M. Czösz, B. Rusterholz, W. Simon, U. E. Spichiger, *Application of Calcium Optode in Human Plasma*, Fresenius' J. Anal. Chem., **337,** 109 (1990).

[56]　K. Seiler, W. Simon, *Theoretical Aspects of bulk optode membranes*, Anal. Chim. Acta, **266**, 73 (1992).

[57] S. S. S. Tan, P. C Hauser, N.Chaniotakis, G. Suter, W. Simon, *Anion-Selective Optical Sensors Based on a Coextrction of Anion-Proton Pairs into a Solvent-Polymeric Membrane*, Chimica, **43**, 257 (1989).

[58] W. E. Morf, K. Seiler, B. Lehmann, C. Behringer, K. Hartmann, W. Simon, *Carriers for Chemical Sensors: Design Features of Opctical Sensors (Optodes) Based on Selective Chromoionophores*, Pure Appl. Chem., **61,** 1613 (1991).

[59] C. Krause, T. Werner, C. Huber, O. S. Wolfbeis, Marc J. P. Leiner, *pH-Insensitive Ion selective optode: A Coextraction Based Sensor for Potassium Ions,* Anal. Chem., **71**, 1544 (1999).

[60] C. Huber, T. Werner, C. Krause, Marc. J. P. Leiner, O. S. Wolfbeis, *Overcoming the pH Dependence of Optical Sensors: A pH-Independent Chloride Sensor Based on Co-Extraction*, Anal.Chim. Acta., **398**, 137 (1999).

[61] C. Huber, T. Werner, C. Krause, O. S. Wolfbeis, *Novel Chloride-Selective Optode Based on Polymer-Stabilized Emulsion Doped with a Lipophilic Fluorescent Polariy Sensitive Dye*, Analyst, **124**, 1617 (1999).

[62] C. Krause, T. Werner, C. Huber, O. S. Wolfbeis, *Emulsion-Based Fluorosensors for Potassium Featuring Improved Stability and Signal Change*, Anal. Chem., **71**, 5304 (1999).

[63] E. Wänninen, *Indicators*, E. Bishop (ed.), Pergamemon Press, Oxford (1972).

[64] B. Valeur, in *Topics in Fluorescence Spectroscopy – Volume 4 Probe Desing and Chemical Sensing*, J. R. Lakowicz (ed.), Plenum Press, New York (1994).

[65] Fluka, *Selectophore Catalog*, Neu-Ulm (1996).

[66] R. P. Haugland, *Handbook of Fluorescent Probes and Research Products*, Molecular Probes, Eugene (2001).

[67] A. W. Czarnik (ed.), *Fluorescent Chemosensors for Ion and Molecule Recognition*, ACS Symposium Series 538, Washington, DC (1992).

[68] J. P. Devergne, A. W. Czarnik (eds.), *Chemosensors of Ion amd Molecule Recognition*, Kluwer Academic Publishers, Dortrecht (1997).

[69] A. P. de Silva, H. Q. Nimal Gunaratne, T. Gunnlaugsson, A. J. M. Huxley, C. P. McCoy, J. T. Rademacher, T. E. Rice, *Signaling Events with Fluorscent Sensors and Switches*, Chem. Rev., **97**, 1515 (1997).

[70] T. Förster, *Zwischenmolekulare Energiewanderung und Fluoreszenz*, Ann. Phys., **2**, 55 (1948).

[71] I. Oehme, S. Prattes, O. S. Wolfbeis, G. J. Mohr, *The effect of polymeric supports and methods of immobilization on the performance of an optcical copper(II)-sensitive membrane based on the colorimetric reagent Zincon*, Talanta, **47**, 595-604 (1998).

[72] H. Kautsky, *Quenching of Luminescence by Oxygen*, Trans. Faraday Soc., **35**, 216 (1939).

[73] D. B. Papkovsky, G. V. Ponomarev, W. Trettnak, P. O´Leary, *Phosphorescent Complexes of Porphyrin Keton: Optical Propeties and Application to Oxygen Sensing*, Anal. Chem., **67**, 4112 (1995).

[74] K. Legg, D. M . Hercules, *Quenching of Lucigenin Fluorescence*, J. Phys. Chem., **74**, 2114 (1970).

[75] J. Biwersi, B. Tulk, A. S. Verkman, *Long Wavelength Chloride-Sensitive Fluorescent Indicators*, Anal. Biochem., **219**, 139 (1994).

[76] C. Huber, K. Fähnrich, C. Krause, T. Werner, *Synthesis and Characterization of New Chlorid-Sensitive*, J. Photochem. & Photobiol., **128**, 111 (1999).

[77] C. Huber, I. Klimant, C. Krause, O. S. Wolfbeis, *Dual Lifetime Referencing as Applied to a Chloride Optical Sensor*, Anal. Chem., **73**, 2097 (2001).

[78] C. Sanchez-Pedreno, J. A. Ortuno, M. I. Albero, M. S. Garcia, M. V. Valero, *Development of a new bulk optode membrane for the determination of mercury (II)*, Anal. Chim. Acta, **414**, 195 (2000).

[79] W. H. Chan, R. H. Yang, K. M. Wang, *Development of a mercury ion-selective optical sensor based on fluorescence quenching of 5,10,15,20-tetraphenylporphyrin*, Anal. Chim. Acta., **444**, 261 (2001).

[80] N. Malcik, O. Oktar, M. E. Ozser, P. Caglar, L. Bushby, A. Vaughan, B. Kuswandi, R. Narayanaswamy, *Immobilised reagents for optical heavy metal ion sensing*, Sens. Actuators B, **53**, 211 (1998).

[81] A. A. Vaughan, R. Narayanaswamy, *Optical fibre reflectance sensors for the detection of heavy metal ions based on immobilised Br-PADAP*, Sens. Actuators B, **51**, 368 (1998).

[82] N. Mahendra, P. Gangaiya, S. Sotheeswaran, R. Narayanaswamy, *Investigation of a Cu(II) fibre optic chemical sensor using fast sulphon black F (FSBF) immobilised onto XAD-7*, Sens. Actuators B, **81**, 196 (2002).

[83] E. Anticó, M. Lerchi, B. Rusterholz, N. Ackermann, M. Badertscher, M. Valiente, E. Pretsch, *Monitoring Pb^{2+} with optical sensing films*, Anal .Chim. Acta, **388**, 327 (1999).

[84] F. Szurdoki, D. Ren, D. R. Walt, *A Combinatorial Approach To Discover New Chelators for Optical Metal Ion Sensing*, Anal. Chem., **72**, 5250 (2000).

[85] A. V. Legin, Y. G. Vlasov, A. M. Rudnitskaya, E. A. Bchkov, *Cross-sensitivity of chalcogenide glass sensors in solution of heavy metal ions*, Sens. Actuators B, **34**, 456 (1996).

[86] W. Rettig, B. Strehmel, S. Schrader, H. Seifert (eds). *Applied Fluorescence in Chemistry, Biology and Medicine,* Springer, Berlin (1999).

[87] O. S. Wolfbeis (ed.), *Fluorescence Spectroscopy*, Springer, Berlin (1993)

[88] J. R. Lakowicz, R. B. Thompson (eds.), *Advances in Fluorescence Sensing Technology IV*, SPIE Proc., **3602**, 452 (1999).

[89] X. F. Wang, B. Herman (eds.), *Fluorescence Imaging Spectroscopy and Microscopy,* Wiley, New York (1996).

[90] D. F. Wilson, G. J. Cerniglia, *Localisation of Tumors and Evaluation of their State of Oxygenation by Phosphorescence Imaging,* Cancer. Res., **52**, 3988 (1992).

[91] S. Nomura, M. Nakao, T. Nakanishi, S. Takamatsu, K. Tomita, *Real-Time Imaging of Microscopic pH Distribution with a Two-Dimensional pH Imaging Aparatous*, Anal. Chem., **69**, 977 (1997).

[92] J. R. Lakowicz, H. Szmacinski, K. Nowaczyk, M. L. Johnson, *Fluorescence Lifetime Imaging of Calcium Using Quin-2*, Cell Calcium, **13**, 131 (1992).

[93] G. Gauglitz, *Optical Sensors Arrays Based on Microtiterplates Dimensions*, Mikrochim. Acta, **131**, 9 (1999).

[94] G. Liebsch, I. Klimant, B. Frank, G. Holst, O. S. Wolfbeis, *Luminescence Lifetime Imaging of Oxygen, pH and Carbon Dioxide Distribution Using Optical Sensors*, Appl. Spec., **54**, 548 (2000).

[95] G. Liebsch, I. Klimant, C. Krause, O. S. Wolfbeis, *Fluorescent Imaging of pH with Optical Sensors Using Time Domain Dual Lifetime Referencing*, Anal. Chem., **73**, 4354 (2001).

[96] G. Holst, B. Grunwald, *Luminescence Lifetime imaging with transparent oxygen optodes,* Sens. Actuators B, **74**, 78 (2001).

Chapter 2

Fluorimetric Determination of Copper(II) Ions in Aqueous Solution Using Lucifer Yellow CH as Selective Metal Reagent

Lucifer yellow CH is shown to be a highly selective fluorescent reagent for the determination of copper(II) in the µg/l concentration range. The fluorophore is statically quenched by copper(II); the carbohydrazide group was assigned as the complexing part of the dye molecule. A total range of copper(II) determination from 0.06 mg/l (1 µM) to 6.3 mg/l (100 µM) with a limit of detection of 0.019 mg/l (0.3 µM) was obtained, along with surprisingly high selectivity. There was no interference from alkaline and earth alkaline metal ions. The cross sensitivity to heavy metal ions was evaluated by the separate solution method and by competitive binding experiments. Calibration plots are shown for copper(II) determination at different pH and the dissociation constant was determined. The application of the reagent was demonstrated by the determination of the copper(II) content of tap water samples.

2.1. Introduction

The determination of copper by photometric methods is well established [1,2]. More recently, the developments in supramolecular chemistry brought new receptors for metal ions to the light. These ionophores linked with a fluorophore yields in so called fluoroionophores. Within these, a recognition and a transducing element is combined in one molecule. Numerous publications deal with this field of molecular recognition. Thiocrown ethers, aza-crown ethers, cyclame, thiourea, thiadiazole, bithiazole, and azo derivatives have been reported as recognition elements [3-9]. Furthermore, polyamines were published as receptor unit [10-13]. Czarnik et al. report the hydrolysis of rhodamine B hydrazide catalyzed by copper(II) [14].

Most of these reagents, however, suffer from considerable disadvantages– e.g. excitation or emission maxima in the UV range, poor solubility, the need of an additional reagent, or, most importantly, the lack of selectivity – which make their application difficult. Mitchel et al. [12] and Ramachandram and Samanta [13] have described the effect of heavy metal ions on the fluorescence of substituted 1,8-naphthalimides. In a search for specific indicators for the application in optical sensors we found that the fluorescent naphthalimide derivative Lucifer yellow carbohydrazide (**LY**) binds copper(II) selectively. The carbohydrazide group is a known complexing agent for copper(II) and other heavy metal ions in the photometric reagent diphenylcarbohydrazide [15].

The commercially available **LY** (see Figure 2.1) was synthesized by Stewart in 1981 [16] and is widely used for staining neurons [17]. LY absorbs at 430 nm with an emission maximum at 535 nm; it can thus be excited with a blue 430 nm LED. The compound has a quantum yield of approximately 0.21 and its photostability is excellent. The absorbance and emission maxima are not effected by pH between 2 and 9 [16]. Because of its two sulfonic acid groups, the solubility of **LY** in water is good.

Lucifer Yellow-CH   Lucifer Yellow-VS
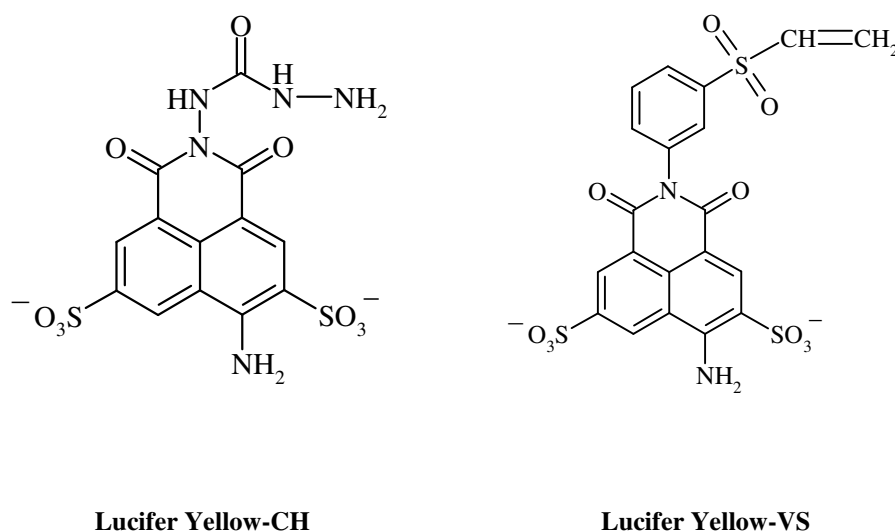
Fig. 2.1. Chemical structures of the naphthalimide derivatives lucifer yellow–CH (LY) and lucifer yellow–VS (LY-VS).

2.2. Theory of Fluorescence Quenching

The term fluorescence quenching refers to any process which decreases fluorescence intensity of a substance. These processes include excited state-reactions, molecular rearrangements, energy transfer, ground state complex formation and dynamic or collisional quenching [18,19]. In addition to this mechanisms decrease in fluorescence can be observed by the so called inner-filter effect. This trivial type of quenching occurs in presence of substances, which absorb a significant proportion of the excitation or fluorescent radiation.

2.2.1. Dynamic Quenching

Quenching is termed dynamic or collisional, if a fluorophore is radiationless deactivated by the collision with a quencher during the lifetime of its excited state (see Figure 2.2). The quenching species must diffuses to the fluorophore and upon contact, the fluorophore returns to the ground state, without emission of a photon. Quenching occurs without any permanent change of the molecule, that is without a photochemical reaction.

The mechanism of collisional quenching is described by the Stern-Volmer equation:

$$\frac{F_0}{F} = \frac{\tau_0}{\tau} = 1 + k_q \tau_0 [Q] = 1 + K_D [Q] \qquad \qquad 2.1$$

where F_0, τ_0 and F, τ are the fluorescence intensities and lifetimes in the absence and presence of a quencher, respectively, k_q is the bimolecular quenching constant for the dynamic reaction of the quencher with the fluorophore and [Q] is the quencher concentration. K_D is the Stern-Volmer constant (KSV) given by equation 2.2.

$$K_D = k_q \cdot \tau_0 \qquad \qquad 2.2$$

A plot of *(F_0/F)* vs. *[Q]* is expected to be linear with a slope equal to K_D. Note that K_D^{-1} is the quencher concentration at which *F_0/F=2*, or 50% of the intensity is quenched.

According to equation 2.1 dynamic quenching can also be determined by fluorescence lifetime measurements of the fluorophore because there is an equivalent decrease in fluorescent intensity and lifetime.

2.2.2. Static Quenching

The formation of non-fluorescent complex of the fluorophore with the quencher in the ground state is described as static quenching. When this complex absorbs light, it immediately returns to the ground state without emission of a photon.

$$F+Q \rightleftharpoons F\text{-}Q$$

fluorescent, τ_0 non-fluorescent

2.3

The association constant for the complex formation is given by

$$K_S = \frac{[F-Q]}{[F][Q]}$$

2.4

where [F-Q] is the concentration of the complex, [F] is the concentration of uncomplexed fluorophores and [Q] the quencher concentration. The total concentration of fluorophores [F_0] is the sum of complexed and uncomplexed fluorophores (equation 2.5) and replacing [F-Q] yields in equation 2.6.

$$[F_0]=[F]+[F-Q]$$

2.5

$$K_S = \frac{[F_0]-[F]}{[F][Q]}$$

2.6

Substituting the fluorophore concentration with the fluorescence intensities and rearranging equation 2.7 yields a similar Stern-Volmer equation.

$$\frac{F_0}{F}=1+K_S[Q]$$

2.7

Apparently, the dependence F_0/F vs. [Q] is linear and is identical to that observed for dynamic quenching, but the quenching constant K_S is now the association constant. In static quenching the observed fluorescence is solely from the uncomplexed fluorophores, since the complexed fluorophores are non-fluorescent. The uncomplexed fraction is not affected by the quencher and hence the lifetime is τ_0. Consequently, for static quenching $\tau_0/\tau=1$, in contrast to dynamic quenching were $\tau_0/\tau = F_0/F$.

2.2.3. Differentiation between Dynamic and Static Quenching

In the previous sections the mechanisms of collisional and static quenching were described. Regarding equations 2.1 and 2.6, fluorescence intensity data are insufficient to distinguish between static and dynamic quenching. The most effective way to differenciate is the measurement of fluorescence decay time, since in case of static quenching a fraction of fluorophores is removed by complex formation and this, of course, does not affect fluorescence lifetime. Besides investigation of the fluorescence lifetime the static and dynamic quenching can be distinguished, recording Stern-Volmer plots at different temperatures. Dynamic quenching is a diffusion depending process. Thus, increasing temperature results in larger diffusion coefficients, and consequently, increasing bimolecular quenching constants K_D are expected. In contrast, the complex formation constant K_s decreases with increasing temperatur because the stability of the complexes usually decreases. Furthermore, the absorption spectra of the fluorophore in absence and presence can be used for the differentiation. Since collisional quenching, only affects the excited states of the fluorophores, no changes in variation in the absorption spectra are expected. In contrast, variation of absorption spectra are observed in static quenching, due to ground-state complex formation.

2.3. Materials and Methods

2.3.1. Chemicals

All chemicals used were of analytical grade and used without further purification. Lucifer yellow CH dipotassium salt (**LY**) and lucifer yellow VS dilithium salt (**LY**) were obtained from Fluka (Buchs, Switzerland). Water was doubly distilled. All inorganic salts were of analytical grade and obtained from Merck (Darmstadt, Germany) or Fluka. The metal ion solutions were prepared from nitrate salts. Sodium acetate and chloroacetic acid were from Merck. Acetic acid was from Roth (Karlsruhe, Germany) and sodium chloroacetate from Riedel-de Haën (Seelze, Germany). 3-[N-Morpholino]propanesulfonic acid and the respective sodium salt (MOPS) were obtained from Sigma (Vienna, Austria). Microtiterplates (96 wells) with flat bottoms were obtained from Greiner (Frickenhausen, Germany).

2.3.2. Instrumentation and Measurements.

2.3.2.1. Fluorescence Measurements

Fluorescence excitation and emission spectra were acquired with an Aminco Bowman Series 2 luminescence spectrometer from SLM-Aminco (Rochester, NY 14625, USA) equipped with a continuous wave 150 W xenon lamp as a light source, as shown in Figure 2.2.

Fig. 2.2. SLM-Aminco luminescence spectrometer

2.3.2.2. Fluorescence Decay Time Measurements

Fluorescence decay time measurements were obtained with an ISS K2 multi-frequency phase-modulation fluorimeter using a 150 W continuous xenon lamp (PS 300–1, ILC technology) as

excitation light source and two 2022D signal generators from Marconi Instruments (Hertfordshire, UK). The light was passed through a Pockels cell which provided modulated light. Emission was detected at 90° to the excitation, through a conventional filter (bandbass filter with transmission at 445–495 nm, FITCA from Schott (Mainz, Germany). The apparatus is shown in Figure 2.3.

Fig. 2.3. ISS K2 multi-frequency phase-modulation fluorimeter

2.3.2.3. *Fluorescence Measurements in Microtiterplates*

Fluorescence measurements in microtiterplates were obtained by means of an Ascent Fluoroscan microtiterplate reader from Labsystems (Helsinki, Finland, see Figure 2.4) equipped with excitation and emission filters at wavelengths of 420 and 530 nm. A quartz halogen lamp was used as light source.
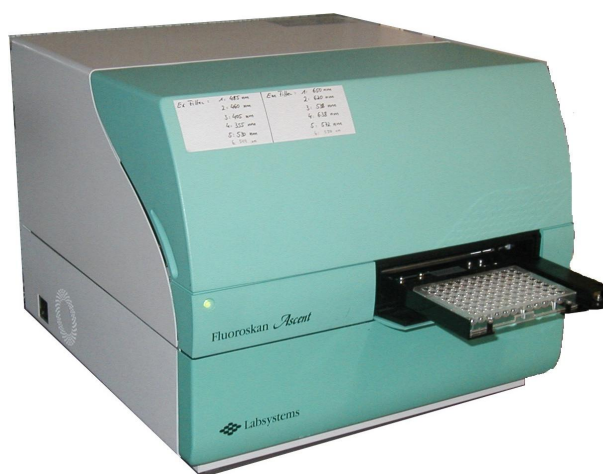
Fig. 2.4. Labsystems Ascent Fluoroscan Microtiterplate Reader

2.3.2.4. *Atom Absorption Spectroscopy*

A SpectrAA-30 Varian Graphite Furnace Atomizer GTA 96 equipped with a copper hollow-cathode lamp was used for the determination of the copper content at an electrothermic atomization temperature of 2400 °C.

2.3.3. Preparation of Buffers

Buffer compositions were calculated according to Perrin [20]. This calculation is based on the Debeye Hückel theory and allows the calculation of buffer composition a defined pH, buffer concentration and ionic strength. The pH was adjusted by use of acetate, chloroacetate, or MOPS buffer ($c_{acid}+c_{base}$=10 mM). The constant ionic strength was adjusted to I=10 mM by use of sodium nitrate as background electrolyte. The pH of the solutions were monitored by use of a digital pH-meter (Knick, Berlin, Germany) calibrated with standard buffers of pH 7.00 and 4.00 at 21±1 °C.

2.3.4. Performance of Measurements

For measurement of the excitation and emission spectra, and for decay time measurements, a 1 mM copper(II) stock solution was prepared by dissolving the appropriate amount of copper(II) nitrate in 10 mM acetate buffer, pH 5, containing 1 µM **LY** or **LY–VS**. From this other solutions were prepared by dilution with the buffer/**LY** solution.

The pH-dependence was investigated by use of 96-well microplates. A 100 mM copper(II) nitrate stock solution and 500 µM stock solution of **LY** were prepared. From the latter solution a 5 µM **LY**/buffer solution at the appropriate pH was prepared and this solution was then used to prepare 1000 µM copper(II) solution with a fluorophore concentration 4.95 µM. **LY**/buffer filling up solution (4.95 µM) was then prepared. From this solution and the 1000 µM copper(II)/**LY** solution measuring solutions containing copper(II) concentrations from 0.1 to 1000 µM were prepared and transferred to 96-well microtiterplates. The standard deviations were calculated from at least six measurements.

Cross-sensitivity to other heavy metal ions was measured in microtiterplates. Stock solutions for all heavy metal ions were prepared by dissolving the respective amount of nitrate salt in 10 mM acetate buffer (pH 5) containing 5 µM **LY**. All solutions were prepared with the same buffer/**LY** solution. The microtiterplates were filled with solutions (100 µL) containing **LY** (5 µM) in acetate buffer and different heavy metal ions at concentrations of 0,

2, 20, 200, and 2000 µM. Copper(II) solutions (100 µL) at concentrations of 0, 2, 20, and 200 µM containing 5 µM **LY** in acetate buffer were then added. Measurements were taken immediately after filling. The standard deviations were calculated from at least six measurements.

The copper(II) content of tap water samples was determined by mixing sample (90 µl) with 10 µl buffered 50 µM **LY** solution (100 mM acetate buffer at pH 5) in microplates. The measured pH of the resulting mixture was 6.1. The solutions for calibration were prepared from 50 µM copper(II) stock solution in 10 mM acetate buffer at pH 6.1. Fluorescence measurements were performed immediately after filling. The average values and standard deviations were calculated from at least six measurements. The copper(II) content of the tap water samples was also investigated by an extraction method with the photometric reagent diethyl dithiocarbamate, as described by Krump and Krist [24].

2.3.5. Fitting Function and Calibration Curves

Calibration curves were fitted with the Boltzmann function shown in Eq. (2.1):

$$F = \frac{Z-Y}{1+\exp(\log(c/\mu M)-X/W)} + Y \tag{2.1}$$

where F is the fluorescence and W, X, Y, and Z are empirical parameters describing the initial value (Z), final value (Y), centre (X), and width (W) of the fitting curve. The 50% decrease in fluorescence intensity [$c_{1/2}(Cu^{2+})$] was calculated by determining the point of inflection of the calibration curve.

2.4. Results and discussion

2.4.1. Quenching of the Fluorescence of Lucifer Yellow–CH by Copper(II)

The excitation and emission spectra of a 1 µM **LY** solution at pH 5 in the presence of copper(II) at different concentrations are shown in Figure 2.5. Increasing the copper(II) concentration from 0 to 1000 µM leads to decrease of the fluorescence intensity of **LY**. The effect appears at a copper(II) concentration of 0.1 µM where 2% of the fluorescence intensity at the emission maximum (λ_{em}=535 nm) is quenched. For a 100 µM (6.3 mg/l) copper(II) concentration the fluorescence is reduced to 17% of the original value.
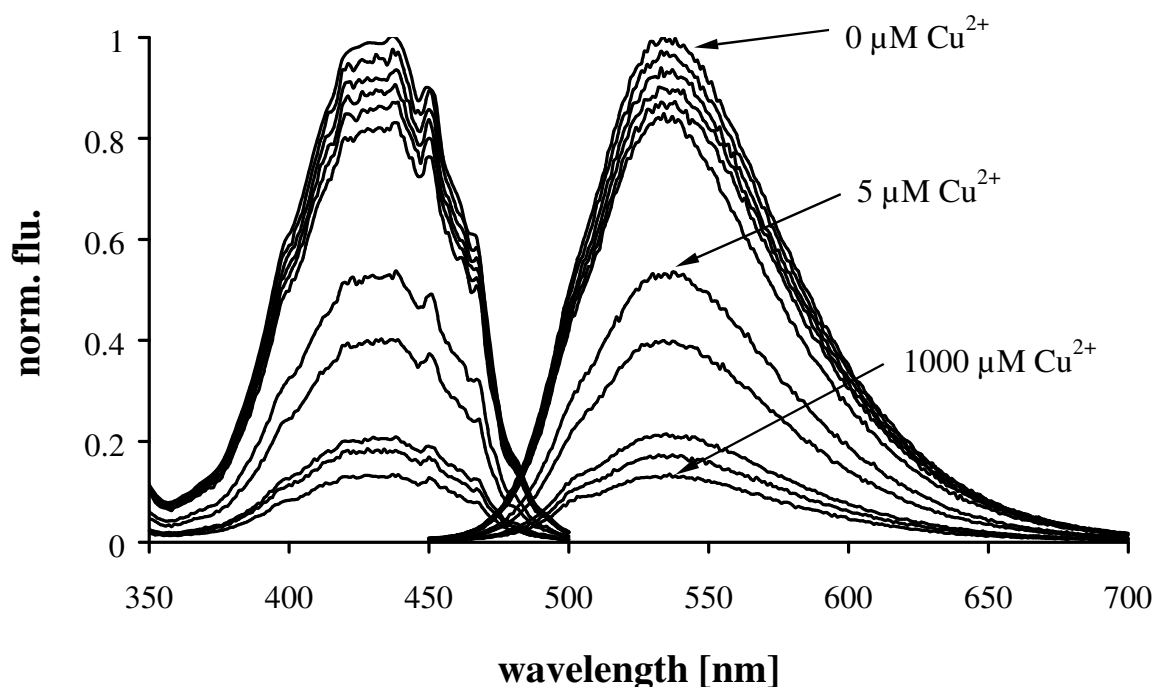
Fig. 2.5. *Fluorescence excitation and emission profiles of 1 µM **LY** solutions in presence of copper(II) in concentrations 0, 0.1, 0.3, 0.5, 0.8, 1, 5, 10, 50, 100, 500, 1000 µM (from top to bottom).*

The calibration plot for pH 5, which can be seen in Figure 2.6, has a sigmoidal shape. The response is nearly linear in the range between 2 and 20 µM. The total range for detection covers the concentration range up to 100 µM (6.3 mg/l) with a limit of detection of 300 nM (0.019 mg/l). The point of inflection ($c_{1/2}$) was calculated to be at 4.4 µM indicating that at this concentration 50% of the fluorescence is quenched.
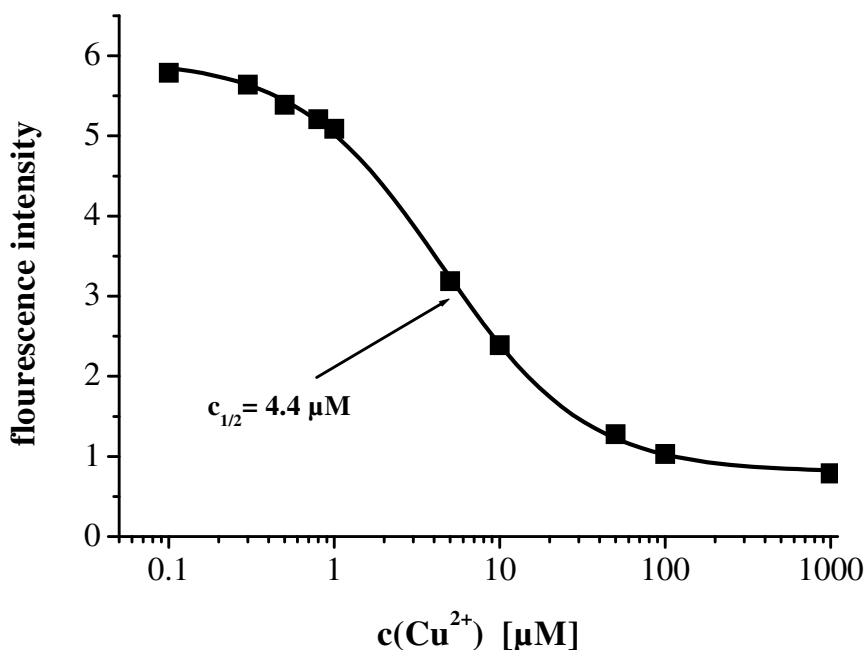
*Fig. 2.6. Calibration plot of 1 µM **LY** solutions in presence of copper(II).*

The fluorescence lifetimes of the solutions were investigated to distinguish between static and dynamic quenching. In dynamic or collisional quenching, increasing the analyte concentration influences the lifetime of the excited state [18]. Solutions containing **LY** and copper(II) at concentrations of 0, 0.1, 1, 10, and 100 µM have a constant fluorescence decay time of 5.3 ns. This indicates that the present quenching effect is static. The dye and the quenching molecule form complex, which is non-fluorescent. The proposed mechanism is given by equation 2.3.

A plot F_0/F- against $c(Cu^{2+})$ shown in Figure 2.7 – analogous to the Stern–Volmer plot for dynamic quenching – is highly linear for copper(II) concentrations <5 µM). At concentrations >10 µM this plot has downward curvature. We attribute this to the poor availability of the fluorophores compared with an excess of copper ions. From the linear part of this plot the quenching constant $K_s = 0.15$ µM was obtained. In static quenching the quenching constant equals the association constant, so a dissociation constant $K_D = 6.6$ µM was calculated [18]. The dissociation constant can also be obtained by plotting $(F–F_{min})/(F_{max}–F)$ against [Q], where the slope is the association constant [24], if we assume a 1:1 complex. For our data such a plot is linear over the whole concentration range and a dissociation constant $K_D = 4.9$ µM was calculated, which is comparable with the result from the Stern–Volmer plot.
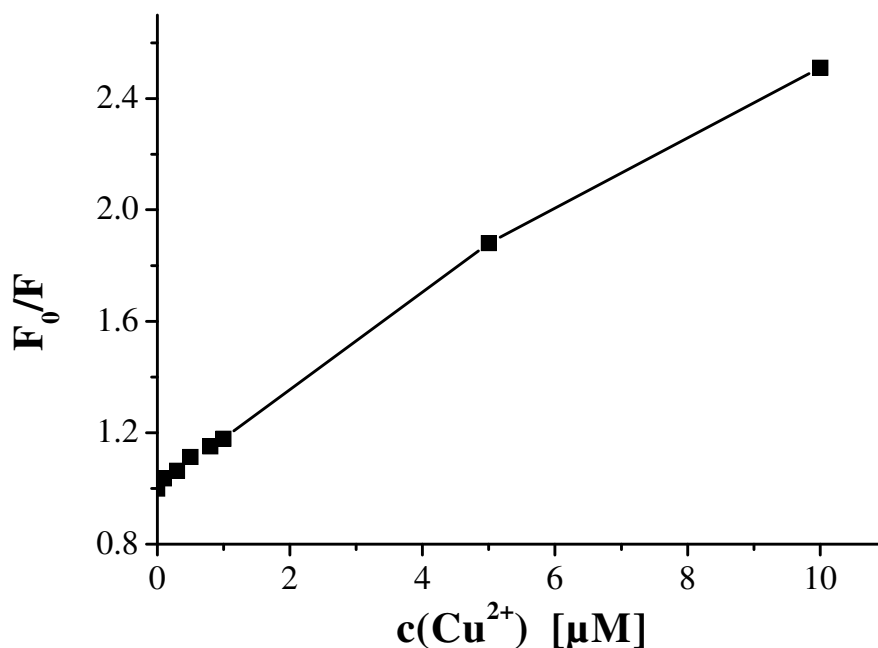
Fig. 2.7. *Stern-Volmer plot for **LY** in presence of copper(II).*

In contrast to Mitchel et al. and Ramachandra et al. we can exclude a PET (photoinduced electron transfer) mechanism, because of the constant decay time [12, 13]. Also, a fluorescence decrease was observed when the copper(II) ion concentration was increased. This is in contrast to a PET mechanism, where the opposite effect would be observed.

In further investigations the naphthalimide derivative **LY–VS** was examined. In this substance the carbohydrazide group is replaced by a vinylsulfonylphenyl group (see Figure 2.1). It was found that copper(II) ions do not reduce the fluorescence of **LY–VS** and therefore the carbohydrazide group is suggested as complexing part of **LY**. Attempts to obtain information about the structure of the complex by NMR-titration failed, because of the paramagnetic nature of copper(II).

2.4.2. Influence of pH

The influence of pH on the quenching by copper(II) is illustrated in Fig. 2.8. The calibration curves are shifted to lower concentrations on turning to lower acidity, as well as the $c_{1/2}$ values decrease on going from pH 2 to pH 6. This effect of pH disappears at pH 7, as is apparent from the calibration plots for pH 6 and 7, which have almost the same shapes and $c_{1/2}$ values. Because of competitive copper hydroxide formation, a distinct increase in fluorescence intensity is observed for solutions of pH>8. The observed pH effect can be explained by an

acid–base equilibrium. The terminal nitrogen atoms of the hydrazide group are protonated in solutions of high acidity (see Figure 2.1). Consequently the complexation of copper(II) is hindered because the necessary lone electron pairs are occupied by protons. Reported acidity constants of $pK_{a1}=2.09$ and $pK_{a2}=4.14$ for carbodihydrazide [22] support this suggestion.
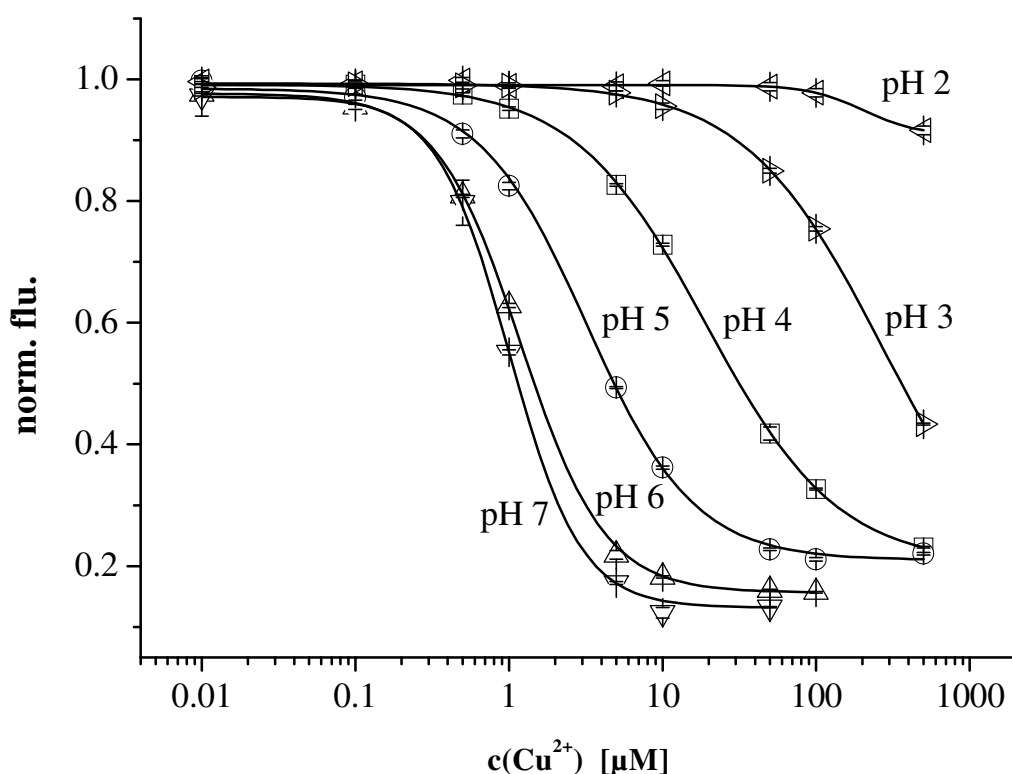
Fig. 2.8: Calibration plots for fluorescence measurements of 4.95 µM LY solution at various pH and copper(II) concentrations. Calculated $c_{1/2}$ values: 27.3, 19.2, 3.2, 1.2, 1.0 for pH 3, 4, 5, 6, 7 respectively.

2.4.3. Selectivity for Copper(II)

LY has high selectivity for copper(II) even in the presence of other metal ions. No interference from the alkali or alkaline earth metals or from the heavy metal ions zink(II), silver(I), cadmium(II), and lead(II) was found in the concentration range investigated (0.1 – 1000 µM). The interference from several heavy metal ions are depicted by the columns in Figure 2.9 for 0 µM copper(II). Selectivity coefficients relative to a 10 µM copper(II) solution were determined by the separate solution method (SSM) $logK_{Cu2+}$ that are 1.5 for mercury(II), 1.9 for iron(III), 2.3 for nickel(II), and 2.9 for cobalt(II).
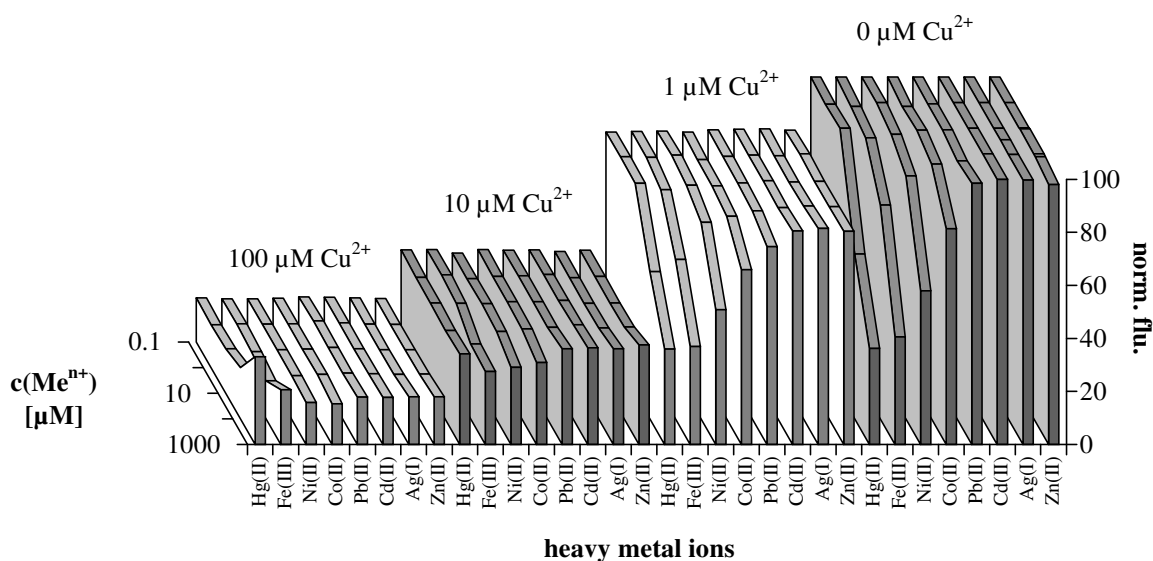
Fig. 2.9. *Fluorescence of 5 μM **LY** solutions in presence of various heavy metal ions in concentrations 0.1, 1, 10, 100, 1000 μM and simultaneous presence of 0, 1, 10, 100 μM copper(II).*

2.4.4. Experiments on Competitive Binding of Heavy Metal Ions

For application of **LY** as a fluorimetric reagent for copper(II), investigation in the simultaneous presence of copper(II) and heavy metal ions is necessary. Figure 2.9 shows a three dimensional plot for different heavy metals at different concentrations in the presence of 0, 1, 10, and 100 μM copper(II). As expected, the fluorescence in presence with zink(II), silver(I), cadmium(II), and lead(II) is just affected by the quenching of copper(II). No influence is observed for the ions mercury(II), iron(III), nickel(II), and cobalt(II) at concentrations up to 1 μM for all copper(II) concentrations. Interfering ion concentrations >1 μM have a noticeable effect. Table 2.1 shows the deviation of the fluorescence from the original value, i.e. without additional heavy metal ion, in the presence of different concentrations of copper(II) and 10 μM heavy metal ion. The fluorescence intensity of solutions containing 10 or 100 μM interfering ion is always lower than that for the interfering ion in the absence of copper(II). From this we conclude that the fluorescence is quenched by the interfering ion and the copper(II) ion, forming two different complexes with **LY**, so quenching is additive. The additive quenching effect was also observed for solutions containing 100 μM interfering ion, with exception of mercury(II). The fluorescence of solutions containing 1000 μM mercury(II) is approximately the same. Consequently,

quenching is not additive and results from mercury(II) forming a more stable complex with **LY** than does copper(II). This was not observed for 1000 µM iron(III), cobalt(II), and nickel(II) and is attributed to the paramagnetism of these ions, which is in contrast with the diamagnetic mercury(II) and its quenching due to the heavy atom effect.

Table 2.1. *Differences in fluorescence intensities for solutions containing 10 µM mercury(II), iron(III), nickel(II), cobalt(II) and different copper(II) concentrations (F_{Cu2+} - $F_{Interferent}$).*

$c(Cu^{2+})$ [µM]	Hg^{2+}	Fe^{3+}	Ni^{2+}	Co^{2+}
0	0.06	3.60	2.29	0.75
1	0.06	2.64	1.12	1.00
10	0.40	1.02	-0.12	0.44
100	-0.18	0.70	-0.14	-0.02

2.4.5. Application to Tap Water Samples and Comparison with Standard Methods

The method was applied to real samples and compared with the standard methods AAS and photometry. The samples were taken at different times from hot and cold water supplied by copper pipes in a regional household. The tap water samples were mixed in microtiterplates with **LY**/buffer solution and the fluorescence was measured. The copper(II) content was calculated from the calibration plot shown in Figure 2.10. The results obtained are listed in Table 2.2, and are in good agreement with those obtained by standard methods.
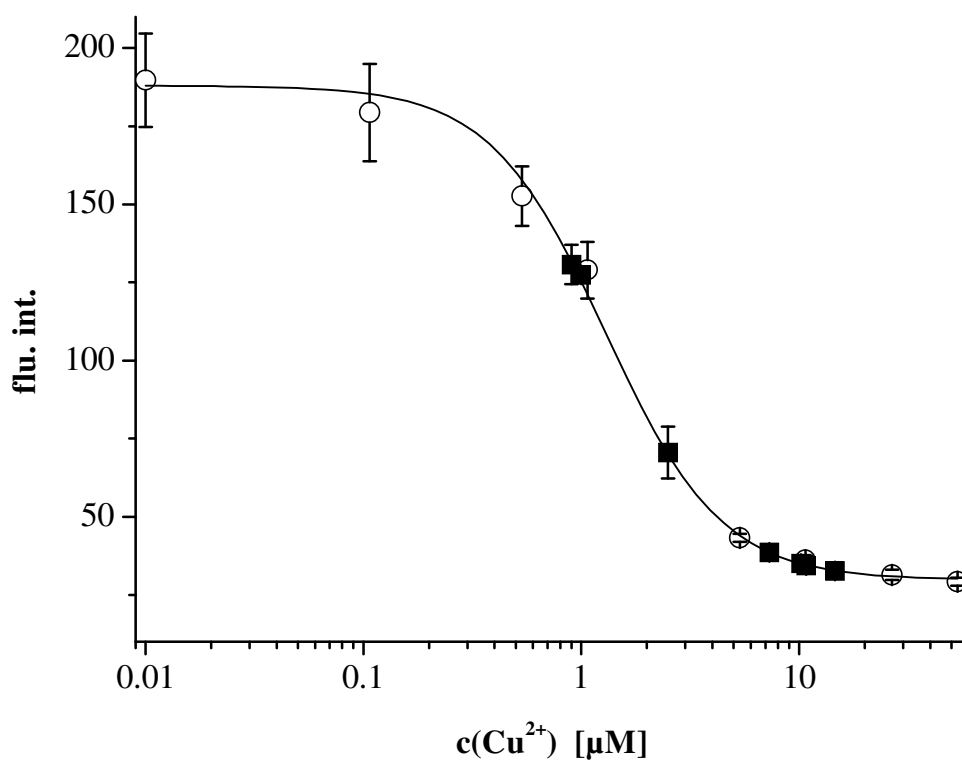
Fig. 2.10. *Calibration plot (circles) and determined copper(II) values for tap water samples (squares) measured with the fluorescence microtiterplate reader at excitation- emission wavelengths of 420 and 530 nm. Average values and error bars were calculated from at least six measurements.*

Table 2.2. *Application of **LY** for the determination of copper(II) in tap water samples. Comparison of fluorescence method and standard methods.*

	Copper(II) content in µM (µg/l)		
Sample no.	*Fluorimetric*	*GF-AAS*	*photometric* [a]
1	10.2 (666)	9.1 (580)	-
2	14.6 (928)	11.6 (740)	12.6 (800)
3	10.8 (686)	9.4 (600)	9.4 (600)
4	0.9 (57.2)	0.7 (44)	-
5	2.5 (159)	2.2 (140)	-
6	1.0 (63.6)	1.0 (64)	-

[a] Determination with diethyl dithiocarbamate according to reference 21

2.5. Conclusion

Detection of copper(II) is possible at concentrations below those recommended for drinking water by the EU and the WHO. The determination of is not affected by the pH in the range from 6–8. The cross-sensitivity towards other ions was also investigated. Although the interference is not negligible, the concentration range at which interference was found was much higher than the concentration expected in a real sample. This selectivity, the independence of pH between 6 and 8, and the good water solubility makes **LY** an ideal reagent for the determination of Copper(II) in drinking or surface water – it can just be added to the sample. The quick and simple method was successfully applied to real samples and the accuracy was proved by reference methods. Another potential application of **LY** is in flow-injection instrumentation. In the next chapter an optical sensor application in presented in which **LY** is incorporated in a polymeric film.

2.6. References

[1]   W. Fresenius, K. E. Quentin, W. Schneider, *Water Analysis*, Springer, Berlin (1988)

[2]   J. Fries, H. Getrost, *Organische Reagenzien für die Spurenanalyse*, Merck, Darmstadt (1977).

[3]   G. De Santis, L. Fabrizzi, M. Licchelli, C. Mangano, D. Sacchi, N. Sardone, *A Fluorescent Chemosensor for the Copper(II) Ion*, Inorgan. Chim. Acta, **257**, 69 (1997).

[4]   G. E. Collins, L. S. Choi, *Fluorescent diaza crown ether sensitive to complexation, confirmation and mircroenvironment*, Chem. Comm., 1135 (1997).

[5]   A. M Josceanu, P. Moore, S. C. Rawle, P. Sheldon, S. M Smith, *1,4,8,11-Tetrakis{(2,2´-bibyridyl-5´-ylmethyl)-bis(2,2´-bipyridyl)ruthenium(II)}-1,4,8,11-tetraazacyclotetra-decane, a Macrocyclic pH and Transition Metal Ion Fluorescence Sensor*, Inorgan.Chim. Acta, 240, 159 (1995).

[6]   M. Schuster, M. Sander, *N-Dansyl-N-ethylthiourea for the Fluorometric Detection of Heavy Metal Ions,* Fresenius J. Anal. Chem., **356**, 326 (1996).

[7]   G. Hennrich, H. Sonnenschein, U. Resch-Genger, *Redox Switchable Fluorescent Probe Selcetive for either Hg(II) or Cd(II) and Zn(II)*J. Am. Chem. Soc., **121**, 5073 (1999)

[8]   S. Pellet-Rostaing, J. Regnouf-de-Vains, R. Lamartin, S. Meallierm, S. Guittonneau, B. Fenet, *Fluorescence Quenching of 2,2´-Bithiazole-Containing Calix[4]arenes by Copper(I)*, Helv. Chim. Acta., **80**, 1229 (1997).

[9]   Q. Cao, K. Wang, Z. Hu, Q. Xu, *Syntheses of three new dervatives of 8-aminoquinoline and its applications for fluorimetric determination of copper(II),* Talanta, **47**, 921 (1998).

[10]   F. Pina, M. A. Bernardo, E. Garcia-Espana, *Fluorescent Chemosensors Containing Polyamine Receptors,* Eur. J. Inorg. Chem., 2143 (2000).

[11]   J. Yoon, N. E. Ohler, D. H. Vance, W. D Aumiller, A. W. Czarnik, *A Fluorescent Chemosensor Signaling only Hg(II) and Cu(II) in Water,* Tetrahedron Lett., **38**,: 3845 (1997).

[12]   K. A. Mitchel, R. G. Brown RG, D. Yuan, S-C. Chang, R. E. Utecht, D. E. Lewis, *A Fluorescent Sensor for Copper(II) at the sub-ppm Level*J. Photochem. and Photobiol. A: Chemistry, **115**, 157 (1998).

[13]   B. Ramachandram, A. Samanta, Modulation of Metal-Fluorophore Communication to Develop Structurally Simple Fluorescent Sensors for Transition Metal Ion, Chem. Comm., 1037 (1997).

[14]   V. Dufols, F. Ford, A. W. Czarnik, *A Long-Wavelength Fluorescent Chemodosimeter Selective for Cu(II) Ion in Water,* J. Am. Chem. Soc., **119**, 7387 (1997).

[15]   K. L. Cheng, K. Ueno, T. Imamura, *Handbook of Organic Analytical Reagents*, CRC Press, Florida (1982).

[16]   W. W. Stewart, *Synthesis of 3,6-Disulfonated 4-aminonaphtalimides*, J. Am. Chem. Soc., **103**, 7615 (1981).

[17]   W. W. Stewart, *Lucifer dyes--highly fluorescent dyes for biological tracing,* Nature 292:17-20(1981).

[18]   J. R. Lakowicz, *Principles of Fluorescence Spectroscopy – 2nd Edition*, Kluwer Academic/Plenum Publishers, New York (1999).

[19]   Mauric Eftink, in *Fluorescence Quenching: Theory and Applications* in *Topics of Fluorescence Spectroscopy –Volume 2*, J . R. Lacowicz (ed.), Plenum Press, New York (1991).

[20]   D. D. Perrin, B. Dempsey, *Buffers for pH and Metal Ion Control*, Chapman and Hall Laboratory Manuals, London (1974).

[21]   H. H. Rump, H. Krist, *Laborhandbuch für die Untersuchung von Wasser, Abwasser und Boden*, VCH, Weinheim (1987).

[22]   E. Campi, G. Ostacoli, A. Vanni, R. Casorati, *Complessi della carboidrazide con ioni meallici in soluzione acquosa,* La Ricerca Scientifica, **6**, 341 (1964)

Chapter 3

Highly Selective Optical Sensing of
Copper(II) Ions Based on Fluorescence Quenching
of Immobilized Lucifer Yellow

The development of an optical sensing scheme for the determination of copper(II) in drinking or waste water is described. It is based on static quenching of the fluorescence of Lucifer Yellow immobilized on anion exchanger particles, embedded in a hydrogel. The sensing membrane allows the determination of copper(II) in the 0.01 µM (0.63 mg/l) to 100 µM (6300 mg/l) concentration range with an outstanding high selectivity. The change in fluorescence on exposure to a significant concentration of 31 µM (2000 mg/l) is 260%. The response time is concentration dependent and varies from 100 to 3 min. Selectivity was investigated by the separate solution method; mercury(II) was found to be the only interferent. The effect of pH was evaluated in the range 4.0–6.8. The application of the sensing membrane as a single shot test was demonstrated using microtiterplates for copper(II) determination in tap water samples.

3.1. Introduction

Recommended procedures for the detection of copper in solution include photometric methods, atomic absorption spectrometry (AAS), inductively coupled plasma atomic emission spectrometry (ICP-AES) and anodic stripping voltammetry (ASV) [1-3]. These methods offer good limits of detection LODs and wide linear ranges, but require expensive analytical instrumentation and are not suitable for on-line or field monitoring. Optical chemical sensors meet these requirements and can therefore be an alternative analytical tool.

A large number of optical sensing schemes for copper(II) with varying working ranges and LODs have been described. Nearly all of them are based on absorbance or reflectance measurements of immobilized colorimetric reagents. Copper(II) ions have been determined

using lipophilized zincon dissolved in a hydrogel gel membrane [4,5]. Sensor membranes containing bathocuproin immobilized on lipophilic resin [6], Nafion ion exchanger [7] or dissolved in plasticised PVC [8] have been reported, but suffer from the requirement for a reducing agent to convert copper(II) into copper(I), which is then complexed by bathocuproin. Zeltser and Bychenko used aluminon immobilized on silica gel for the determination of copper(II) in food [9]. The binding properties of lipophilized 8-hydroxyquinoline have been studied in plasticised PVC [10]. The colorimetric reagent PAN was adsorbed on Dowex 50W resin [11] or dissolved plasticised PVC [12]. Malcik *et al.* [13] reported on sensor membranes with certain immobilized coloured sequestrants on XAD-4, XAD-7 and Dowex. A few publications have dealt with fluorescent sensors, such as calcein covalently bound cellulose [14] or Rhodamine 6G electrostatically immobilized on Nafion ion exchanger [15]. Unfortunately, all of these sensing membranes suffer from being highly unspecific. Birch et al. described the selective detection of copper(II) using time-resolved fluorescence energy transfer from Rhodamine 800 entrapped in a Nafion matrix [16]. However, most optical copper sensing membranes described did not possess sufficient selectivity for copper(II).

This chapter describes the development of a novel copper(II) sensing membrane that is based on static quenching of the fluorescence of Lucifer Yellow CH (**LY**). Unlike previously described sensors, it exhibits an outstanding selectivity for copper(II). The fluorescent dye was immobilized on cellulose anion exchanger particles, embedded in a hydrophilic polymer. The features of the sensing membrane include high selectivity, large signal changes, compatible with a blue 430 nm LED and no necessity for sample pre-treatment. Additionally, the sensing membrane is capable of measuring copper(II) in the concentration range set by the official guidelines for drinking water.

3.2. Materials and Methods

3.2.1. Chemicals and Solutions

Lucifer Yellow CH dipotassium salt (**LY**) was obtained from Fluka (Buchs, Switzerland), bead-form cellulose ion exchanger (DEAE-Sephacel) from Pharmacia (Uppsala, Sweden), the polyurethane hydrogel D4 from CardioTech (Ringo, NJ, USA), ethanol from J. T. Baker (Deventer, The Netherlands), the polyester support (LS 1465585) from Goodfellow (Cambridge, UK), microtiterplates (96 wells) with a round bottom from Greiner (Frickenhausen, Germany), sodium acetate and all inorganic salts of analytical-reagent grade from Merck (Darmstadt, Germany), acetic acid from Roth (Karlsruhe, Germany) and 3-(*N*-morpholino)propanesulfonic acid and its sodium salt (MOPS) from Sigma (Vienna, Austria).

Aqueous solutions were prepared from doubly distilled water. Stock standard solutions of all heavy metal ions were prepared by dissolving the respective amount of the nitrate salt in 10 mM buffer solution. Buffers were prepared and controlled as described in chapter 2.3.3.

The determination of the copper(II) content in tap water was performed by filling the wells of the coated microtiterplate with 180 ml of sample solution and adding 20 ml of 100 mM MOPS buffer solution (pH 6.8) to each well. Further, the wells were filled with solutions containing 0.1, 0.5, 1, 5, 10 and 100 µM copper(II) buffered to pH 6.8. In order to obtain equilibrium signals, the microtiterplate was measured for 3h every 10 min. The mean value and the standard deviation were calculated from the measured values of at least four wells.

3.2.2. Membrane Preparation

3.2.2.1. Preparation of LY-Cellulose Beads

A 500 mg amount of DEAE-Sephacel cellulose particles was added to 10 ml of a solution containing 1 mM **LY** and stirred for at least 24 h. The particles were washed first with water until the filtrate showed no yellow coloration, then three times with dry ethanol. The highly fluorescent yellow cellulose was vacuum dried in a desiccator, then powdered in a mortar.

3.2.2.2. Preparation of Sensing Membranes

A cocktail was prepared by dissolving D4 polymer and the **LY**–cellulose beads in water and ethanol. The compositions of the cocktails are listed in Table 3.1. The mixture was stirred overnight and spread on a dust-free polyester support using a home-made knife coating

device, as shown in the schematic view in Figure 3.1, having a spacer distance of 60 µm. After evaporation of the solvent, the membranes were stored in buffer solution. The thickness of the membranes **M1** and **M2** was calculated from the amounts of membrane components applied as approximately 4 and 1.5 µm, respectively.

3.2.2.3. Preparation of Microtiterplates

The bottoms of the wells were coated with the sensing membrane by pipetting 2 µl of cocktail **M3** into each well. After drying overnight the microtiterplates were ready for use.

Table 3.1. *Composition of the membranes*

	LY-beads/mg **(%, w/w)**[a]	**D4/mg** **(%, w/w)**	**Ethanol/mg** **(%, w/w)**	**Water/mg** **(%, w/w)**
M1	20 (1.9)	50 (4.9)	860 (84.1)	93 (9.1)
M2	20 (1)	20 (1)	1800 (88.2)	200 (9.8)
M3	10 (1.3)	25 (3.3)	650 (86.5)	67 (8.9)

[a] per unit weight matrix
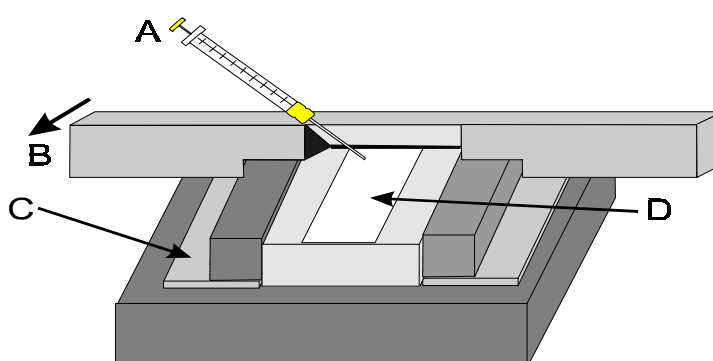
Fig. 3.1. *Schematic view of the knife coating device, with A= pipette containing the membrane cocktail, B = coating device, C= spacer and D= polyester support (Mylar)*

3.2.3.   Instrumentation and Measurements

3.2.3.1. Fluorescence Measurements for Membrane Characterization

Fluorescence excitation and emission spectra and the response curve were acquired with an Aminco Bowman Series 2 luminescence spectrometer from SLM-Aminco (Rochester, NY, USA) as described in chapter 2.3.2.1. The excitation light from the source passed through a monochromator and was focused on one branch of a bifurcated fiber bundle of randomized glass fibres (diameter 6 mm). The light was carried outside the spectrometer to the sensing membrane, fixed in a laboratory-made flow-through cell, as shown in Figure 3.2. The emitted light was guided by the other branch of the fibre bundle through a monochromator and the photomultiplier tube (PMT) inside the spectrometer.

Characterization of the membranes was carried out by passing solutions of known pH and analyte concentrations at a rate of 1 ml/min through the flow cell. The sample solutions were transported by a Minipuls-3 peristaltic pump (Gilson, Villiers-le-Bel, France) via silicone-rubber tubing of 1.0 mm i. d. from the storage bottle through the measuring cell.

3.2.3.2. Fluorescence Measurements of Sensor Integrated Microtiterplates

Fluorescence measurements on the microtiterplates were carried out using an Ascent Fluoroscan microtiterplate reader from Labsystems (Helsinki, Finland) equipped with excitation and emission filters at wavelengths of 420 and 530 nm. A quartz halogen lamp was used as the light source. The instrument is shown in chapter 2.3.2.3. The signal was referenced by measuring the fluorescence of the coated wells before (F_{ref}) and after (F) filling the wells with buffered solutions containing copper(II) at various concentrations.
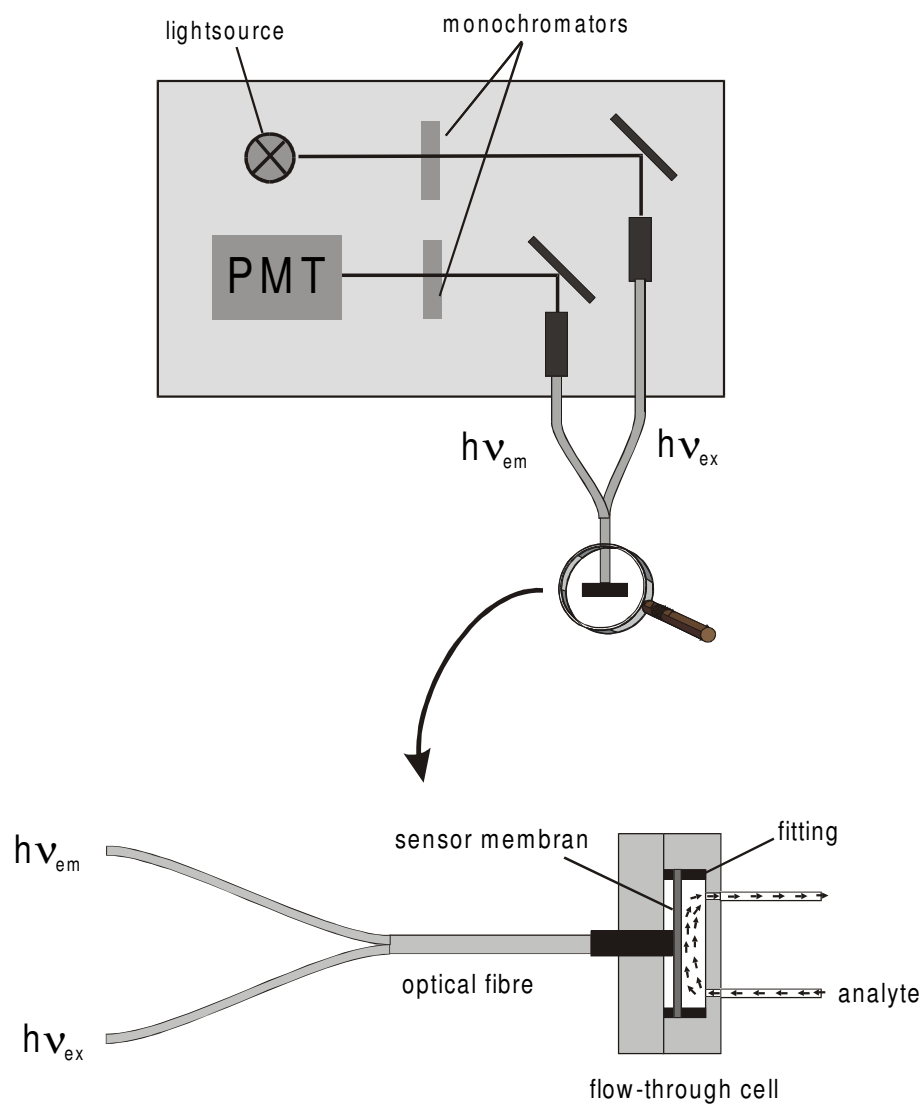
Fig. 3.2: Schematic representation of the measuring set-up.

3.3. Results and Discussion

3.3.1. Choice of Indicator

A variety of fluorescent reagents for the determination of heavy metals, in particular copper ions, have been described in the literature [17,18]. For application in sensors, these probes need to meet the following criteria: (a) a sufficiently large change in the fluorescence (enhancement or quenching) in solution, (b) an excitation maximum higher than 420 nm to allow the use of blue LEDs as stable light sources, (c) a large Stokes shift, (d) high fluorescence quantum yields, (e) high photostability and (f) ease of immobilization.

LY was found to fulfill many of these requirements. It is widely used for staining neurons [19] and its exceptionally high selectivity for copper(II) was discussed in the previous chapter. **LY** is commercially available and does not require any chemical modification for the application presented here. **LY** absorbs at 430 nm with an emission maximum at 535 nm, hence it can be excited with a blue 430 nm LED. The compound has a quantum yield of about 0.21 and shows excellent photostability. Neither the absorbance nor the emission maxima are affected by pH changes between 2 and 9 [21].

3.3.2. Immobilization

The dye was electrostatically immobilized on a cellulose anion exchanger via its two aromatic sulfonate groups. The protonated, positively charged diethylamino groups of the cellulose bind the negatively charged indicator. The cellulose material was chosen among other ion-exchange materials because of its high ion-exchange capacity and homogeneous particle size. The strong ion exchanger used offers an effortless route to immobilization of the indicator by stirring the material in the indicator solution. After immobilization, the highly fluorescent particles were embedded in D4 hydrogel. The polymeric support based on polyurethane is hydrophilic and ion permeable and is commonly used for ion sensors [21]. Since all the materials chosen show high physical and chemical stability, good longterm stability for the sensing membrane was achieved.

Other attempts for immobilization were binding **LY** covalently to polymer matrix. **LY** contains two amino-groups for a potential linking of the molecule to a carboxylic group of a matrix, namely one part of the carbohydrazide group and an aromatic (Figure 3.2) . Thus, **LY** was immobilized via an one-step carbodiimide coupling method [22] to carboxy-cellulose.

Membranes containing **LY** bound to cellulose were highly fluorescent and showed no signal drift, but a response was observed for concentration of >100 µM only.

3.3.3. Membrane characteristics

The fluorescence spectra of immobilized **LY** differ from those in solution by a blue shift in excitation and red shift in emission of about 10 nm due to the more lipophilic environment of the dye. On exposure to solutions containing copper(II), membrane **M1** undergoes a strong decrease in fluorescence intensity. The excitation and emission spectra of **M1** in the presence of 0.1 and 500 µM copper(II) are depicted in Figure 3.3. The copper(II) ions penetrate the membrane, come into contact with the immobilized **LY** and subsequently the fluorescence intensity is quenched.
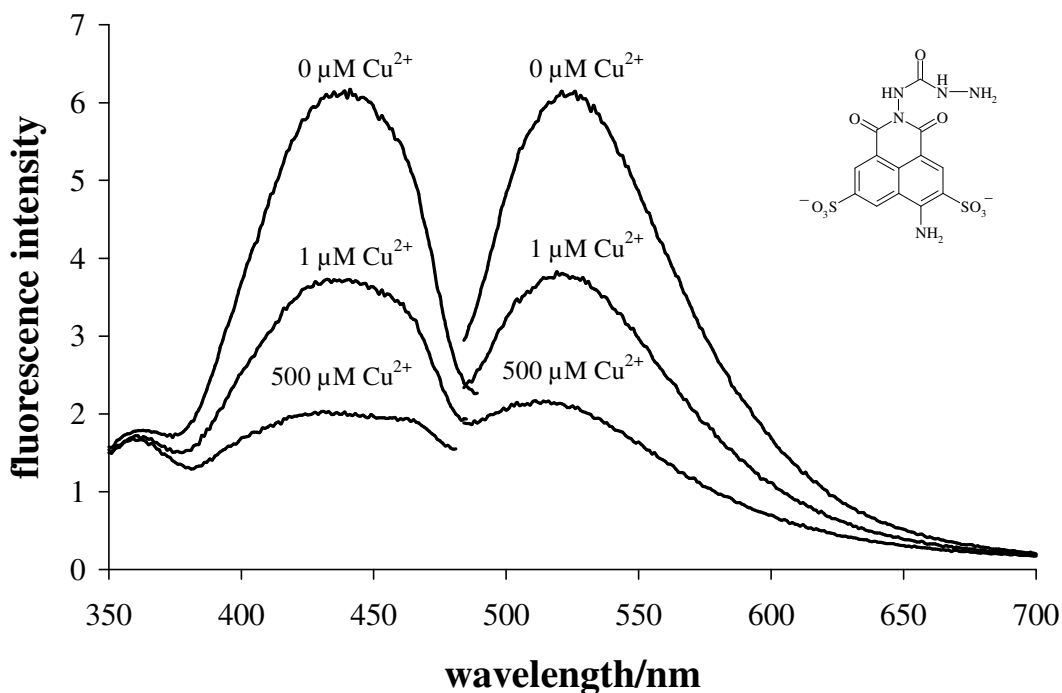
Fig. 3.3. *Fluorescence excitation and emission spectra of **M1** when exposed to 0, 1 and 500 µM Cu^{2+}.*

The response curve of **M1** exposed to various copper(II) concentrations and the respective calibration plot is illustrated in Figure 3.4. **M1** responds to 1, 5, 10, 50 and 100 µM copper(II) by changing the fluorescence by -38, -49, -54, -62 and -64%, respectively. A signal change of -60% was found for the recommended guideline concentration of 2 mg/l (31µM). The dynamic range of the expose to copper(II) is 0.1- 100 µM. This wide range can be explained by the different microenvironment of immobilized **LY** in the membrane compared with the

response of free **LY** to copper(II) in solution. Furthermore, a signal change of 10% was determined for a concentration of 0.01 µM copper(II). Owing to the long response time t_{90} (time to reach 90% of the equilibrium signal) of about 100 min, this was the lowest concentration investigated. The t_{90} for concentrations of 10–500 µM copper(II) is in the range 2–3 min, which is of same order as the time needed for exchanging the sample in the flow-through cell. At lower concentrations the response time increases to 10 min for 5 µM and 30 min for 1 µM copper(II). The source of the slow response at low concentrations is attributed to several reasons. On the one hand, the response is limited by diffusion of ionic copper(II). This was examined by reducing the membrane thickness in membrane **M2**. As a result, the response time is shortened to < 5 min, but slight leaching of the indicator was observed, resulting in a signal drift of ~ 5% per hour. On the other hand, for extremely dilute solutions the mass transfer from the bulk of the sample to the membrane interface becomes rate-limiting, which was described by Bakker et al. for optodes [23] and Morf et al. for electrodes [24].
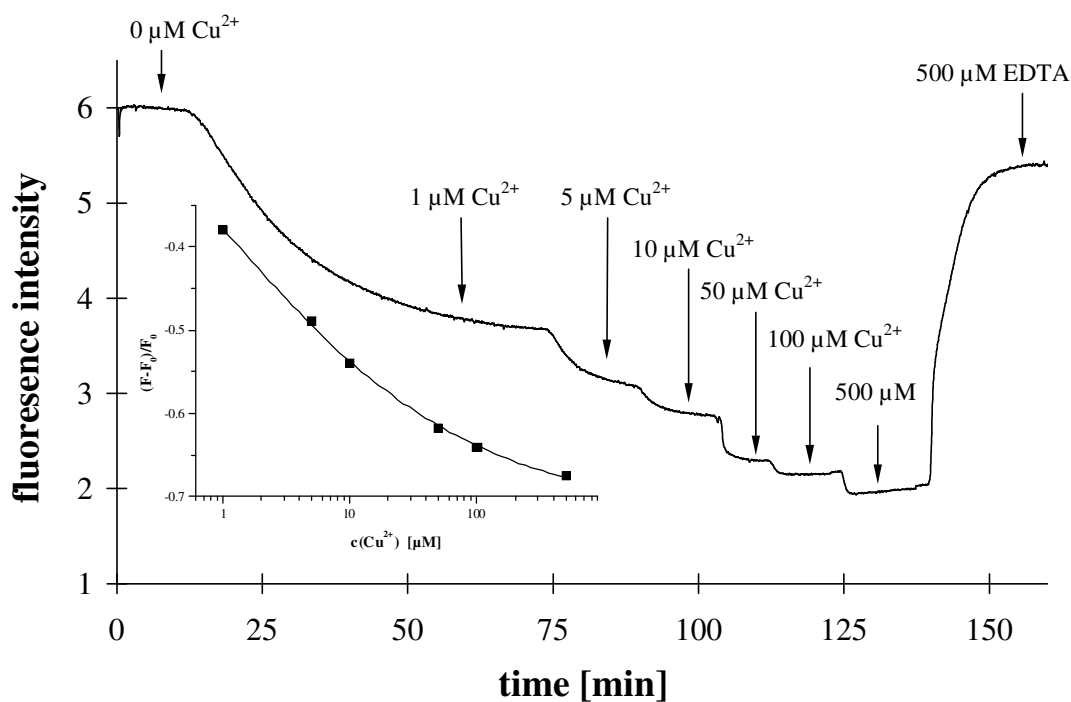
Fig 3.4. *Response curve and calibration plot of sensing membrane M1 at various copper(II) concentrations. Solutions were buffered to pH 6.0 and the ionic strength was adjusted to 10 mM by NaNO₃.*

3.3.4. Selectivity

Sensors for heavy metals often suffer from unspecific binding. This is in complete contrast to the sensing membrane presented here, which is highly selective for copper(II). In the previous chapter **LY** was shown to be a highly selective reagent, with negligible interference from mercury(II), iron(III), cobalt(II) and nickel(II). In comparison, sensing membranes incorporating immobilized **LY** show an improved selectivity for copper(II). The cross-sensitivities of membranes **M2** for mercury(II), iron(III), cobalt(II), nickel(II), cadmium(II), zinc(II) and lead(II) were investigated in concentrations up to 1000 µM at pH 5. Contrary to our expectations, no interference was found for iron(III), cobalt(II) or nickel(II). The only interferent found was mercury(II), which is also the strongest interferent of **LY** not immobilized. Fig. 3.5 displays the relative signal changes caused by mercury(II) and copper(II). The selectivity coefficient relative to copper(II) for a 10 µM ion solution, determined by the separate solution method (SSM), $\log K_{Cu(II)}$, was found to be 0.97. However, the concentration range where interference occurs is far from levels that can be expected in real samples. Other heavy metal ions such as cadmium(II), zinc(II) or lead(II) did not influence the signal intensity.
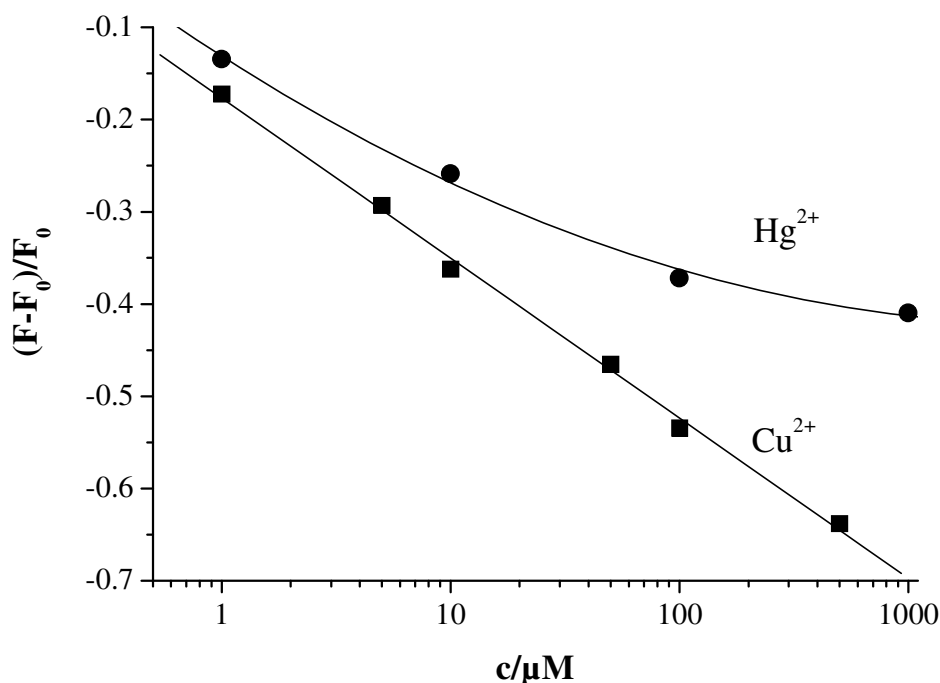
Fig. 3.5. *Calibration plot for membrane M2 for copper(II) and mercury(II) at pH 5 and a constant ionic strength of 10 mM.*

3.3.5. Effect of pH

Although the absorbance and emission spectra of **LY** are not affected by pH in the range 2–9, the quenching of the fluorescence by copper(II) in solution is strongly pH dependent as the sensitivity is increased from pH 3 to 7 (see chapter 2.4.2). The carbohydrazide group is the complexing part of the dye molecule and binding of copper(II) is hindered in solutions of high acidity owing to an acid–base reaction of the terminal nitrogen atom. Therefore, quenching at low pH values is less efficient. A similar behavior is observed for immobilized **LY**. The calibration plots for membrane **M2** for the determination of copper(II) in buffers of varying pH values are shown in Fig. 3.6. The calibration plots for pH 4.0 and 5.0 show superior linearity in the concentration range shown ($r > 0.98$, $s > 0.015$), while the plots for pH 5.8 and 6.8 display parts of a typical sigmoidal shape. Note that linearity is only obtained in the investigated concentration range. The relative signal changes decrease on going to higher acidity with a substantial change between pH 5.0 and 5.8. The observed higher quenching efficiency at higher pH agrees with the results found for **LY** solution, whereby the influence of pH can be interpreted as an acid–base reaction of the hydrazide group.
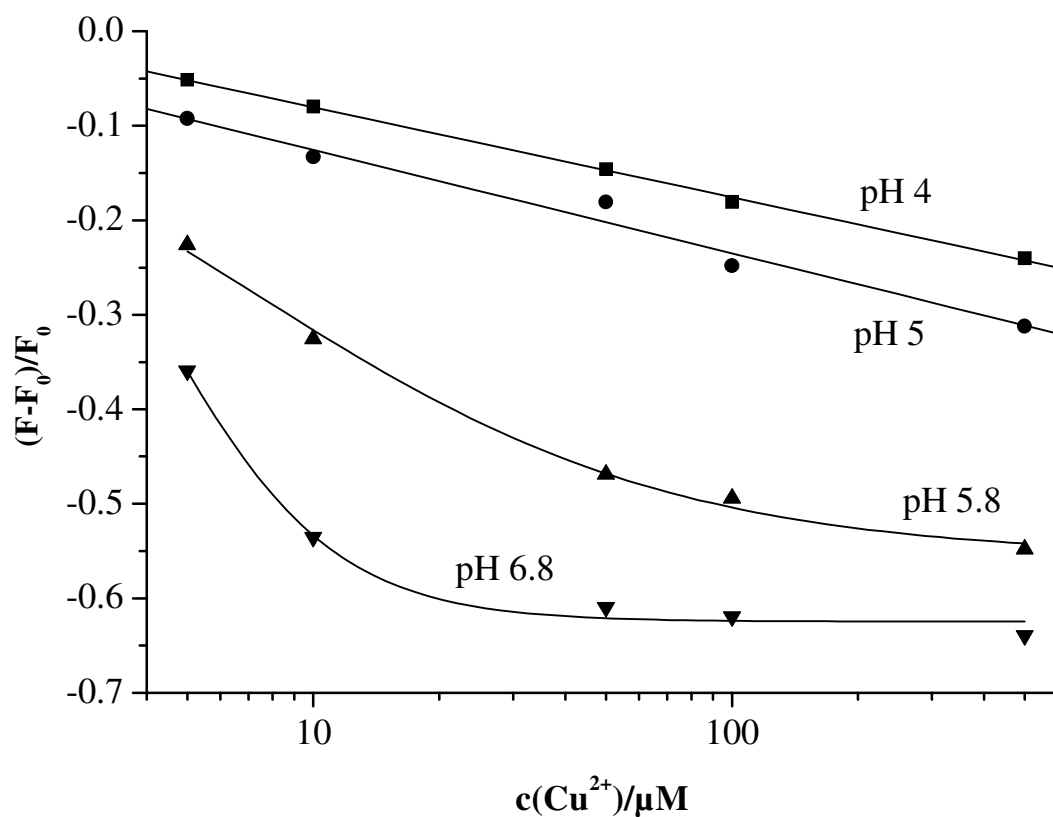
Fig. 3.6. *Calibration plot for membrane **M1** at various pH values.*

3.3.6. Regeneration of the membrane

The response of membrane M1 to copper(II) is not fully reversible, but can be regenerated with EDTA solution. The membrane was consecutively rinsed with buffer, 100 μM copper(II) and 100 µM EDTA within three cycles. After exposure to EDTA and buffer the signal reached 94–96% of the original level in every cycle. The decrease in signal can be attributed to copper(II) remaining in the membrane, strongly bound to **LY** or to **LY** exchanged by negatively charged EDTA on the cationic cellulose. On exposure to a solution containing 100 µM copper(II) the signal was found to vary by ±4.5%.

3.3.7. Determination of copper(II) in tap water

The sensing membrane was applied to test real samples and to compare the results with those given by the AAS reference method. The bottoms of 96-well microtitre plates were coated with a layer containing hydrogel and immobilized **LY**. Real samples were taken from the hot and cold water supplies through copper pipes in a domestic household. A high pH of 8.2 was found, which made acidification necessary. This was achieved by adding buffer solution (pH 6.8) to a fixed volume of tap water sample. The content of copper(II) was calculated from the calibration plot shown in Fig. 3.7. The results obtained are given in Table 3.2 and are in good agreement with data obtained by the reference method. Note that this method is able to measure the amount of free copper(II). This has to be taken into consideration when the results are compared with those given by the standard method, where the total amount is determined. However, chelating molecules are not expected to be present in the investigated tap water samples.

Table 3.2. *Copper(II) determination in tap water samples by applying sensing material on microtitre plates and comparison with AAS reference method.*

	Copper(II) content/μM (µg/l)		
Sample no.	*Value from calibration plot* [a]	*Corrected value* [b]	*GF-AAS*
1	1.1	1.0 (64)	1.07 (68.0)
2	2.4	2.1 (133)	2.2 (139.8)
3	0.8	0.7 (44)	0.69 (43.8)

[a] Value for stable signals after 180 min. [b] Value taking into consideration dilution by the buffer
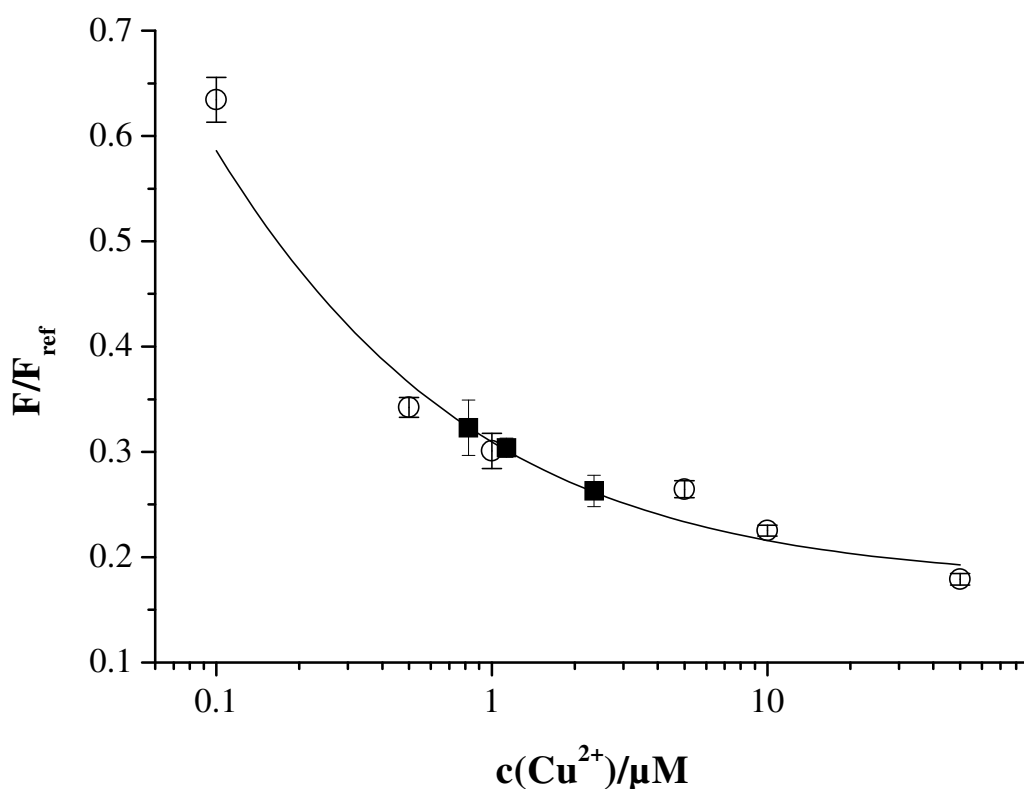
Fig. 3.7. *Calibration plot (circles) and determined Cu(II) values for tap water samples (squares). F_{ref} is the fluorescence measure for the empty wells. F is the fluorescence when wells were filled with sample solution. Average values and error bars were calculated from at least four measurements.*

3.4. Conclusion

A sensing membrane has been presented for the determination of copper(II) in weakly acidic solutions based on static quenching of **LY**. The method is advantageous in displaying an outstanding high selectivity for copper(II) and possessing a fully LED-compatible excitation maximum. The sensing spots are easily produced by immobilizing **LY** on anion exchanger beads, incorporated in a hydrogel. The response to copper(II) extends over the $0.01-100$ μM concentration range and thus matches perfectly the guidelines set by the WHO and the EC. The response time is of the order of a few minutes for high concentrations and longer for low concentrations. The sensing membrane can be regenerated with EDTA with a slight signal decrease. Consequently, the application of the proposed material for use in single shot tests seems to be more practical, as was successfully demonstrated by the determination of the

copper(II) content in tap water samples. In order to improve reproducibility and accuracy, the dual lifetime reference (DLR) scheme was applied and is presented in the next chapter.

3.5. References

[1]   E. Merian, ***Metals and Their Compounds in the Environmen**t*, VCH, Weinheim (1991).

[2]   W. Fresenius, K. E. Quentin, W. Schneider, ***Water Analysis***, Springer, Berlin (1988).

[3]   U. Förstner, G. T. Wittmann, ***Metal Pollution in the Aquatic Environment***, Springer, Berlin (1981).

[4]   I. Oehme, B. Prokes, I. Murkovic, T. Werner, I. Klimant, O. S. Wolfbeis*, **LED-compatible copper(II)-selective optrode membrane based on lipophilized Zincon***, Fresenius J. Anal. Chem., **350**, 563 (1994).

[5]   I. Oehme, S. Prattes, O. S. Wolfbeis, G. J. Mohr, ***The effect of polymeric supports and methods of immobilization on the performance of an optical copper(II)-sensitive membrane based on the colourimetric reagent Zincon,*** Talanta, **47**, 595 (1998).

[6]   A. M. Ervin, K. J. Ewing, R. A. Lamontagne, I. D. Aggarwal and D. A. Rowley, ***Development of a fiber-optic sensor for trace metal detection in aqueous environments***, Applied Optics, **32,** 4287 (1993).

[7]   A. M. Ervin, K. J. Ewing, G. Nau, D. A. Rowley, R. A. Lamontagne, I. D. Aggarwal, ***Investigation of a robust flow through Cu(I) sensor using 2,9 dimethyl-4,7-diphenyl-1,10-phenanthroline immobilized into a Nafion film,*** Sens. Act., **B 53,** 104 (1998).

[8]   T. Saito, ***Sensing of Trace Copper Ion by Solid Phase Extraction-Spectrophotometry Using a Poly(Vinyl Chloride) Membrane Containing Bathocuproin***, Talanta, **41,** 811 (1994).

[9]   L. E. Zeltser, A. V. Bychenko, ***Immobilized Aluminon as sensitive layer of a copper optical sensor***, Zh. Anal. Khim., **481**, 659 (1993).

[10] E. Wang, K. Ohashi, S. Kamata, ***Optical Sensing Properties of PVC Membrane incoporating lipophilic 8-hydroxchinoline derivative***, Chem. Lett., 939 (1992).

[11] F. Lazaro, M. D. L. de Castro, M. Valcarcel, ***Integrated reaction/spectrophotometric detection in unsegmented flow systems***, Anal. Chim. Acta, **214,** 217 (1988).

[12] C. Sanchez-Pedeno, J. A. Ortuno, M. I. Albero, M. S. Garcia, *A new procedure for the construction of flow-through optodes. Application to determination of Copper*, Fresenius J. Anal. Chem., **366**, 811 (2000).

[13] N. Malcik, P. Caglar, R. Narayanaswamy, *Investigations into optical sensing of cupric ions using several immobilized reagents*, Quím. Anal., **19,** 94 (2000).

[14] L.A. Saari, W.R. Seitz, *Immobilized Calcein for metal ion preconcentration*, Anal. Chem., **56**, 810 (1984).

[15] F. V. Bright, G. E. Poirer, G. M. Hieftje, *A new ion sensor based on fiber optics*, Talanta, 113 (1988).

[16] D. J. S. Birch, O. J. Rolinski, D. Hatrick, *Fluorsecence lifetime sensor of copper ions in water*, Rev. Sci. Instrum., **67(8)**, 2732 (1996).

[17] V. Dujols, F. Ford, A. W. Czarnik, *A long-wavelength fluorescent chemodosimeter selective for Cu(II) ion in water*, J. Am. Chem. Soc., **119**, 7387 (1997).

[18] G. De Santis, L. Fabrizzi, M. Licchelli, C. Mangano, D. Sacchi, N. Sardone, *A fluorescent chemosensor for the copper(II) ion*, Inorgan. Chim. Acta., **25, 7**69 (1997).

[19] W. W. Stewart, *Lucifer dyes-highly fluorescent dyes for biological tracing*, Nature, **292,** 17 (1981).

[20] W. W. Stewart, *Synthesis of 3,6-Disulfonated 4-aminonaphtalimides*, J. Am. Chem. Soc., **103**, 7615 (1981).

[21] C. Krause, T. Werner, O. S. Wolfbeis, *Multilayer Potassium Sensor Based on Solid-State Coextraction*, Anal. Sci., **14**, 163 (1998).

[22] D. G. Hoare, D. E. Koshland, *Procedure for the selective modification of carboxyl groups in proteins*, J. Amer. Chem. Soc., **88**, 2057 (1966).

[23] E. Bakker, P. Bühlmann, E. Pretsch, *Carrier Based Ion-Selective Electrodes and Bulk Optodes, 1. General Characteristics*, Chem. Rev., **97**, 3083 (1997).

[24] W. E. Morf, E. Lindner, W. Simon, *Theoretical Treatment of the Dynamic Response of Ion-Selective Membrane Electrodes,* Anal. Chem., **47**, 1596 (1975).

Chapter 4

Dual Lifetime Referenced (DLR) Optical Sensor Membrane for the Determination of Copper(II) Ions

A sensor membrane has been developed for the determination of copper(II) ions that displays excellent performance due to internal referencing of luminescence intensities. The applied sensing scheme (dual lifetime referencing) makes use of the indicator lucifer yellow and an inert reference luminophore (a ruthenium complex entrapped in poly(acrylonitrile) beads). Both are contained in a hydrogel matrix. The copper-dependent fluorescence intensity change of lucifer yellow can be converted in either a phase shift or time dependent parameter. The sensing membrane is capable of determining copper(II) with an outstanding high selectivity over a dynamic range between 5 and 1000 µM in neutral or weakly acidic conditions. The advantages of the referencing method over intensity based measurements was demonstrated by the measurement of turbid solutions. The scheme was also applied to 2-dimensional measurements in the time domain. Sensor-integrated microtiterplates were imaged with a CCD-camera gated with square pulses in the microsecond range

4.1. Introduction

In the previous chapter a highly selective sensing membrane for coppper(II) based on fluorescence intensity measurements was described. In the following section this scheme was extended by a new and general logic which enables the measurements in the frequency- or time-domain. This new scheme uses a couple of luminophores with different decay times and similar excitation spectra and is referred to as Dual Lifetime Referencing (DLR) [1-3].

The recent years have seen a large number of publications dealing with optical copper sensing. Most of them are based on absorbance or reflectance measurements of immobilized colorimetric reagents in various matrices including lipophilized zincon, aluminon, lipophilized 8-hydroxychinoline, bathocuproine, or various coloured sequestrants [4-6].

Although fluorescence is advantageous over absorbance and reflectance in terms of sensitivity, only few fluorescent sensors are published. Calcein was covalently bound to cellulose [7] or rhodamine 6G electrostatically to Nafion ion exchanger [8], but suffer from being highly unspecific. In addition, a fluorescent copper sensor with noteable high selectivity was presented in the previous chapter. However, all these sensors use fluorescence intensity as the analytical information. The measurement of intensity is simple in terms of instrumentation, but its accuracy is often compromised by drifts in the opto-electronic setup, loss of light in the optical path, and variations in the optical properties of sample e. g. turbidity or coloration. Such adverse effects can be partially overcome by applying referencing methods to achieve precise measurements. Among those, the ratio of the intensities at two wavelengths (ratiometry) is commonly used [9]. In this approach, the fluorescence intensity of a single fluorophore is measured at two or more wavelengths. Alternatively, the decay time can be an attractive parameter, because it is virtually independent of the overall signal intensity. Birch et al. describe the selective detection of copper(II) using time-resolved fluorescence energy transfer from rhodamine 800 encapsulated in a nafion matrix [10] but the method requires complicated and expensive instrumentation due to the short decay time (2 ns) of the dye. For this reason luminophores with longer life-times are favorable [11].

A recently published method allows the conversion of fluorescence intensity information into either a phase-shift or time-dependent parameter by using a couple of luminophores having different decay times [3,12-14]. In this chapter, the application of this scheme to a sensing membrane for copper(II) is described. Specifically, the highly selective indicator **LY**, immobilized on cellulose particles, was combined with phosphorescent inert beads containing the ruthenium luminophore Ru(dpp), both contained in a polyurethane hydrogel. The determination of copper(II) was performed in the frequency domain as well as the time-domain. The new sensors show outstanding selectivity and are capable of measuring copper(II) in the concentration range set by the official guideline for drinking water. The benefits of the reference method for the measurement of real samples was demonstrated by turbid solutions. Additionally, time-resolved imaging was applied by mapping microtiterplate integrated sensor spots with a CCD-camera.

4.2. Materials and Methods

4.2.1. Chemicals and Solutions

Lucifer Yellow CH dipotassium salt (**LY**) was obtained from Fluka (Buchs, Switzerland). The bead-formed cellulose ion exchanger (DEAE Sephacel) was from Pharmacia (Uppsala, Sweden). The reference particles PS100 (Ru(dpp)) was a gift from Presens (Regensburg, Germany). The polyurethane hydrogel D4 was obtained from CardioTech (Ringo, NJ). The polyester support (prod. No. LS 1465585) was obtained from Goodfellow (Cambridge, UK). Microtiterplates (96 wells) were obtained from Greiner (Frickenhausen, Germany). All inorganic salts and sodium acetate were of analytical grade and obtained from Merck (Darmstadt, Germany) or Fluka (Buchs, Switzerland). 3-[N-Morpholino]-propane sulfonic acid and the respective sodium salt (MOPS) were obtained from Sigma (Vienna, Austria). Titanium(IV)oxide was from Aldrich (Steinheim, Germany).

Aqueous solutions were prepared from double-distilled water. Stock solutions for all heavy metal ions were prepared by dissolving the respective amount of nitrate salt in 10 mM buffer solution. Turbid solutions were generated suspending 10 mg TiO_2 in 100 ml buffer. Buffers were prepared and controlled as described in chapter 2.3.3.

4.2.2. Membrane Preparation

4.2.2.1. *Preparation of LY-Cellulose Beads*

A 500 mg amount of DEAE-Sephacel cellulose particles was added to 10 ml of a solution containing 1 mM **LY** and stirred for at least 24 h. The particles were washed first with water until the filtrate showed no yellow coloration, then three times with dry ethanol. The highly fluorescent yellow cellulose was vacuum dried in a desiccator, then powdered in a mortar.

4.2.2.2. *Preparation of Sensing Membranes*

A cocktail was prepared by suspending **LY**/cellulose particles, reference particles PS100 and D4 polymer in water and ethanol. The mixture was stirred overnight and spread on a dust-free polyester support using a knife having a spacer distance of 120 µm (see chapter 3.2.2.2). After evaporation of the solvent, the membranes were stored in buffer solution. The compositions of the cocktails and the estimated membrane thickness are listed in Table 5.1. A cross-section of the membranes is schematically shown in Figure 5.1. Sensor spots of membrane **M3** (∅ 4

mm) were placed on the bottom of the wells of microtiterplates for the performance of imaging measurements.

Table 5.1. Composition of the sensing membranes

membrane	LY-beads /mg (w/w)	PS100 /mg (w/w)	D4 /mg (w/w)	Ethanol /mg (w/w)	Water /mg (w/w)	Thickness /μm
M1	9.75 (0.9)	9.8 (0.9)	20 (1.8)	936 (86.6)	106 (9.8)	4.5
M2	10 (1)	5 (0.5)	15 (1.5)	841.5 (86.4)	103.5 (10.6)	3.5
M3	24.6 2.6	12.3 1.3	53 5.7	757.7 81.1	87 9.3	11.5
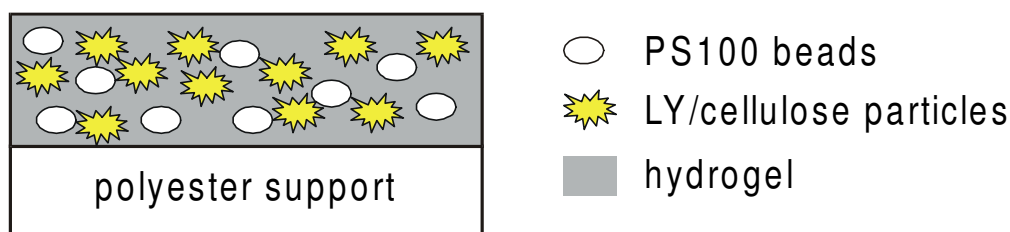
Fig. 5.1. *Cross-section of membrane M1-M3 (not to scale). The polyester support serves as an inert and optically transparent mechanical support.*

4.2.3. Instrumentation and Measurements

4.2.3.1. Fluorescence Measurements

Fluorescence excitation and emission spectra and the response curve were acquired with an Aminco Bowman Series 2 luminescence spectrometer from SLM-Aminco (Rochester, NY, USA) as described in chapter 2.3.2.1.

4.2.3.2. Fluorescence Measurements of Sensor Integrated Microtiterplates

Fluorescence measurements on the microtiterplates were carried out using an Ascent Fluoroscan microplate reader from Labsystems (Helsinki, Finland) equipped with excitation and emission filters at wavelengths of 420 and 530 nm. A quartz halogen lamp was used as the light source. The instrument is shown in chapter 2.3.2.3. The signal was referenced by the ratio of the fluorescence fluorescence intensity measured at wavelengths of 530 nm and 620 nm, when excited at 420 nm.

4.2.3.3. Phosphorescence Decay Time Measurements

Phase angle measurements were performed using a system recently described [14]. A dual-phase lock-in amplifier (DSP 830; Stanford Research Inc., see Figure 5.2 A) was used for sine-wave modulation of the LED at a frequency of 45 kHz and for detection. The optical system consisted of a blue LED (383 UBC; λ_{max} 430 nm; Roithner, Vienna, Austria) equipped with a blue band-pass filter (BG12; Schott, Mainz, Germany), a bifurcated glass fiber bundle of 2 mm i. d. and a red-sensitive PMT module (H5701-02; Hamamatsu; Herrsching, Germany) equipped with a long-pass filter (OG 530; Schott; Mainz, Germany). The fiber-bundle was placed on a flow-through cell as shown in figure 5.2 B.

Characterization of the membranes was carried out by passing solutions of known pH and analyte concentrations at a rate of 1 ml/min through the cell. The sample solutions were transported by a Minipuls-3 peristaltic pump (Gilson, Villiers-le-Bel, France) via silicone tubings of 1.0 mm i. d. from the storage bottle to the flow-through cell and then to the waste.

(A)   **(B)**
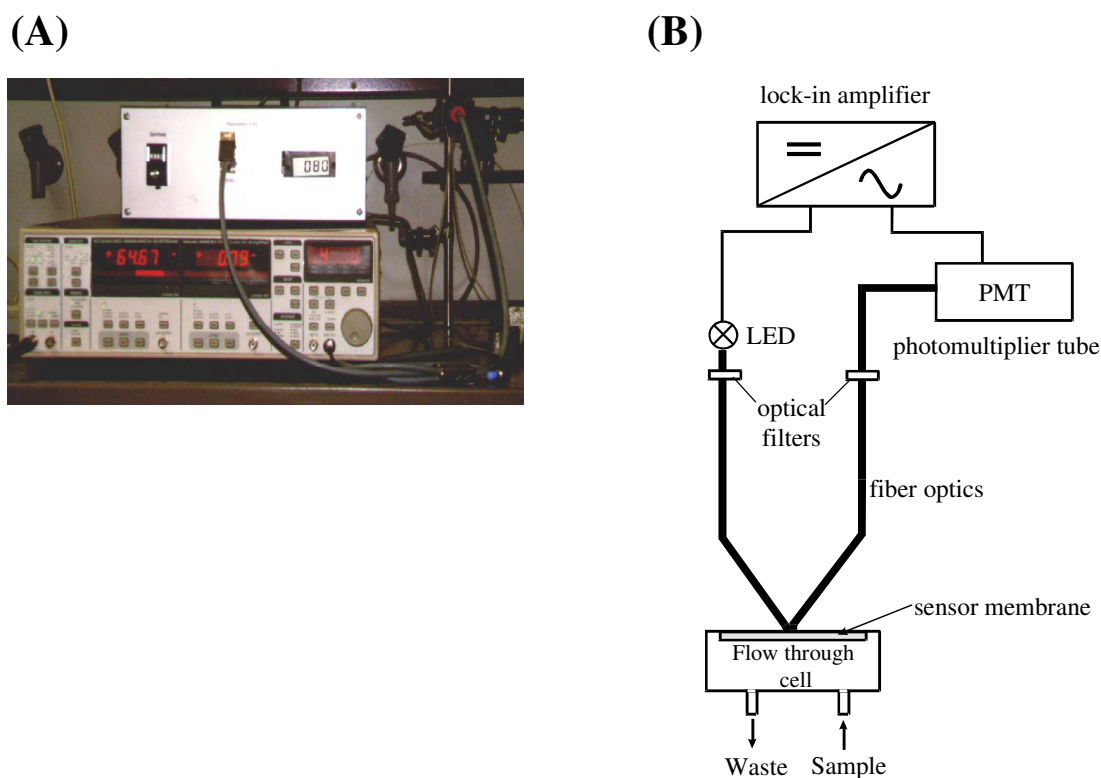
Fig. 5.2. (A) Lock-in amplifier; (B) Optical arrangement for decay time measurements

4.2.3.4. Imaging Set-up

Time-resolved imaging was performed as described in chapter 5.3.4. The set-up comprises a self-developed pulsable LED array, consisting of 12 blue LEDs (383 UBC, λ_{max}= 430 nm) as the light source, a blue short-pass filter (BG12; Schott, Mainz, Germany), a long-pass filter (OG515; Schott; Mainz, Germany), a fast gate-able CCD-camera (SensiMod; PCO; Kelheim, Germany), and a pulse generator for triggering the camera and LEDs. A personal computer controls the components and visualises the results. The camera has a half-in monochrome lens-on-chip CCD sensor with 640x480 pixels and a 12-bit resolution which is equivalent to 4096 greyscale values.

4.2.4. Dual lifetime Referencing (DLR)

The measurement of luminescence decay time is favorable regarding the adverse effects of intensity measurement mentioned above. Therefore the recently reported DLR scheme was

applied. This new scheme takes advantage of measuring a phase shift Φ of a couple of luminophores by the phase modulation (frequency-domain) method [3, 14]. One of the luminophores, referred to as the indicator, has a nanosecond decay time, the other (acting as the reference) has a decay time in the µs range. The two luminophores have similar spectral properties so that they can be excited at the same wavelength and their emission can be detected using the same detector. The phase shift Φ_m of the overall luminescence depends on the ratio of intensities of the reference luminophore and the indicator dye. The reference luminophore gives a constant background signal (ref) while the fluorescence of the indicator (ind) depends on the analyte concentration (see Figure 5.3). Therefore, the average phase shift Φ_m directly reflects the intensity of the indicator dye and, consequently, the analyte concentration. The linear relation between $\cot(\Phi_m)$ and the ratio of A_{ind}/A_{rer} is given by equation 5.1:

$$\cot \Phi_m = \cot \Phi_{ref} + \frac{1}{\sin \Phi_{ref}} \cdot \frac{A_{ind}}{A_{ref}}$$

4.1

where A is the amplitude of either indicator (ind) or luminophore (ref), and Φ is the phase angle of either the overall signal (m) or the luminophore (ref).
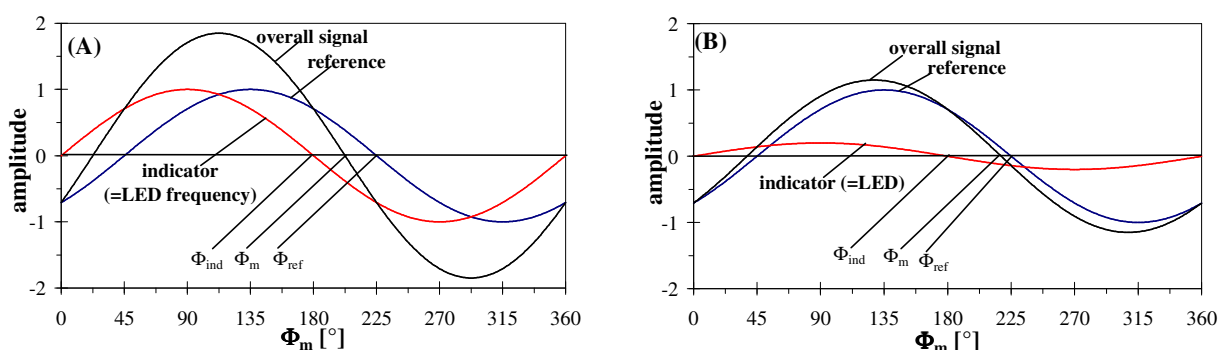
Fig. 5.3. Phase shift of the overall luminescence (Φ_m), the reference (Φ_{ref}) and the indicator (Φ_{ind}). Fluorescence of the indicator in (A) absence and (B) presence of the analyte.

4.2.5. Time domain DLR (t-DLR) imaging

Two-dimensional measurements were applied making use of the previously reported t-DLR scheme [13]. In this scheme, the fluorescence intensity information is converted into a time-dependent parameter. Similar to the DLR-scheme (see above), two luminophores with largely

different decay time are used. The luminescence is periodically excited by squared pulses of light. Two images are recorded during the measuring cycle. The first is recorded during excitation and reflects the luminescence of both the reference and the indicator. The second image which is measured after a certain delay (after switching off the light source), is solely caused by the long-lived (µs) reference. The ratio of the two recorded images displays a referenced intensity distribution. The ratio can be described by the following relationship:

$$R = \frac{A_{REF-exc} + A_{IND}}{A_{REF-em}} \qquad\qquad 4.2$$

$A_{REF-exc}$ and A_{IND} are the signal intensities of the reference and the indicator in the excitation window respectively. A_{REF-em} is the signal intensity of the reference in the emission window. A more detailed description of this elegant way to reference out inhomogeneities of the excitation light-field and the indicator distribution in the sensing membrane is given in chapter 5.2.

4.3. Results and Discussion

4.3.1. Choice of Materials

The application of DLR in fluorescence sensing requires a reference luminophore and a fluorescent indicator meeting the following criteria: (a) the reference luminophore and the indicator fluorophore have large different decay times, (b) spectral properties including decay time, quantum yield and spectral shape of the reference luminophore are not affected by the sample, (c) the indicator fluorophore changes its fluorophore intensity as a function of the analyte concentration, (d) the indicator and the reference can be excited at a single band of wavelength due a strong overlapp of the excitation spectra, (e) the emission of both the indicator and reference can be detected at a common wavelength or band of wavelength using a single photodetector [1].

LY was chosen as fluorescent indicator because of its exceptional selectivity for copper(II). The decay time of **LY** in aqueous solution is sufficiently short (approx. 5 ns). It is commercially available and provides an effortless immobilization without any chemical modification. **LY** absorbs at 430 nm with an emission maximum at 535 nm, thus it can be excited with a blue 430 nm LED. Its quantum yield is ~0.21 and its photostability is excellent [15]. **LY** was electrostatically immobilized on cellulose anion exchanger particles as shown in chapter 3.2.2.1.

PS100 beads were selected as the reference standard. The particles comprise of ruthenium(II)-tris-4,7-diphenyl-1,10-phenantroline   [Ru(dpp)]   incorporated   in poly(acrylonitrile) (PAN). Ru(dpp) turned out to be a good reference luminophore [3,14] because of its quantum yield of > 0.3 and luminescence decay time of approximately 6 µs [16]. However, the luminescence of Ru(dpp) is known to be quenched by molecular oxygen [17] and oxidative or reductive compounds [18]. For this reason Ru(dpp) is incorporated in gas impermeable PAN beads, which minimizes the problem of oxygen quenching, as shown previously [19]. Furthermore, the encapsulation into PAN beads protects Ru(dpp) from quenching by either oxidants or reductants. A preliminary experiment revealed that the luminescence of PS100 beads is not affected by heavy metal ions.

The PS100 beads and the **LY**/cellulose particles were homogeneously dispersed in the hydrogel. This polymeric support based on polyurethane is hydrophilic and ion permeable.

The spectral properties of the indicator and the reference dye are shown in Figure 5.4. The strong overlap of the excitation spectra allows the excitation of both, **LY** and Ru(dpp),

with the 430-nm LED. Although the emission spectra differ, the signals of both compounds can be detected with one detector using an appropriate long-pass filter.
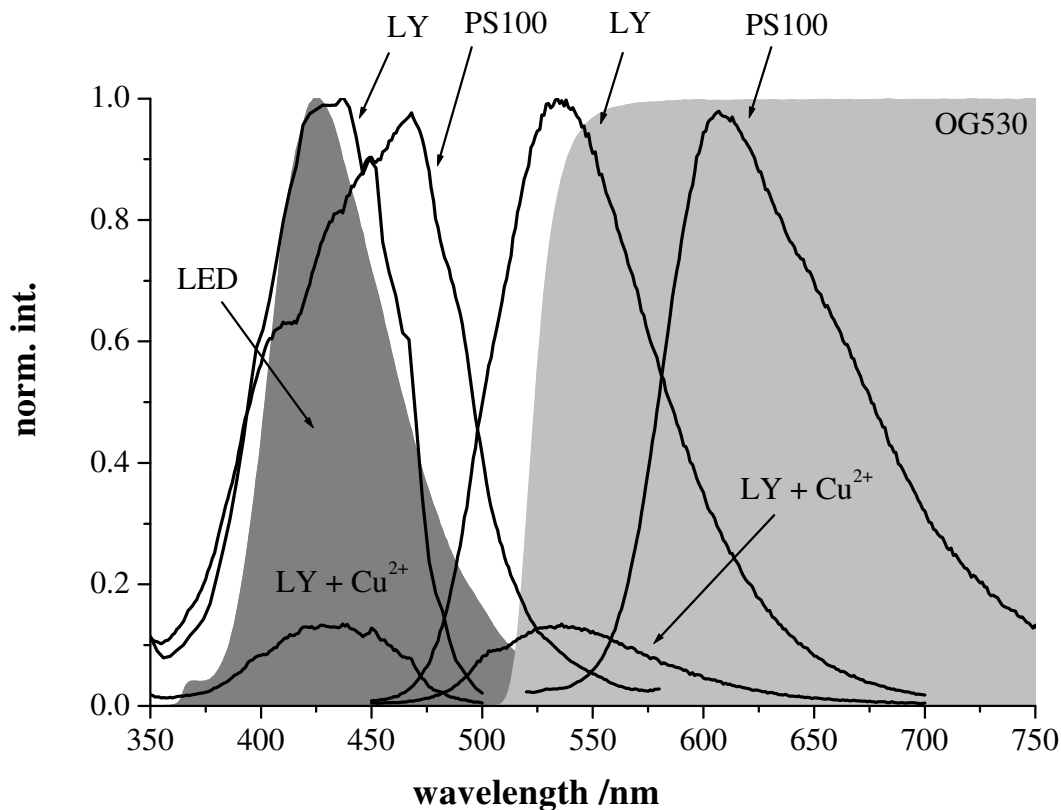
Fig. 5.4. *Excitation and emission spectra of **LY** and Ru(dpp) in presence and absence of copper(II). The dark gray area gives the spectrum of the LED. The light gray area displays the transmission characteristics of the long-pass filter (OG530) and simultaneously represents the signal detected by the photodetector.*

4.3.2. Membrane Characteristics

The fluorescence of the indicator dye **LY** is a strongly quenched by copper(II). Whilst, the luminescence of Ru(dpp) is not affected by copper(II). Consequently, the spectral overlap of the reference beads and the indicator dye is diminished. As a result the emission is dominated by the luminescence of the reference.

Figure 5.5 displays the response curve of membrane **M2**, when exposed to copper(II) in various concentrations. Response times are in the order of minutes and concentration depending. The response of membrane **M2** is not fully reversible because of high affinity

complex formation of **LY** with copper(II). Nevertheless, the membrane can be regenerated by a strong complexing agent such as EDTA.
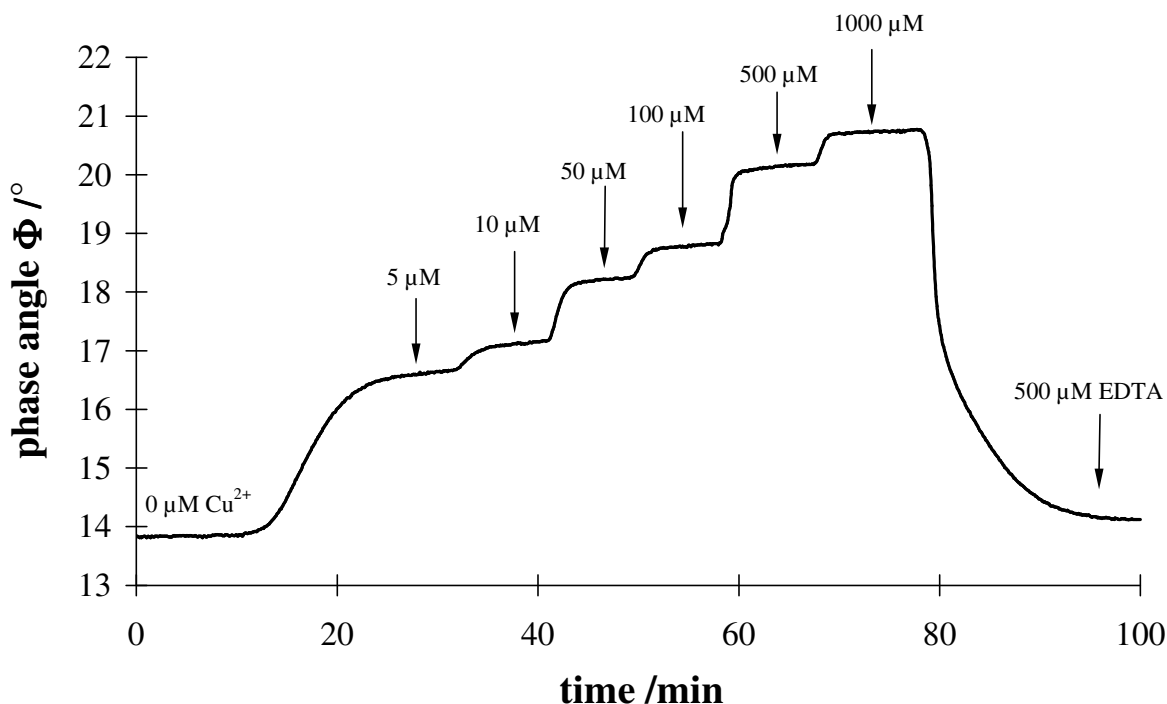
*Fig. 5.5. Response curve of sensor membrane **M2** to copper(II). Solutions are buffered to pH 5.0, and the ionic strength is adjusted to 10 mM by NaNO₃.*

The overall emission derives from the fluorescence of the indicator and the constant background luminescence of the reference. Increasing the copper(II) concentration results in a growing phase shift because the emission is dominated by the luminescence of the ruthenium complex.

Apparently, the phase shift depends on the ratio of the indicator and the reference. Any change in this ratio results in a change in the phase angle. **M1** and **M2** were prepared from cocktails (see Table 1) having indicator/reference ratios of 1:1 and 2:1, respectively. In absence of copper(II) the phase angle for **M1** is about 38.6° and it increases to 49.0° in presence of 1 mM copper(II), which is close to a phase shift of 55° measured for pure PS100 beads dispersed in hydrogel. The higher indicator/reference fraction in **M2** leads to a phase shift of ~ 13.8° in the absence of copper(II) which increases to 20.7° for 1 mM copper(II).

4.3.3. Selectivity

Sensing of heavy metal ions is usually accompanied by severe interferences of various ions species. In contrast, the sensor presented here exhibits an outstanding selectivity. Interference by mercury(II), iron(III), cobalt(II) and nickel(II) are negligible, as shown in chapter 2.2.4 and chapter 3.3.4. The cross-sensitivities of membranes **M2** for mercury(II), iron(II), cobalt(II), nickel(II), cadmium(II), zinc(II), and lead(II) were investigated in concentrations up to 1 mM. As expected, the ions cadmium(II), zinc(II), and lead(II) did not affect the measured signal. Contrary to our expectations, no interference was found for iron(III), cobalt(II), nickel(II). The only interferent was mercury(II), which is also the strongest interferent in solution. The calibration plots of membrane **M2** for copper(II) and mercury(II) is given in Figure 5.6. A selectivity coefficient log $K_{Cu(II)}$ relative to copper(II) for a 10 µM ion solution that is 2.5 was determined by the separate solution method (SSM). However, the concentration range where interference occurs is far from levels that can be expected in real samples.
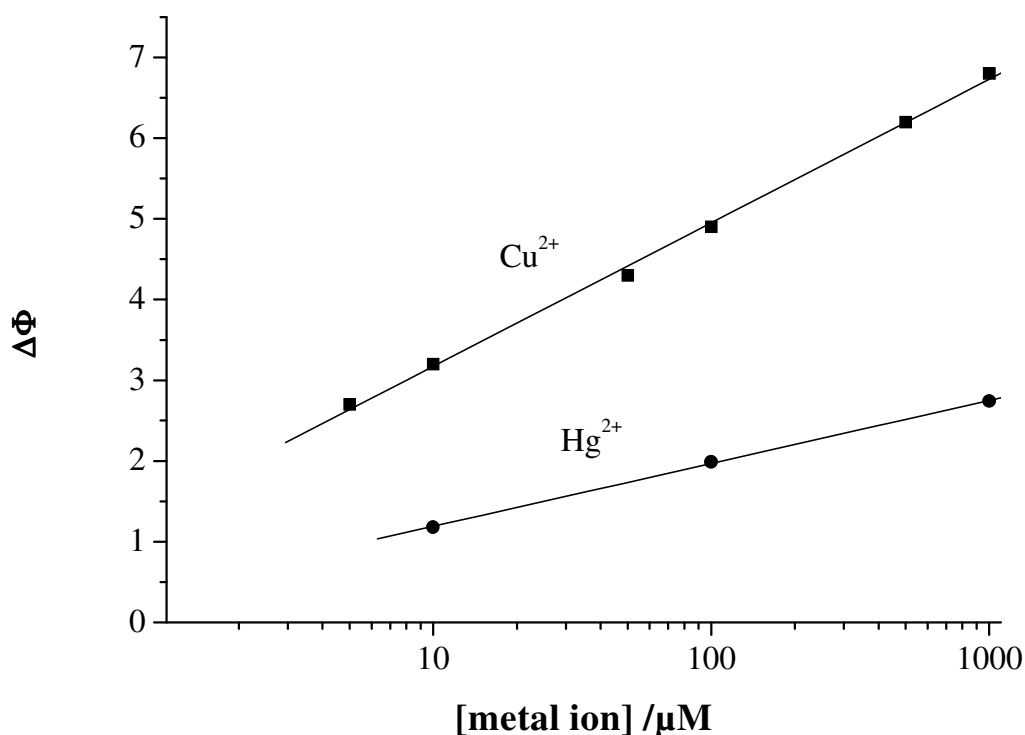
Fig. 5.6. *Calibration plot of membrane M3 for copper(II) and mercury(II) at pH 5 and constant ionic strength of 10 mM . $\Delta\Phi = \Phi\text{-}\Phi_0$, Φ = phase angle, Φ_0 = phase angle at 0 µM copper(II).*

4.3.4. Effect of pH

Fluorescence quenching of **LY** in aqueous solution by copper(II) is strongly pH-dependent because sensitivity is increased from pH 3 to 7 (see chapter 2.4.2 and chapter 3.3.5). The quenching is less efficient at low pH because of an acid base reaction of terminal nitrogen atom of the carbohydrazide group which is the complexing part of the indicator. Consequently, complexation of copper(II) is hindered in solutions of high acidity. A similar behaviour is observed for immobilised **LY** within the DLR-scheme. Figure 5.7 displays the calibration plots for membrane **M1** exposed to copper(II) in buffers of varying pH-values. The phase shifts increase on going to higher acidity indicating a more efficient quenching of the indicator at higher pH. The more efficient quenching at higher pH is in agreement with the results in solution. Again, the effect of pH can be interpreted as an acid base reaction of the hydrazide group.
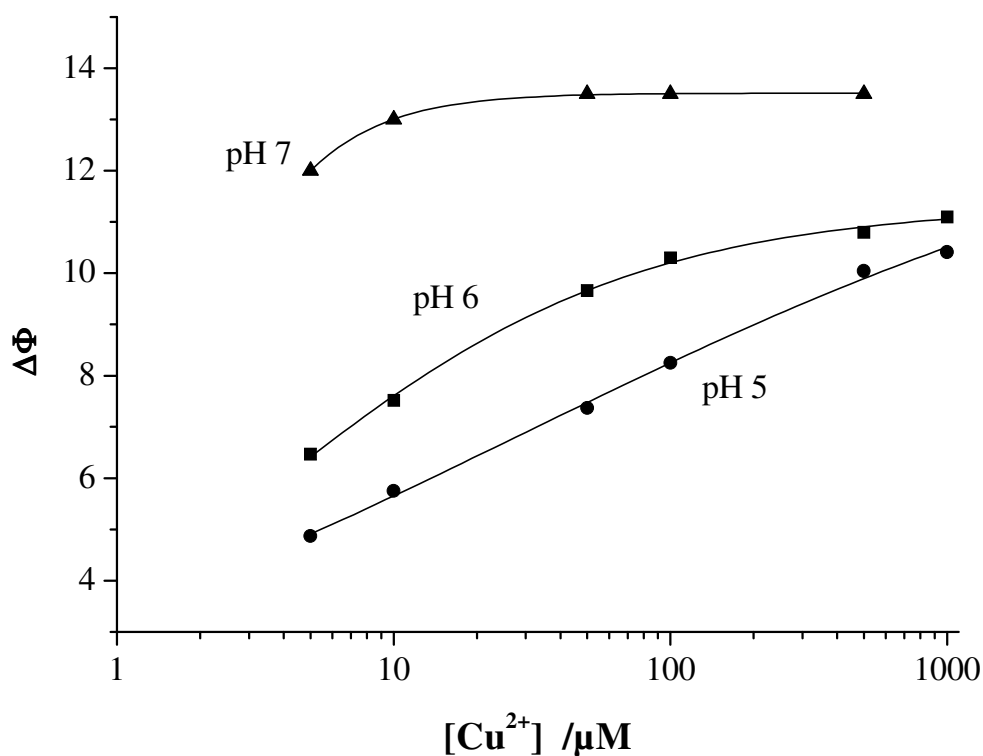
Fig. 5.7. *Calibration plot of membrane M3 for copper(II) at various pH-values. $\Delta\Phi = \Phi$-Φ_0, Φ = phase angle, Φ_0 = phase angle at 0 μM copper(II).*

4.3.5. Effect of solution turbidity

The DLR sensing scheme offers the possibility to eliminate adverse effects occurring in fluorescence measurements. Unlike in the laboratory, real samples are often filthy or soiled, which affects fluorescence. Hence, turbidity has to be taken into consideration for calibration routines. Figure 5.8 demonstrates that the effects of turbid solutions can be referenced out by DLR measurements. Membrane **M2** was subsequently exposed to clear and turbid solutions, resulting in changes of the fluorescence intensity, while the phase shifts remained constant.
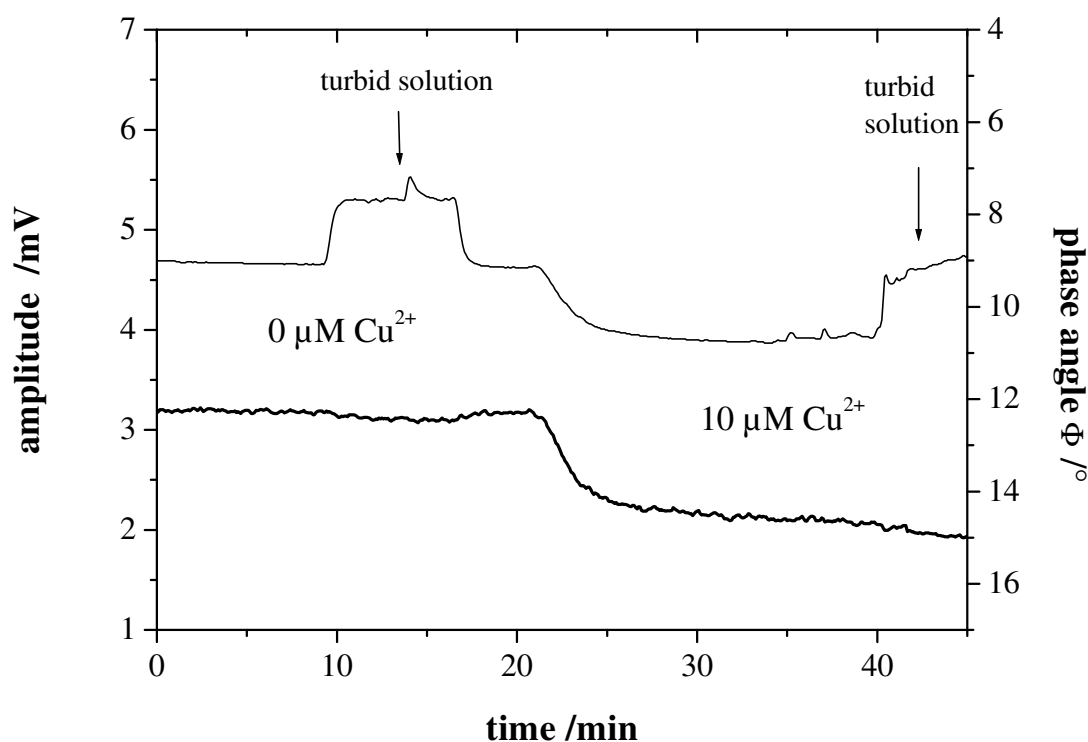
Fig. 5.8. *Effect of turbid solutions on the intensity signal (doted line) and the referenced signal of M2 simulated by the addition of titan(IV)oxide. The sensing membrane was consecutively rinsed with solution containing 0 μM copper(II) (0 to 10 min.), 0 μM copper(II) and titan(IV)oxide (10 to 18 min.), 0 μM copper(II) (18 to 22 min.), 10 μM copper(II) (22 to 40 min.), 10 μM copper(II) and titan(IV)oxid (>40 min.), respectively*

4.3.6. t-DLR imaging of sensors integrated in microtiterplates

The DLR sensor presented were also exploited for time-resolved luminescence imaging. Therefore the DLR scheme is transferred from the frequency domain into the time domain [21]. In this case, the luminescence can be detected by a CCD-camera because no sinusoidal modulation is necessary. The camera maps an area of 20 wells of a microtiterplate with integrated sensor spots of type **M3.** The wells were filled with copper(II) solution of various concentrations. The uniform illumination of the areas is crucial and for this reason a source for inhomogeneities. However, this effect can be eliminated to a large extent by forming the ratio of the excitation window and the emission windows representing (a) the luminescence of both the indicator and the reference and (b) the solely emission of the reference standard. Figure 5.9 shows the grey-scale image of the wells and the surface plot of the image. R reflects the copper(II) concentration of the solution in each well. The effects of nonhomogeneous excitation (through a nonhomogeneous lightfield) or nonhomogeneous dye distribution are referenced out, which is displayed by the uniform grey distribution of the sensor spots. Furthermore, the pixel data of each well were averaged and plotted vs. the copper(II) concentration (see Figure 5.10). In addition, Figure 5.10 displays the calibration plot of a conventional intensity measurement at two wavelengths. Apart from the scale, the calibration plots show identical shape. The homogeneous intensity distribution of the sensor spots demonstrates successful referencing.
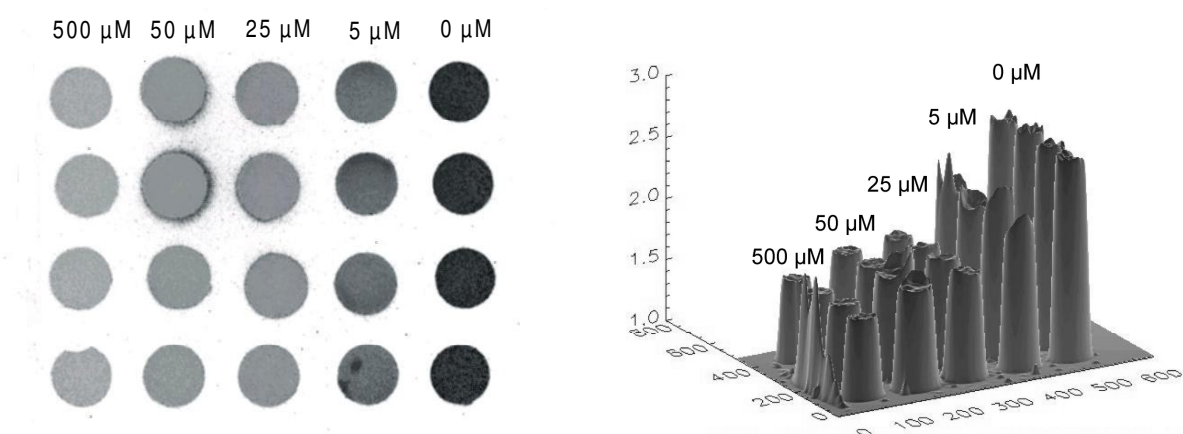
Fig. 5.9. *Referenced grey-scale picture (left) and surface plot (right) of the mapped area of the microtiterplates with sensor spots integrated into the wells. X and y-axes represent the pixels of the image, R values (eq. 2) are plotted in direction of the z-axes.*
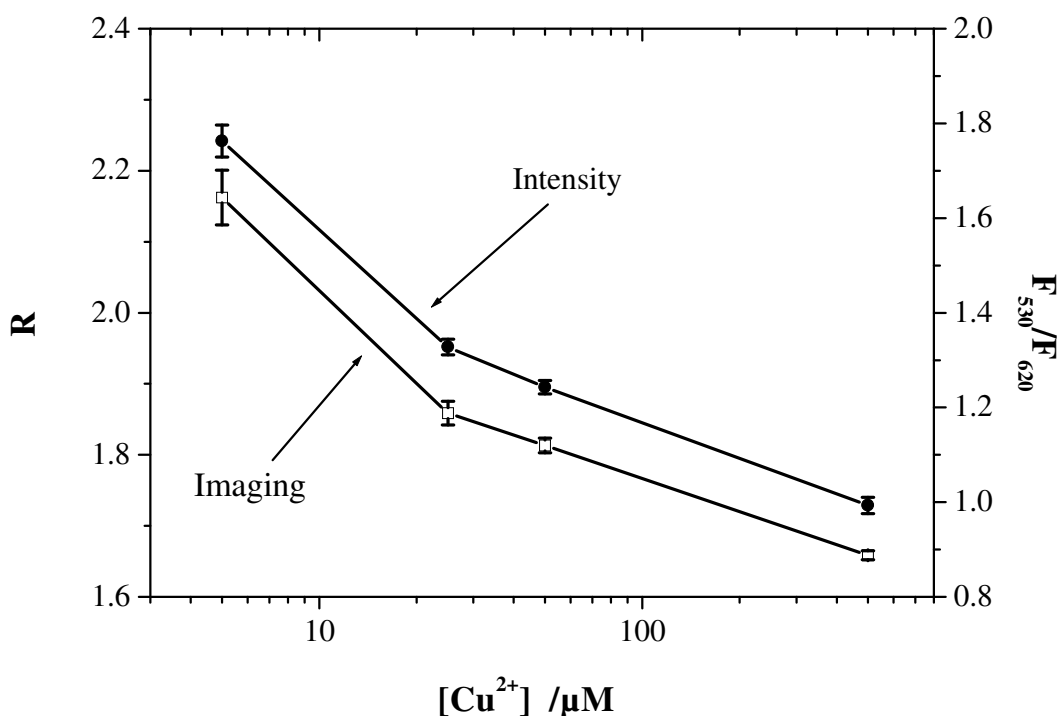
Fig. 5.10. *Calibration plots of (a) the imaging measurement and (b) the ratiometric intensity measurement. R is the fraction of the intensity of the reference and the indicator in the excitation window and the intensity of the reference in the emission window. F_{530} is the intensity measured at 530 nm and F_{620} at 620 nm, respectively, when excited at 420 nm.*

4.4. Conclusion

A powerful sensor scheme for the determination of copper(II) with internal referencing of luminescence intensities is presented. The scheme is based on combining a fluorescent indicator with a phosphorescent reference standard. The method provides the conversion of a copper(II)-dependent fluorescence intensity into a phase shift that can be detected by non-sophisticated instrumentation. The sensing membrane is capable of measuring copper(II) with an outstandingly high selectivity over a wide range. The dynamic range is between 5 and 1000 µM which matches the guide line set by the WHO and the EC. The advantages of the referencing method over intensity-based measurements was demonstrated by the measurement of turbid solutions. The intensity signal changes strongly, while the phase shift remains at a constant level. This simplifies determination of copper(II) of real samples where turbidity is likely to occur.

In addition, the sensing scheme enables measurements both in the frequency domain and in the time domain. This was demonstrated by performing 2-dimensional measurements by time-resolved imaging of sensors integrated into microtiterplates. The images obtained show a homogenoeus intensity distribution due to a efficient intrinsic referenciation of the heterogeneous light-field and of dye distribution. The method also demonstrates its high potential over sequential methods in view of a data acquisition in less than 1 s and the collection of the data in one image which allows further interpretation.

4.5. References

[1]   I. Klimant, Ch. Huber, G. Liebsch, G. Neurauter, A. Stangelmayer, O. S. Wolfbeis, in *New Trends in Fluorescence Spectroscopy*, B. Valeur, J. C. Brochon (eds.), Springer Verlag, Berlin, (2001).

[2]   I. Klimant, (inv.) *German Patent Application*, DE 198.29.657, Aug. 1 (1997).

[3]   C. Huber, I. Klimant, C. Krause, O. S. Wolfbeis, *Dual lifetime referencing as applied to a chloride optical sensor*, Anal. Chem., **73**, 2097 (2001).

[4]   I. Oehme, O. S. Wolfbeis, *Fundamental Review – Optical Sensors for Determination of Heavy Metal Ions*, Microchim. Acta, **126**, 177 (1997).

[5]   C. Sanchez-Pedeno, J. A. Ortuno, M. I. Albero, M. S. Garcia, *A new procedure for the construction of flow-through optodes. Application to determination of Copper*, Fresenius J. Anal. Chem., **366***, 811 (2000).

[6]   N. Malcik, P. Caglar, R. Narayanaswamy, *Investigations into optical sensing of cupric ions using several immobilized reagents*, Quím. Anal., **19,** 94 (2000).

[7]   L.A. Saari, W.R. Seitz, *Immobilized Calcein for metal ion preconcentration*, Anal. Chem., **56**, 810 (1984).

[8]   F. V. Bright, G. E. Poirer, G. M. Hieftje, *A new ion sensor based on fiber optics*, Talanta*, 113 (1988).

[9]   J. W. Parker, O. Laksin, C. Yu, M. L. Lau, S. Klima, R. Fischer, I. Scott, B. W. Atwater, *Fiber-Optic Sensor for pH and Carbon Dioxide Using a Self-Reerencing Dye*, Anal. Chem., **65** 2329 (1993).

[10]   D. J. S. Birch, O. J. Rolinski, D. Hatrick, *Fluorsecence lifetime sensor of copper ions in water*, Rev. Sci. Instrum., **67(8)**, 2732 (1996).

[11] J. R. Lakowicz, *Principles of Fluorescence Spectroscopy*, Plenum Press, New York (1999).

[12] J. R. Lakowicz, F. N. Castellano, J. D. Dattelbaum, L. Tolosa, G. Rao, I. Gryczynski, *Low-Frequency Modulation Sensors Using Nanosecond Fluorophores*, Anal. Chem., **70**, 5115 (1998).

[13] G. Liebsch, I. Klimant, C. Krause, O. S. Wolfbeis, *Fluorescent Imaging of pH with Optical Sensors Using Time Domain Dual Lifetime Referencing*, Anal. Chem., **73**, 4354 (2001).

[14] C. Huber, I. Klimant, C. Krause, T. Werner, T. Mayr, O. S. Wolfbeis, *Optical Sensor for Seawater Salinity*, Fresenius J. Anal. Chem., **368**, 196 (2000).

[15] W. W. Stewart, *Synthesis of 3,6-Disulfonated 4-aminonaphthalimides*, J. Am. Chem. Soc., **103**, 7615 (1981).

[16] C. T. Lin, W. Boettcher, W. Chou, C. Creutz, N. Sutin, J. Am. Chem. Soc., *Mechanism of the Quenching of the Emission of Substituted Polypyridineruthenium(II) Complexes by Iron(III), Chromium(III) and Europium(III) Ions*, **98,** 6536 (1976).

[17] I. Klimant, O. S. Wolfbeis, *Oxygen-Sensitive Materials Based on Silicon-Soluble Ruthenium Complexes,* Anal. Chem., **67,** 3160 (1995).

[18] A. Juris, V. Balzani, F. Barigelletti, S. Campagna, P. Belser, A. von Zelewsky, *Ru(II) Polypyridine Complexes: Photophysics, Photochemistry and Chemiluminescence,* Cood. Chem. Rev., **84**, 85 (1988).

[19] G. Liebsch, I. Klimant, O. S. Wolfbeis, *Luminescence lifetime temperature sensing based on sol-gels and poly(acrylonitrile)s dyed with ruthenium metal-ligand complexes*, Adv. Mater. **11** 1296 (1999).

Chapter 5

Multi-Ion Imaging Using Selective Fluorescent Sensors in a Microtiterplate Array Format

A novel type of sensor array destined for water analysis is described. The sensor array delivers simple on/off patterns of complex ion mixtures. Fluorescent indicators for calcium(II), sodium(I), magnesium(II), sulfate, chloride and mercury(II) were dispersed in thin films of water-soluble polymer on the bottom of the wells of microtiterplates. Indicator and polymer dissolve after adding the aqueous sample and the interaction of analyte and dissolved indicator result in a fluorescence signal that can be quantified. The fluorescence intensity of the indicators was transferred into a time-dependent parameter applying a scheme called dual lifetime referencing (DLR). In this method, the fluorescence decay profile of the indicator is referenced against the phosphorescence of an inert reference dye added to the system. The intrinsically referenced measurements were performed using blue LEDs as light sources and a fast gateable CCD camera.

5.1. Introduction

The arrangement of several chemical sensors in an array format enables the simultaneous determination and assessment of multiple chemical information. This is essential in the design of, for example, artificial noses and tongues. Existing sensing schemes employ a variety of chemical interaction strategies. These include the use of conductive polymers [1], metal oxide field effect transistors [2], surface acoustic wave devices [3], catalytic (tin oxide) [4,5], electrochemical [6,7] or optical sensors [8-14]. By making use of certain sensors out of the multitude of existing sensors for environmental contaminants, almost any species may be sensed, but this is associated with a considerable instrumental effort, since practically all sensors are different in terms of sensing scheme and hence instrumentation. Ideally, however,

a sensor array for monitoring a variety of environmental parameters is based on a single technology (*e.g.* optical), can sense all parameters simultaneously, yet is compatible with standard methods for sample preparation. We have tackled this challenge by (a) using a uniform analytical protocol, (b) using fluorescent indicators with very similar excitation and emission wavelengths, (c) integrating the format into microtiterplate technology (in order to form disposable sensor arrays), (d) making use of chemical imaging (which allows fast reading of all parameters simultaneously), and (e) using comparative and inexpensive semiconductor and optical components. This combination paves the way for analyzing aqueous solutions for a large number of parameters using a single opto-electronic system, in a short time.

The sensing array introduced here incorporates sensor spots yielding signals at almost identical excitation and emission wavelengths and within the same range of decay times. It parallels a recent report (using different materials) to 'see' a variety of odors by making use of a set of sensors spots whose coloration is affected by vapors of certain odorants [8]. In contrast to previous work by McDevitt and co-workers who have described arrays based on micro-beads contained in micromachined cavities [9]. The scheme presented here does not require any highly sophisticated steps in peparation and signal processing, but rather makes use of the widely accepted microtiterplate technique.

5.2. Time-domain Dual Lifetime Referenced (t-DLR) Imaging

Fluorescence intensity is a widely used parameter in fluorometry, but it is a poor parameter for the use in quantitative imaging because it depends on a number of variables other than the concentration of the species to be assayed. These include the variation of light intensity over the whole area to be imaged and inhomogeneities of the dye distribution of the sensing layer. Ratiometric calibration schemes were employed in order to overcome these drawbacks by rationing intensities at two excitation or emission wavelengths [15]. The most effective way to eliminate the mentioned adverse effects is the measurements of decay time. Since it is a intrinsically referenced parameter, decay time is superior to intensity in that it is independent of local concentrations of fluorescent probes and of fluctuations in light source intensity. On the other hand, lifetime imaging requires sophisticated and expensive instrumentation [16], especially for approaches employing nanosecond-decaying fluorescent probes. Nevertheless, a recently developed scheme allows to generate intrinsically referenced readouts by measuring these short-decaying indicators using a microsecond resolving system with

comparatively simple instrumentation [17,18]. This scheme, referred to as time-domain dual lifetime referencing (t-DLR), converts the intensity information in a time dependent parameter.

Specifically, a phosphorescent dye is added to the sample containing the fluorescent indicator. For a successful application of the scheme it is mandatory that the excitation and emission spectra of the phosphore overlap the respective spectra of the indicator. During the measuring cycle both the indicator and the reference are excited simultaneously and two images are taken at different time gates detected by a CCD camera, one recorded in the excitation period (A_{ex}) when the light source is on, the other in the decay period (A_{em}) when the light source is off. Consequently, the first image reflects the luminescence signal of both the fluorescent indicator dye and the phosphorescent reference dye. The second image which is measured after a certain delay (after the indicator fluorescence has decayed), is solely caused by the long-lived phosphorescent dye. A schematic representation of the t-DLR scheme is given in Figure 5.1. Since the intensity of the fluorophore contains the information on the respective analyte, whereas phosphorescence is inert to it, the ratio of the images displays a referenced intensity distribution that reflects the analyte at each picture element (pixel). The ratio can be described by the following relationship:

$$R = \frac{A_{ex}}{A_{em}} = \frac{A_{REF-exc} + A_{IND}}{A_{REF-em}} \qquad\qquad 5.1$$

where the image A_{ex} represents the sum of both luminescences $A_{REF-exc}$ and $A_{IND,}$ which are the signal intensities of the reference and the indicator in the excitation window, respectively. The second image A_{em} is equal to A_{REF-em}, which is the signal intensity of the reference in the emission window.

$$R = \frac{A_{ex}}{A_{em}} = \frac{A_{REF-ex} + A_{FLU}}{A_{REF-em}}$$
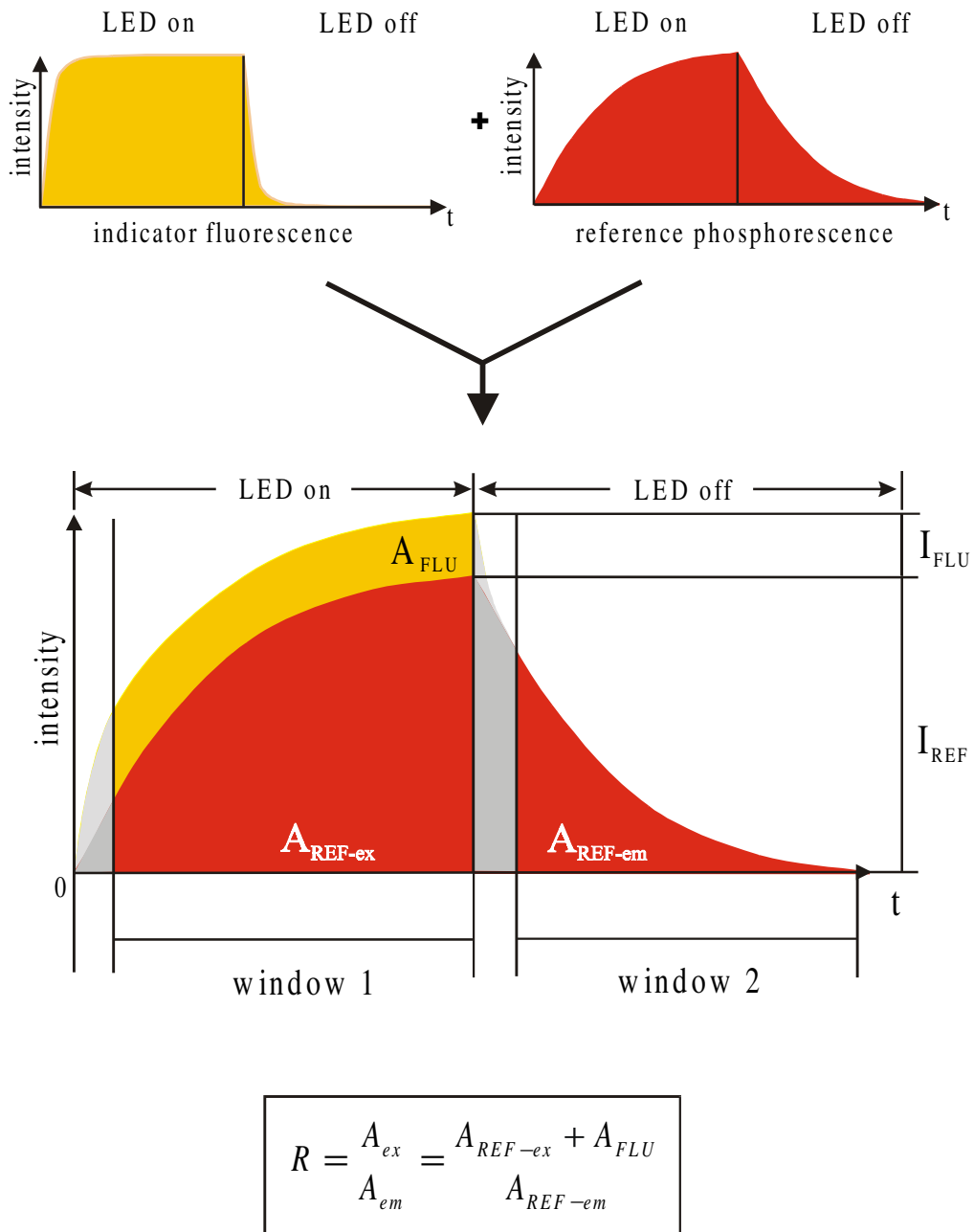
Fig. 5.1. Scheme of time-domain DLR (t-DLR). The short-lived-indicator and the long-lived reference are simultaneously excited and measured in two time gates. The first (A_{ex}) is the excitation period, where the signal obtained is composed of the indicator fluorescence and the phosphorescence of the reference standard. The second gate (A_{em}) is opened in the emission period, where the intensity is exclusively composed of the reference luminescence. Rationing both images results in an intrinsically referenced signal.

5.3. Material and Methods

5.3.1. Chemicals and Solutions

Fluorescent probes Oregon Green BAPTA-5N, Magnesium Green, Sodium Green, Lucigenin, Phen Green FL were obtained from Molecular Probes Europe BV (Leiden, The Netherlands). The phosphorescent reference beads PD containing ruthenium(II)-4,7-diphenyl-1,10-phenanthroline were a friendly gift from Presens (Regensburg, Germany). Poly(ethylene glycol) (PEG 1000) and inorganic salts of analytical-reagent grade from Merck (Darmstadt, Germany), imidazol buffer from Sigma (Vienna, Austria), black microtiterplates (96 wells) with transparent bottom from Greiner (Frickenhausen, Germany).

12 samples were prepared containing different mixtures of calcium(II), magnesium(II), sodium(I), mercury(II), sulfate and chlorid ions in 5 mM imidazole buffer of pH 7. The concentrations of the respective salts were: 5 mM $Ca(NO_3)_2$, 1 mM $Mg(NO_3)_2$, 25 mM NaCl, 1 mM Na_2SO_4, 100 mM $Hg(NO_3)_2$. In the DLR experiments, the samples were mixed with phosphorescent reference beads (0.06% w/w). The arrays were filled with 200 µl of the solution containing mixtures of the above ions. After 5 min, the content of the wells were mixed with a pipette and the arrays were ready for imaging.

Buffer was prepared by dissolving the respective amount of imidazole in doubly distilled water. The pH was adjusted to pH 7 adding hydrochloric acid, monitored by use of a digital pH-meter (Knick, Berlin, Germany) calibrated with standard buffers of pH 7.00 and 4.00 at 21±1 °C.

5.3.2. Preparation of sensor arrays

6 wells of a standard 96 well microtiterplate were filled with stock solutions of the respective indicators. The luminescence intensities were adjusted to a comparable level. Volumes added and concentrations of the respective indicators stock solutions are given in Table. 5.1. Afterwards, 10 µl of a solution of poly(ethylene glycol) (PEG 1000, 0.01 wt%) and 30 ml of doubly distilled water were pipetted into each well. After vaccum drying in a desiccator, the bottom of the wells contain a thin layer of polymer and dispersed indicator that readily dissolves on addition of an aqueous sample.

Table 5.1. *Concentrations of the indicator stock solutions and volumes*
added to the wells of the microtiterplates

Indicator	Concentration /μM	Volume added /μl
OregonGreen BAPTA 5N	216	6.5
Magnesium Green	132	30
Sodium Green	300	23
Oregon Green BAPTA 5N	216	9
Ba(NO₃)₂	saturated	5
Lucigenin	3915	5
Phen Green FL	757	6

5.3.3. Measurements of Fluorescence Spectra

Excitation and emission spectra of the indicators and the reference particles were recorded with a Varian Carry Eclipse Spectrofluorimeter equipped with a microtiterplate accessory, as shown in Figure 5.2.

Fig. 5.2. *The Varian Carry Eclipse Spectrofluorimeter*
equipped with a microtiterplate reader device.

5.3.4. Imaging Setup

A gated CCD camera and a pulsed LED excitation light source were used for time-resolved imaging of the emission intensity as described by Liebsch et al. [18]. An fast puslable LED array consisting of 12 bright blue emitting LEDs (λ_{max}= 470 nm, NSPB, Nichia, Nürnberg, Germany) served as the light source. The array was covered with a short-pass filter (BG12, Schott, Mainz, Germany) for excluding the red fraction of the LED emission. Short pulses (5 µs) of blue excitation light hit the microtiterplate containing the respective probes in its wells. The emitted light passed an emission filter (OG 530, Schott, Mainz, Germany) and was then detected by a CCD camera (SensiMod, PCO, Kehlheim, Germany). The camera had a black/white CCD chip with 640x480 pixels (307 200 pixels, VGA resolution) and a 12-bit resolution, equivalent to 4096 gray-scale values. The CCD chip can be gated directly with a minimal trigger time of 100 ns; additional image intensification is not required. The camera and the light source are triggered by a pulse generator (DG535, Scientific Instruments, West Palm Beach, USA) and the image data are transferred to a personal computer. Hardware and image processing are controlled by software developed in-house [19]. A schematic representation is given in Figure 5.3.
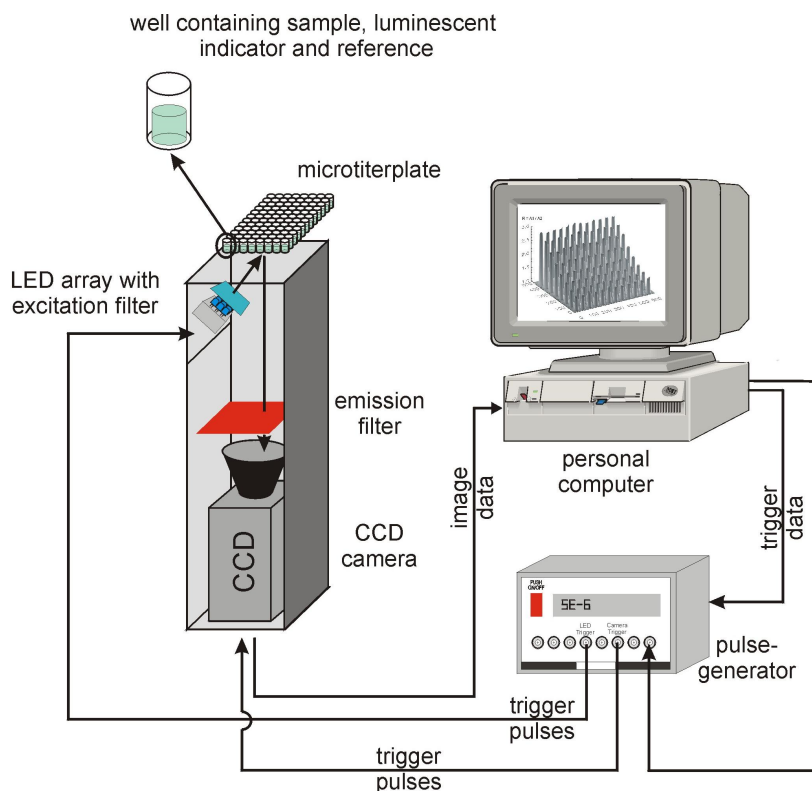
Fig. 5.3. *Schematic view of the imaging setup.*

5.4. Results and Discussion

5.4.1. Choice of Indicators

A manifold of fluorescent indicators or probes for ions were developed in the past decade, in particular for biological and clinical purposes. However, only a few fulfill the demands for the use in the uniform scheme presented here. Indicators were selected meeting the following criteria: a) selectivity for the target ion, b) good watersolubility, c) high quantum yield, d) similar excitation wavelengths, e) decay time in the nanosecond range.

 Oregon Green BAPTA 5N, **Magnesium Green**, **Sodium Green**, **PhenGreen FL** and **Lucigenin** were found to fulfill many of these requirements. The chemical structures are shown in Figure 5.4. All chosen indicators show excellent water-solubility and sufficient quantum yield. They can be excited with blue LEDs (λ_{max}= 470 nm) and then emit light with a maximum at >505 nm. Their fluorescence decay time is in the range of 2-6 ns. Figures of merit are summarized in Table 5.2.

Table 5.2. *Figures of merit for indicators used for detection of respective ions [20].*

Ion	Fluorescent probe	λ_{ex} /nm	λ_{em} /nm	Effect on fluorescence if ion is present
Ca^{2+}	Oregon Green BAPTA-5N	494	521	enhancement
Mg^{2+}	Magnesium Green	506	531	enhancement
Na^+	Sodium Green	506	532	enhancement
Cl^-	Lucigenin	455	505	quenching
Hg^{2+}	Phen Green FL	492	517	quenching
SO_4^{2-}	Oregon Green BAPTA 5N + $Ba(NO_3)_2$	494	521	decrease

The fluorescence of the indicators is either enhanced or decreased depending on the various mechanisms signaling the recognition event of the analyte. Calcium(II), magnesium(II) and sodium(I) ions increased the fluorescence, while chloride, sulfate and mercury(II) ions decreased the fluorescence of the respective indicators. The indicators **Oregon Green BAPTA 5N** and **Magnesium Green** for the earth alkaline ions utilize photon induced

electron transfer (**PET**) for signaling. Either does **Sodium Green**, but within this a second effect contributes to an increase in fluorescence on binding, that is the physical separation of the two intramolecular fluorophores moieties quenching each other in the unbound state. Chloride decreases the fluorescence of **Lucigenin** by dynamic quenching, as well as mercury(II) ions dramatically quenches the fluorescence of **Phen Green FL**. The signal decrease of sulfate is caused by a precipitation reaction with barium(II) ions, which enhance the fluorescence of **Oregon Green BAPTA 5N**. In presence of sulfate, the precipitation of $Ba(SO_4)$ removes barium(II) ions from the probe in a competitive reaction resulting in an decrease of fluorescence. Normalized excitation and emission spectra of the respective indicator in presence and absence of the target ions are shown in Figure 5.5.
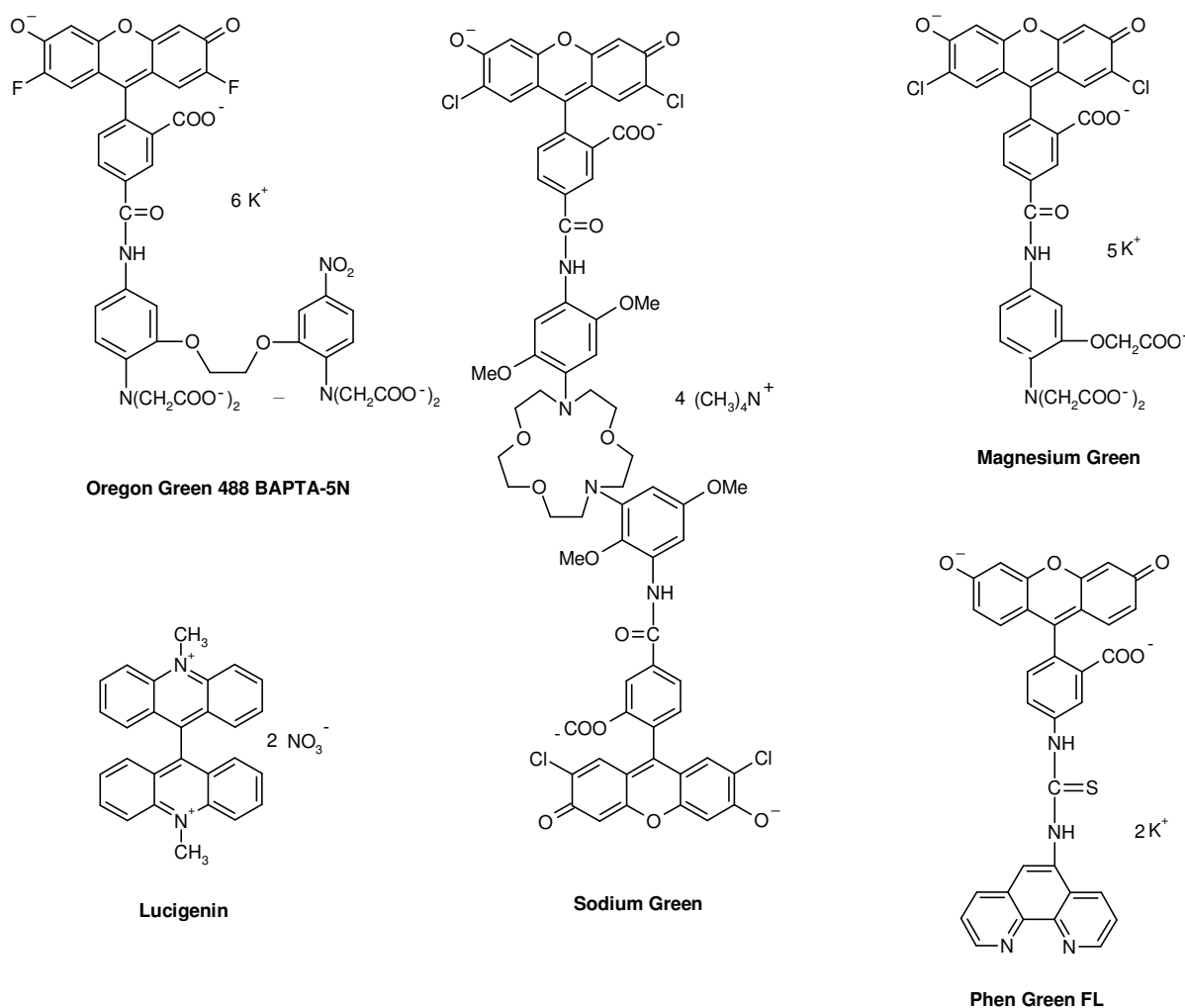
Fig. 5.4. *Chemical structures of fluorescent probes used for the sensor array.*
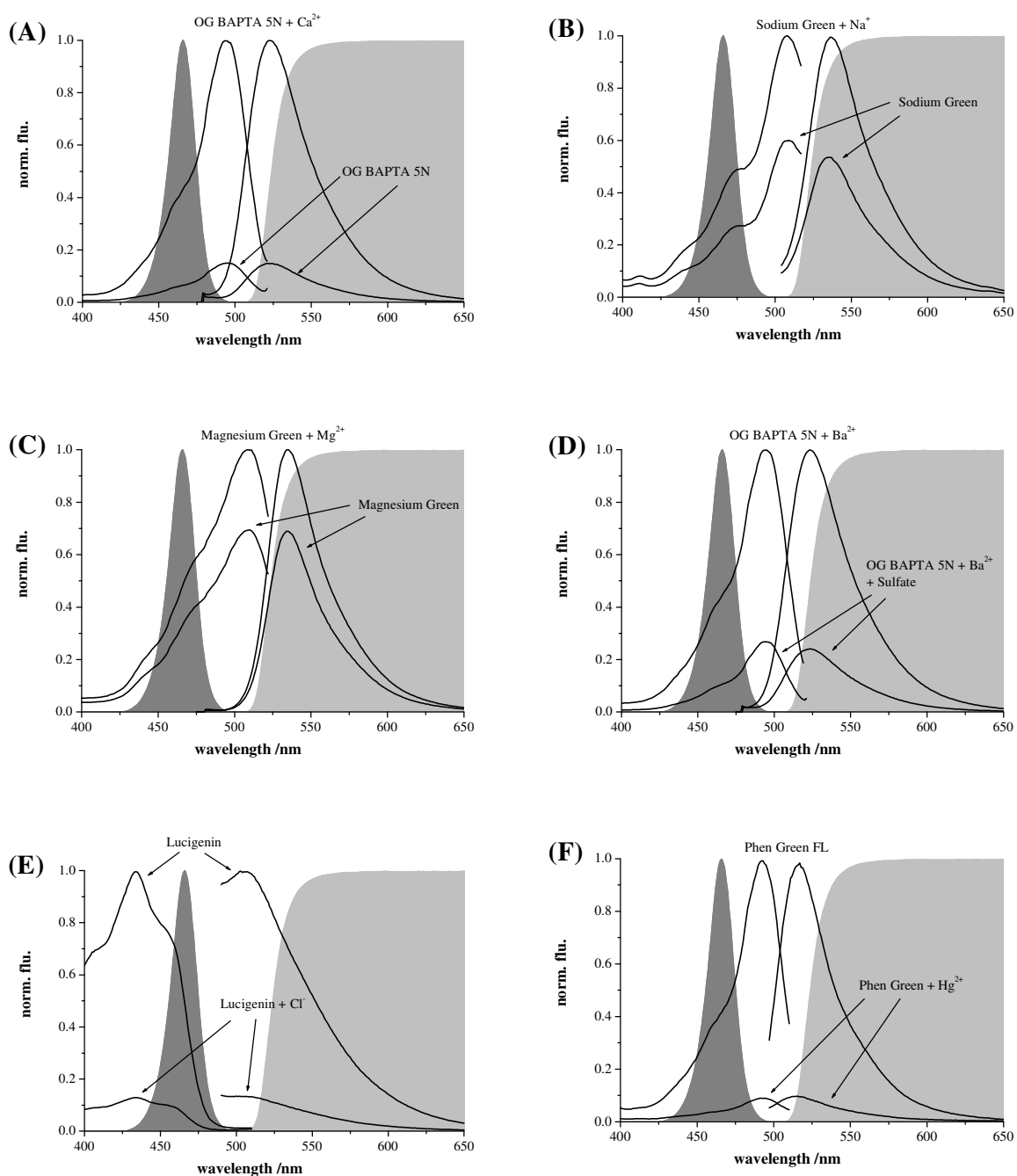
Fig. 5.5. *Excitation and emission spectra of the* **(A)** *Oregon Green BAPTA 5N,* **(B)** *Sodium Green,* **(C)** *Magnesium Green,* **(D)** *Oregon Green BAPTA 5N + barium(II),* **(E)** *Lucigenin,* **(F)** *Phen Green FL in presence and absence of calcium(II), sodium(I), magnesium(II), sulfate, chloride and mercury(II), respectively. Spectra were recorded at the exctiation wavelength of 470 nm and the emission wavelength of 530 nm. The gray areas represent the optical properties of the imaging setup. The dark gray area gives the spectrum of the excitation light derived from a LED combined with a BG12 light filter. The light gray area displays the transmission characteristics of the long-pass filter (OG530) and simultaneously represents the emission signal detected by the CCD-camera.*

5.4.2. Choice of Reference Dye

The criteria for the reference luminophore for the application in t-DLR imaging are: (a) a decay time in the microsecond range for the use of microsecond resolving system compounds, (b) spectral properties including decay time, quantum yield and spectral shape of the reference luminophore are not affected by the sample, (c) the reference can be excited at the same band of wavelength as the indicator due a strong overlap of the excitation spectra, (d) the emission of both the indicator and reference can be detected at a common band of wavelength.

The phosphorescent PD beads were selected as the reference standard. The particles with a size of 10-100 nm comprise of ruthenium(II)-tris-4,7-diphenyl-1,10-phenanthroline [Ru(dpp)] incorporated in poly(acrylonitrile) (PAN). Ru(dpp) has a quantum yield of >0.3 and a luminescence decay time of approximately 6 µs [21]. However, the luminescence of Ru(dpp) is known to be quenched by molecular oxygen [22] and oxidative or reductive compounds [23]. For this reason Ru(dpp) is shielded from the quenching of molecular oxygen by its encapsulation in gas impermeable PAN [24]. Furthermore, a preliminary experiment revealed that the luminescence of PD beads is not affected by the target ions. The excitation and emission spectra of PD beads are depicted in Figure 5.6.
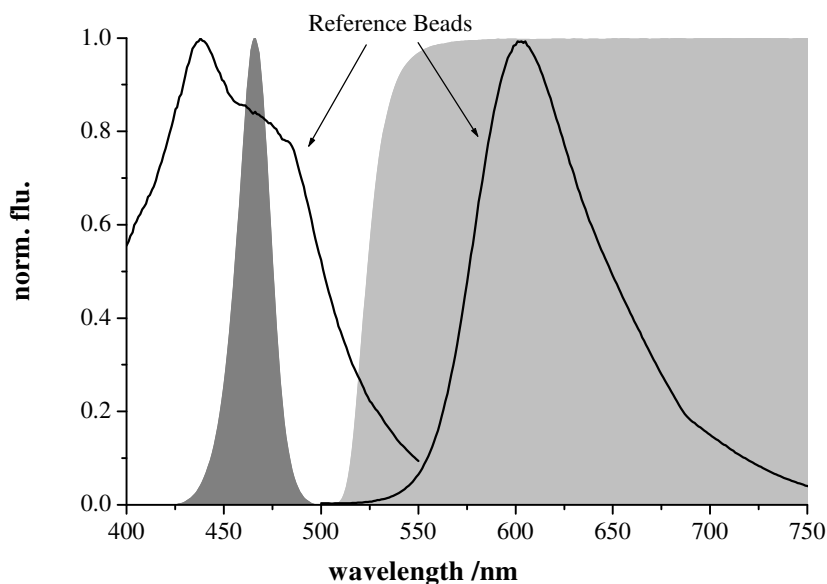
Fig. 5.6. Excitation and emission spectra of the reference dye. The dark gray area gives the spectral characteristics of LED combined with a BG12 excitation filter. The light gray area displays the transmission characteristics of the long-pass filter (OG530).

5.4.3. Choice of Polymer

The indicator dyes were dispersed in thin films of a water-soluble polymer on the bottom of the wells of microtiterplates. Both the polymer and the indicator rapidly dissolve after adding the aqueous sample. The physical immobilization of the indicators in the wells of a microtiterplate offers an effortless array preparation without changing the response characteristics of the indicator, including dynamic range and optical properties, since any chemical modification is required. Furthermore, the goal of forming a disposable water test array makes a permanent immobilization unnecessary. Nevertheless, arrays prepared in this way can be conveniently stored for a long time and used for determinations outside the laboratory .

Poly(ethylene glycol) was selected due its chemical inertness towards ions and its solubility in water in short time. Of course, the latter depends on the molecular weight of the polymeric chains. Thus, PEG 1000 was chosen because it is solid (PEG of lower molecular weights are liquid), dissolves rapidly in water and is expected to show good longterm stability.

5.4.4. Response Characteristics

After filling the arrays with solutions containing varying ion mixtures and the reference luminophore, the selective interaction of analyte ion and indicator result in a fluorescence signal that can be quantified. The sensor spots were arranged according to the patterns given in Figure 5.7. Therefore the response of one spot can be attributed to one respective analyte.
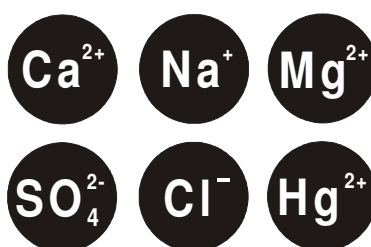
Fig. 5.7. Pattern of the sensors spots contained in the array. Each array was prepared by filling six wells of a microtiterplate with poly(ethylene glycol) along with the respective fluorescent indicator.

The spots were illuminated by LEDs and "viewed" by a CCD-camera. Figure 5.8 displays the resulting gray-scale pictures reflecting the intrinsically referenced luminescence intensity of the spots. The homogeneity of the gray distribution for each spot indicates the successful referencation of the inhomogeneities caused be the heterogeneous lightfield. This is underlined by the surface plot of an array filled with sample containing sodium(I) and chloride, shown in Figure 5.9.

Buffer Mg^{2+} Hg^{2+} Ca^{2+}

$Na^+ + Cl^-$ $Na^+ + Mg^{2+}$ $Na^+ + Cl^- + SO_4^{2-}$ $Ca^{2+} + Mg^{2+}$

$Ca^{2+} + Na^+ + Cl^-$ $Na^+ + SO_4^{2-}$ $Ca^{2+} + Na^+$ $Ca^2 + Mg^{2+} + Na^+$
                                                   $+ SO_4^{2-}$ $Hg^{2+} + Cl^- + SO_4^{2-}$
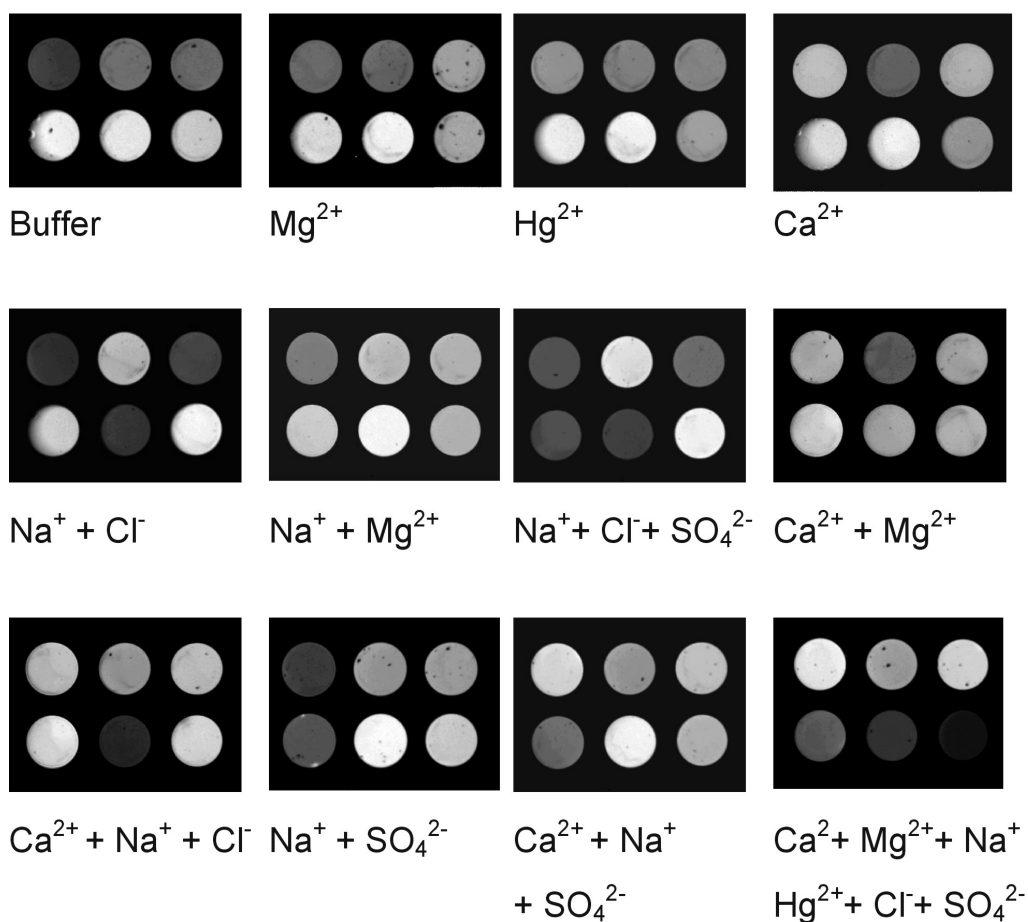
Fig. 5.8. The basic data sets for primary evaluation: Gray-scale pictures of the imaged arrays in presence of the ion mixtures given under the spots. The uniformity of the gray distribution of the spots indicate that local intensity variations have been successfully referenced out by using the DLR method.
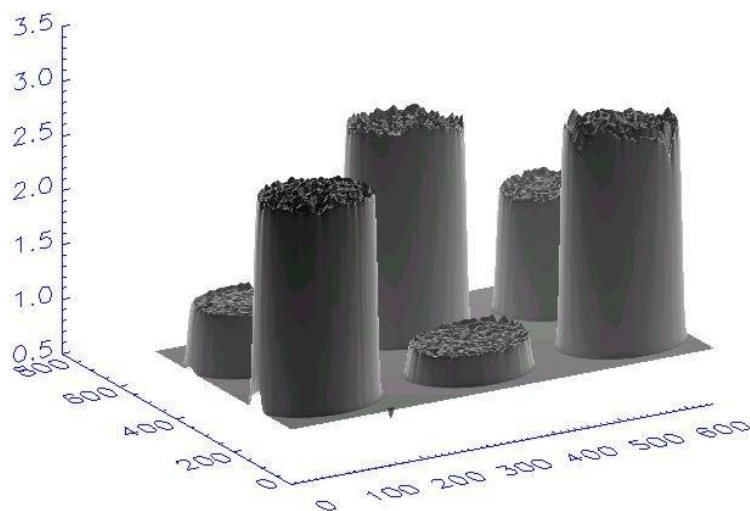
Fig 5.9. *Surface plot of the gray-scale image obtained for a solution containing sodium(I) and chloride.*

For the purpose of demonstration the sensor spots were considered as on/off switches, even though the spectral data contain quantitative information. High and low luminescence intensity can be distinguished by setting threshold values, so that the complex image data can be scaled down into a simple on/off pattern. On exceeding the threshold limit, the color displayed is made to change from blue to yellow. As shown in Figure 5.10, a characteristic pattern for the respective ion mixtures is obtained. Depending on the interaction between ion and indicator, however, fluorescence can be enhanced (calcium(II), sodium(I), magnesium (II)) or quenched (sulfate, chloride and mercury(II)). Therefore, strong luminescence does not necessarily imply presence of an ion, but its absence. The different interactions between ion and analyte were taken in consideration for the array-layout. In the first row the fluorescence is enhanced in presence of the respective ion, while in the second fluorescence is quenched. Hence, a yellow color in the first row indicates presence of the ion and a blue color absence. In the second row the inverse coloring is observed.
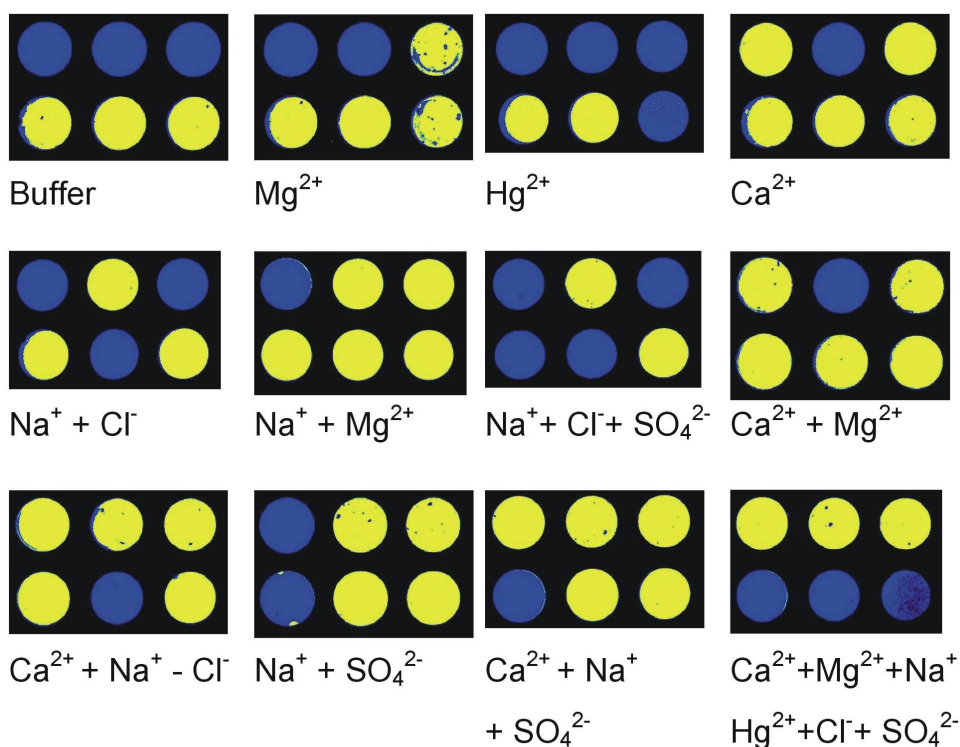
Fig 5.10. *Pseudo-color representation after defining threshold values. Yellow coloration of the spots signals high and blue low luminescence. Depending on the interaction of indicator and analyte, in the first row yellow indicates presence and blue absence, while in the second row blue indicates presence and yellow absence.*

The interpretation of the achieved pattern is rather sophisticated. For the sake of simplicity, the coloring of the spots row in Figure 5.10 (where the presence of an ion is accompanied by low luminescence) were inverted. This leads to an unambiguous on/off pattern. In the pseudo-color representations of Figure 5.10, the so-called traffic light colors green and red signal presence and absence. Note that the ion concentrations were chosen in order to demonstrate the feasibility of the scheme and do not necessarily reflect concentrations found in other situations.

As can be seen from Fig. 5.11, the resulting arrays can clearly differentiate between solutions containing magnesium(II), mercury(II), sulfate, chloride and partly sodium ions. On the other side, calcium(II) interferes in the detection of magnesium due to poor probe selectivity. Consequently, solutions containing calcium(II) (or calcium(II) and magnesium(II)) cannot be discerned. However, this can be improved by evaluating the manifold information of the gray-scale pictures with chemometric tools, e. g. regression models or artificial networks.
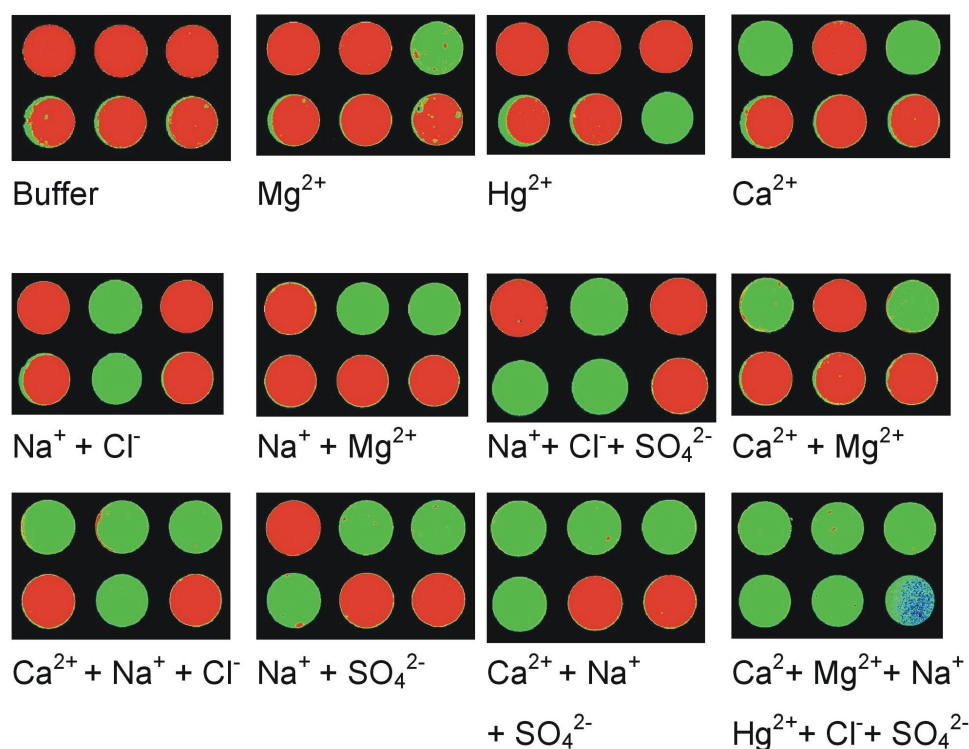
Fig. 5.11. *Typical on/off pattern. Green indicates the presence of an ion, while red indicates its absence.*

5.5. Conclusion

A novel type of sensor array was demonstrated that has high flexibility and is easily prepared. The uniform scheme allows extension of the array by adding further indicators (6 wells from 96 possible were used here) if they match the spectral properties of the system. It is a first step in the development of a multi-analyte microtiterplate for the use in environmental analysis. In addition to the analytical information gained from physically immobilised indicators, the number of parameters can be extended by integration of existing sensors, e.g. oxygen, pH, carbon dioxide, ammonia and nitrate. A further step is the implementation of established chemometrics methods in order to process data of less selective indicators, potential interferents and competing natural chelators. Such an approach is presented in the following chapter.

Additionally, the employment of the imaging scheme, enables to recognize all desired analytical information at a glance, since a multitude of parameters can be collected in one

picture. This can be advantageous for a numerous fields of application. They include the analysis of environmental samples, drinking water, biological fluids and the determination of calcium which is extremely important in studying cellular interactions and in high throughput screening. In particular, the scheme takes it full advantage when turbid or colored samples are to be analyzed.

5.6. References

[1]　B. J. Doleman, R. D. Sanner, E. J. Severin, R. H. Grubbs, N. S. Lewis, *Use of compatible polymer blends to fabricate arrays of carbon black-polymer composite vapor detectors,* Anal. Chem., **70** (13), 2560 (1998).

[2]　T. Eklov, I. Lundström, *Distributed Sensor System for Quantification of Individual Components in a Multiple Gas Mixture*, Anal. Chem., **71**, 3544 (1999).

[3]　J. W. Grate, S. J. Patrash, S. N. Kaganovet, M. H. Abraham, B. M. Wise, N. B. Gallagher, *Inverse least-squares modeling of vapor descriptors using polymer-coated surface acoustic wave sensor array responses*, Anal. Chem., **73**(21), 5247 (2001).

[4]　J. W. Gardner, H. V. Shurmer, T. T. Tan, *Application of an electronic nose to the discrimination of* **coffees**, Sens. Actuators B, **6**, 71 (1992).

[5]　C. Di Natale, F. A. M. Davide, A. D´Amico, G. Sberveglieri, P. Nelli, G. Faglia, C. Perego, *Complex chemical pattern recognition with sensor array: the discrimination of vintage years of* **wine**, Sens. Actuators B, **25**, 801 (1995).

[6]　A. V. Legin, A. Smirnova, A. Rudnitskaya, L. Lvova, E. Suglobova, Y. Vlasov, *Chemical sensor array for multicomponent analysis of biological liquids*, Anal. Chim. Acta, **385**, 131 (1999).

[7]　A. V. Legin, Y. G. Vlasov, A. M. Rudnitskaya, E. A. Bychkov, *Cross-sensitivity of chalcogenide glass sensors in solutions of heavy metal ions***,** Sens. Actuators B, **34**, 456 (1996).

[8]　N. A. Rakow, K. S. Suslick, *A colorimetric sensor array for odour visualization,* Nature, **406**, 710 (2000).

[9]　A. Goodey, J. J. Lavigne, S. M. Savoy, M. D. Rodriguez, T. Curey, A. Tsao, G. Simmons, J. Wright, S-J. Yoo, Y. Sohn, E. V. Anslyn, J. B. Shear, D. P Neikirk, J. T. McDevitt, *Development of Multianalyte Sensor Arrays Composed of Chemically*

Derivatized Polymeric Microspheres Localized in Micromachined Cavities, J. Am. Chem. Soc., **123,** 2559 (2001).

[10] J. A. Ferguson, F. J. Steemers, D. R. Walt, *High-Density Fiber-Optic DNA Random Microsphere Array*, Anal. Chem.,**72**, 5618 (2000).

[12] C. Di Natale, D. Salimbeni, R. Paolesse, A. Macagnano, A. D´Amico, *Porphyrins-based opto-electronic nose for volatile compounds detection*, Sens. Actuators B, **65**, 220 (2000).

[13] C. A. Rowe, L. M. Tender, M. J. Feldstein, J. P. Golden, S. B. Scruggs, B. D. MacCraith, J. J. Cras, F. S. Ligler, *Array Biosensor for Simultaneous Identification of Bacterial, Viral, and Protein Analytes*, Anal. Chem., **71**, 3846 (1999).

[14] K. L. Michael, L. C. Taylor, S. L. Schultz, D. R. Walt, *Randomly Ordered Addressable High-Density Optical Sensor Arrays*, Anal. Chem., **70**, 1242 (1998).

[15] M. Dellian, G. Helmlinger, F. Yuan, R. K. Jain, *Fluorescence Ratio Imaging of Interstitial pH in Solid Tumors: Effect of Glucose on Spatial and Temporal Gradients*, Br. J. Cancer, **74**, 1206 (1996).

[16] T. W. J. Gadella, A. von Hoeck, A. J. W. G. Visser, *Construction and Characterization of a Frequency-Domain Fluorescence Lifetime Imaging Microscopy System*, Cell. Mol. Biol., **44**, 261 (1996).

[17] I. Klimant, Ch. Huber, G. Liebsch, G. Neurauter, A. Stangelmayer, O. S. Wolfbeis, in *New Trends in Fluorescence Spectroscopy*, B. Valeur, J. C. Brochon (eds.), Springer Verlag, Berlin (2001).

[18] G. Liebsch, I. Klimant, C. Krause, O. S. Wolfbeis, *Fluorescent Imaging of pH with Optical Sensors Using Time Domain Dual Lifetime Referencing*, Anal. Chem., **73**, 4354 (2001).

[19] G. Liebsch, I. Klimant, B. Frank, G. Holst, O. S. Wolfbeis, *Luminescence Lifetime Imaging of Oxygen, pH, and Carbon Dioxide Distribution Using Optical Sensors*, Appl. Spec., **54**, 548 (2000).

[20] R. P. Haughland, *Handbook of Fluorescent Probes and Research Products*, Molecular Probes, Eugene (2001).

[21] C. T. Lin, W. Boettcher, W. Chou, C. Creutz, N. Sutin, J. Am. Chem. Soc., *Mechanism of the Quenching of the Emission of Substituted Polypyridineruthenium(II) Complexes by Iron(III), Chromium(III) and Europium(III) Ions*, **98,** 6536 (1976).

[22] I. Klimant, O. S. Wolfbeis, *Oxygen-Sensitive Materials Based on Silicon-Soluble Ruthenium Complexes,* Anal. Chem., **67,** 3160 (1995).

[23] A. Juris, V. Balzani, F. Barigelletti, S. Campagna, P. Belser, A. von Zelewsky, *Ru(II) Polypyridine Complexes: Photophysics, Photochemistry and Chemiluminescence,* Cood. Chem. Rev., **84**, 85 (1988).

[24] J. M. Kürner, I. Klimant, C. Krause, H. Preu, W. Kunz, O. S. Wolfbeis, *Inert Phosphorescent Nanospheres as Markers for Optical Assays*, Bioconjugate Chem., **12**, 883 (2001).

Chapter 6

A Step Towards Imaging of Cross-Reactive Arrays for Metal Ions Evaluated by an Artificial Neural Network

A cross-reactive array in the microtiterplate format for the determination of calcium(II), copper(II), nickel(II), zinc(II) and cadmium(II) is described. The fluorescence of 8 indicators was imaged with a CCD-camera applying the time-resolved dual lifetime referencing (t-DLR) scheme. The unselective response of the indicator generates a characteristic pattern, which was analyzed by an artificial neural network. In a first approximation the model was able to predict a trend for solution containing high concentrations. The microtiterplates were mapped with a modified set-up. Each well was illuminated by one LED, which allows the detection in the nM-range without amplification.

6.1. Introduction

Conventional sensor approaches make use of specific interaction between the analyte and the receptor ("lock-and-key principle"). In recent years, a new sensing strategy emerged that employs an array of unspecific sensors [1,2]. This was inspired by the excellent performance of the biological olfactory systems, which are known to possess both broad-band response and a remarkable sensitivity. The mammalian olfactory system achieves these abilities by using a large array of cross-reactive receptor cells which are not highly selective. In fact, one receptor responds to many analytes and many receptors respond to any given analyte [3,4]. The receptors signal the presence of an odor and spatial and temporal patterns are generated by the neuronal circuitry of the brain. These patterns contain molecular identity information, which are thought to be used to recognize the odorant [5,6].

In the last decade, the sensing principle of the mammalian olfactory system was transferred to a manifold of approaches including electrochemical, catalytic, conductive polymers, piezoelectronic and surface acoustic wave sensors [7]. Few publications dealt with optical sensor array for vapours, so called opto-electronic noses [8-13]. Furthermore, cross-reactive sensor arrays for liquids were developed, so called electronic tongues. Potentiometric

schemes were applied to determine heavy metal ions [14,15] and to discriminate beverages [16]. Heavy metal ions were also determined by fluorescent sensor arrays [17,18]. Goodey et al. describe attempts mimicking the mammalian tongue, by sensing the five primary tastes: sweet, sour, salty, pungency and bitter, which contribute to the sense of taste [19].

All these approaches make use of a collection of unspecific sensors with high chemical diversity. The identification of the analyte is achieved by the recognition of a distinct pattern of responses providing a fingerprint of the analyte (see Figure 6.1). The obtained patterns are evaluated by various models of data analysis including principal component analysis (PCA), factor analysis, multiple linear regression (MLR), artificial neural networks (ANN), linear discriminant analysis (LDA) and nearest-neighbors (NN) classifications [20]. Herein, neural network algorithms, which benefit of the development in microcomputers of the last decade, emerged to be the most accurate classifiers for typical chemical sensor array data, even though a large data set is required for training [21].
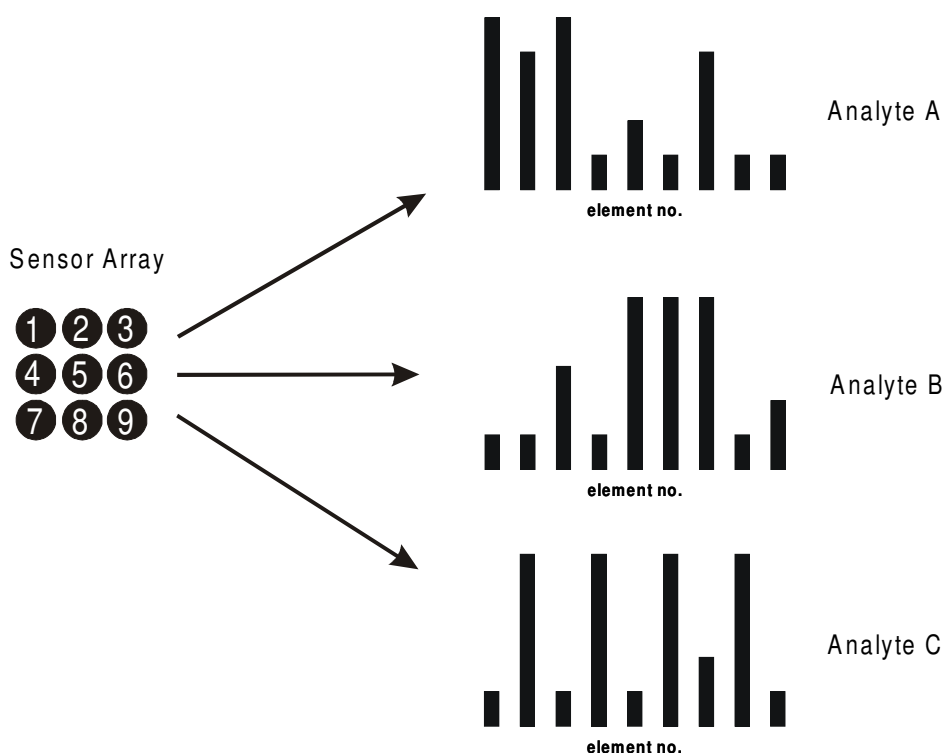
Fig. 6.1. Response of a sensor array, comprised of a set of incrementally different but nonspecific elements. The characteristic patterns generated for an analyte are identified by various possible chemometric algorithms.

Numerous fluorescent chelators for the determination of metal ions are known [22]. In environmental analysis, the fluorimetric determination of heavy metal ions is accompanied by

interference by other metal ions due to the lack of specific indicators. The approach presented here takes advantage of the poor probe selectivity forming cross-reactive arrays of unselective indicators. Selectivity is gained analyzing the obtained response pattern with an artificial neural network. This was realized by the extension of the array concept introduced in chapter 5 to a cross-reactive array for the determination of calcium(II), copper(II), nickel(II), cadmium(II) and zinc(II) mixtures. Again, arrays were prepared in simple steps in the widely accepted microtiterplate format and imaged with a CCD-camera, which in contrast to the sensor array described by Prestel et. al. [18] requires no sophisticated instrumentation.

Figure 6.2. shows an image of a microtiterplate containing various indicators ion mixtures published by Molecular Probes (MP) in November 2001 [23]. The idea is based on the array concept introduced in chapter 5 and was presented by myself at *7th Conference on Methods and Applications of Fluorescence* in Amsterdam in mid September 2001 [24]. Molecular Probes scanned the microtiterplate with an conventional image reader, which is based on intensity measurements. The image displays a heterogeneous luminescence distribution of the wells. As mentioned above, time resolved measurements are superior to intensity measurements. Hence, the approach presented in this chapter applies time resolved imaging using the t-DLR scheme as described in chapter 5.2. However, the imaging set-up described there lacks of insufficient illumination in case of extending the imaged area to the microtiterplate in whole (i.e. 96 wells instead of 6 wells). For the application of a cross-reactive array this was improved by using a self-developed 96-LED array allowing to illuminate each well with one LED.
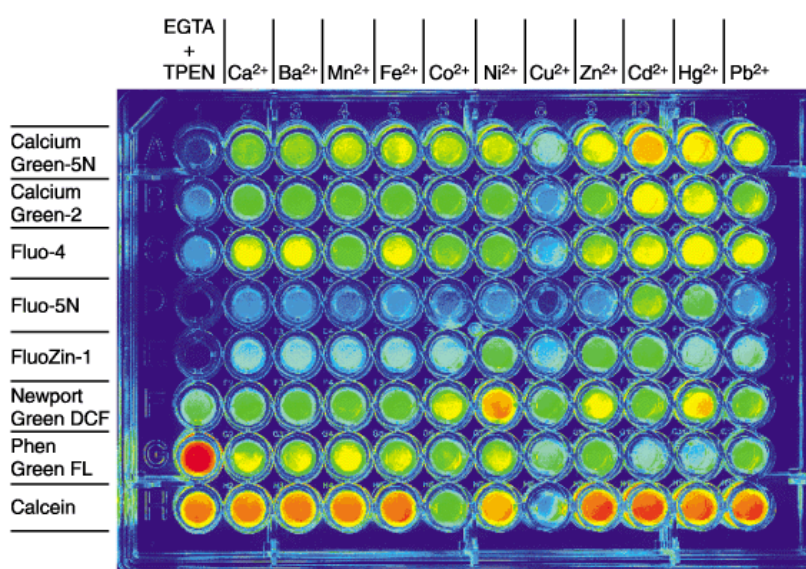
Fig. 6.2. *Pseudo-color picture of a microtiterplate containing various indicators and 1 µM ion solution. This image was recorded and published by Molecular Probes [23].*

6.2. Artificial Neural Networks

Artificial neural networks (ANN) are mathematical constructs that try to mimic way of the computation of the brain, which is entirely different from the conventional digital computer. Nerve cells (neurons) are the structural constituents of the brain. However, neurons are five or six orders of magnitude slower than silicon logic gates. This slow rate of operation is compensated by a truly staggering number of neurons with massive interconnections. In the human cortex is estimated to be the order of 10 billion neurons and 60 trillion synapses or connections. ANNs try to simulate the principles of biological neural systems using artificial neurons. The three basic elements of a neural model are (i) synapses or connecting links (each of which is characterized by a weight or strength of its own), (ii) an adder (for summing up the input signals), (iii) an activation function (limiting the amplitude of the output of neuron). A schematic representation of a model neuron is shown Figure 6.3 [25,26].
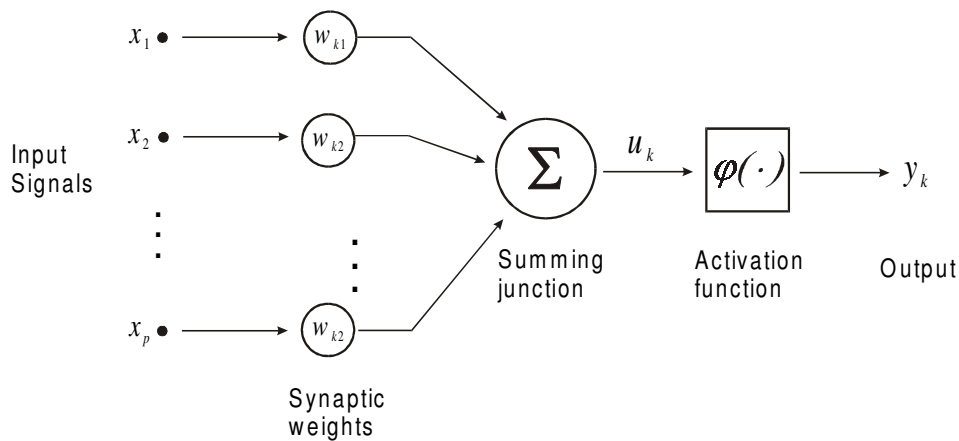
Fig. 6.3. *Nonlinear model of a neuron. A signal x_j at the input of synapse j connected to neuron k is multiplied by the synaptic weight w_{kj}. The weighted input signals are summed up in an adder (here linear combiner). The activation function $\varphi(.)$ limits the amplitude of the output.*

In mathematical terms the model can be described by the following equations:

$$u_k = \sum_{j=1}^{p} w_{kj} x_j \qquad\qquad 6.1$$

and

$$y_k = \varphi(u_k - \Theta_k) \qquad\qquad 6.2$$

where x_1, x_2 ..., x_p are the input signals; w_1, w_2, ..., w_{kp} *are the synaptic weights of neuron k*; u_k is the linear combiner output; Θ_k is the threshold lowering the net input of the activation function; y_k is the ouput signal of a neuron.

Pattern recognition for sensor arrays usually apply multilayer feedforward networks [21]. These networks consists of a set of sensory units (source nodes) that constitute the input layer, one or more hidden layers of computation nodes, and an output layer for computation nodes. The input signal propagates through the network in a forward direction, on a layer-by-layer basis. These neural networks are commonly referred to as mutlilayer perceptrons (MLP). Figure 6.4 give a schematic representation. This popular class of networks employs the error back propagation algorithm. The main principles of this algorithm are: (i) the error of the output signal of a neuron is used to adjust its weights such that the error decreases, and (ii) the error in the hidden layers is estimated proportional to the weighted sum of the (estimated) errors in the layers above.
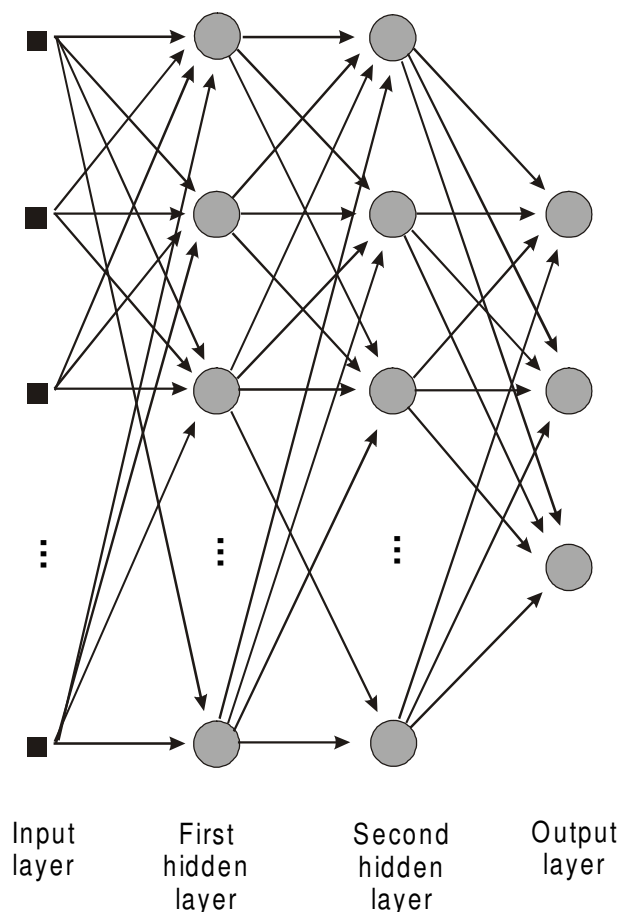
Fig. 6.4. *Architectural graph of a multilayer perceptron with two hidden layers.*

6.3. Material and Methods

6.3.1. Chemicals and Solutions

Fluorescent probes FluoZin-1, BTC-5N, Phen Green, Newport Green, Oregon Green Bapta 5N, Fluo-5N and carboxyfluorescein were obtained from Molecular Probes Europe BV (Leiden, The Netherlands). Calcein and Lucifer Yellow were purchased from Fluka (Buchs, Switzerland). The phosphorescent reference beads PD containing ruthenium(II)-4,7-diphenyl-1,10-phenanthroline were a friendly gift from Presens (Regensburg, Germany). Inorganic salts of analytical-reagent grade were from Merck (Darmstadt, Germany), imidazole buffer from Sigma (Vienna, Austria) and black microtiterplates (96 wells) with transparent bottom from Greiner (Frickenhausen, Germany).

Aqueous solutions were prepared from doubly distilled water. Stock standard solutions of 1000 µM metal ion concentration were prepared by dissolving the respective amount of the nitrate salt in 5 mM buffer solution. From this solutions were prepared containing 10 and 100 µM of the respective metal ion by dilution with the buffer solution.

Buffer solution was prepared by dissolving the respective amount of imidazole in doubly distilled water. The pH was adjusted to pH 7 adding hydrochloric acid, monitored by use of a digital pH-meter (Knick, Berlin, Germany) calibrated with standard buffers of pH 7.00 and 4.00 at 21±1 °C.

6.3.2. Preparation of Arrays

Various ion mixtures were prepared by filling the wells of microtiterplates with 10 µl solutions containing 10, 100 or 1000 µM metal ion using a robotic system from Hamilton (Darmstadt, Germany) as shown in Figure 6.5. Each column contained a different mixture. Depending on the composition of the ion mixture the mixture was filled up to 90 µl with the respective volume of buffer. The source code for programming the dispensing system is given in Appendix A and B.

Assay arrays were obtained by adding 10 µl of solutions containing the fluorescent probes and PD beads to the ion mixture at the same time using a 8-channel electronic pipette. Arrays of 8 elements were arranged in columns. The concentrations of the fluorescent indicators and the PD beads after dilution in ion mixtures are given Table 6.1. After addition of the indicator/bead solutions the concentration of the each ion amount to 0, 1, 10 or 100 µM, respectively. The microtiterplates were immediately imaged after adding the indicator/bead solution.

Fig. 6.5. *The Hamilton Micro Lab S dispensing system*

Table 6.1. *Indicator concentrations after adding to various ion mixtures.*

Indicator	FluoZin-1	BTC-5N	Calcein	Lucifer Yellow
Concentration /μM	2.5	5	1	5

Indicator	PhenGreen	NewportGreen	Oregon Green BAPTA-5N	Fluo-5N
Concentration / μM	5	1	1	2.5

6.3.3. Measurements of Fluorescence Spectra

Excitation and emission spectra of the indicators and the reference particles were recorded with a Varian Carry Eclipse Spectrofluorimeter equipped with a microtiterplate accessory, as shown in Figure 5.2 in chapter 5.3.3.

6.3.4. Imaging Set-Up

A gated CCD camera and a pulsed LED excitation light source were used for time-resolved imaging of the emission intensity as described in chapter 5.3.4 and by Liebsch et al. [27]. The set-up was modified using a array of 96 LED in order to illuminate every well of the microtiterplate by one LED, and different filter for excitation and emission. The LEDs (λ_{max}= 470 nm, NSPB, Nichia, Nürnberg, Germany) were arranged fitting exactly to wells of a 96-well microtiterplate as shown in Figure 6.6. This new LED array, which was developed in house, offers high flexibility, because the LEDs were pined to the electronic board, which enables a quick exchange by LEDs emitting light of different wavelengths.
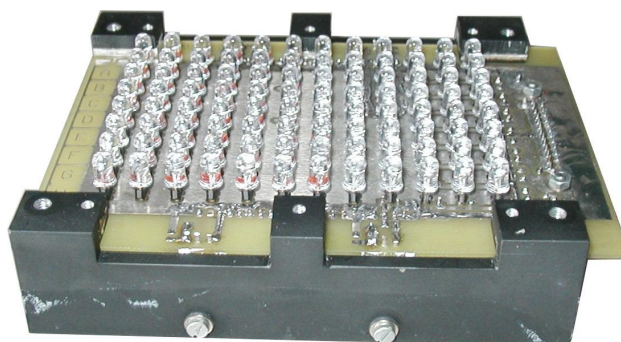
Fig. 6.6. *Picture of the LED-array with 96 LEDs arranged in exact distance of the wells of a 96-well microtiterplate for single illumination of each well by one LED. The LEDs can be quickly changed to LED of other wavelengths.*

The array was covered with a combination of dichroic medium blue filter (Linos Photonics, Göttingen, Germany) and a shortpass filter BG12 (Schott, Mainz, Germany) for excluding the red fraction of the LED emission. Short pulses (5 µs) of blue excitation light hit the microtiterplate containing the respective probes in its wells. The emitted light of each well was collected by a light-guiding adapter to an area of approximately 40x80 mm. This is necessary because the evaluation geometry does not allow to image the area of a whole microtiterplate (96 wells) simultaneously (with the standard set-up a maximum segment of 4 x 5 wells can be imaged). The emission light is guided in optical fibers of 3 mm i. d. (Laser Components, Olching, Germany) between two metal plates as shown in Figure 6.7. After passing through the waveguides the emission light was filtered with a KV 550 (Schott, Mainz, Germany) and was then detected by a CCD camera. The optical path of this set-up is illustrated in Figure 6.8.

(A)   (B)
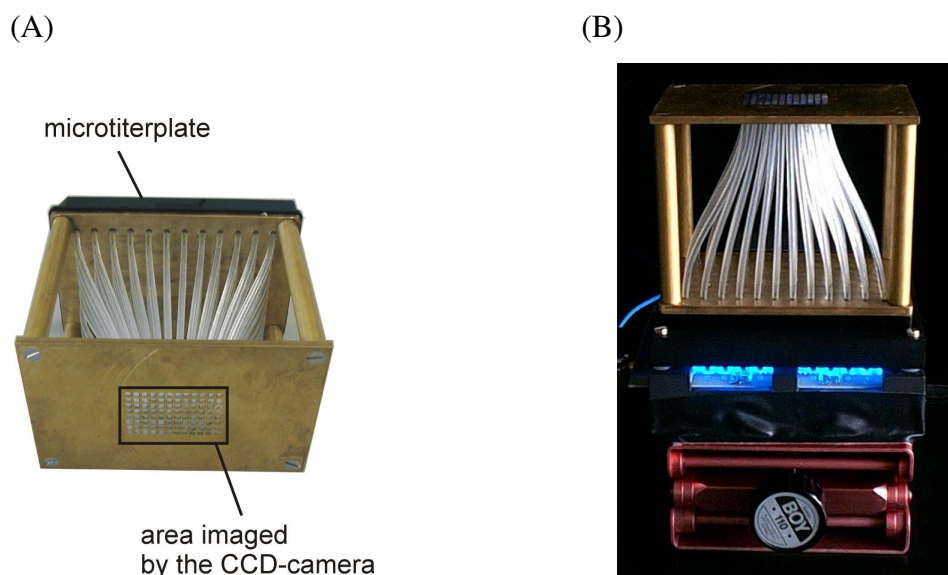
Fig. 6.7. *Light-guiding adapter for imaging of microtiterplates, which reduces the imaged area to fit the standard optics of the imaging set-up. This enables the simultaneous evaluation of 96-wells at the same time. The emission light is guided in optical fibres between two metal plates. (A) Picture of the light-guiding adapter with microtiterplate. The outlined box marks the area imaged by the camera. (B) Photograph of the combination of LED-array, microtiterplate and light-guiding adapter mounted on a laboratory lifter in order to move this device in the right position of the camera.*
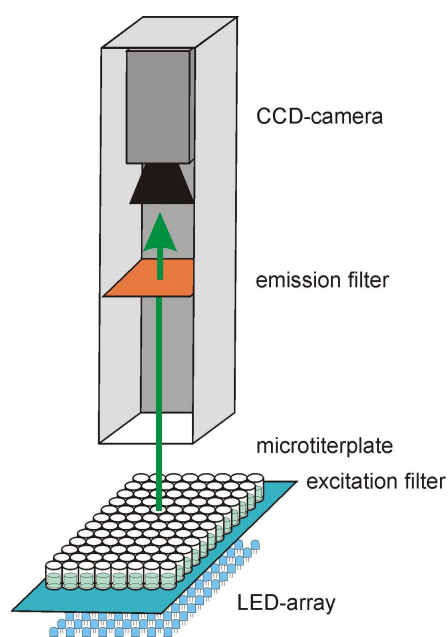
Fig. 6.8. *Schematic representation of the modified imaging set-up. The light from the LEDs passes an excitation filter combination and hits the wells of the microtiterplate. The emitted from the fluorescent indicators light is filtered by an excitation filter and is detected by the CCD-camera.*

6.3.5. Data Analysis

Data were evaluated with standard application of a multilayer perceptron (MLP). A model architecture of 8 neurons in the input layer, one hidden layer consisting of 7 neurons and 5 output signals was used. Sigmoidal nonlinearity is employed as activation function $\varphi(.)$. Specifically, the hyperbolic tangent is used, which is antisymmetric with respect to the origin and for which the amplitude lies in the range of $-1 \le y_j \le +1$. The network was adjusted by 250000 iterations. The network was trained with a learning parameter of $\eta = 0.3$ and momentum constant of $\alpha = 0.9$ according the delta rule of eq. 6.3:

$$\Delta w_{ji}(n) = \alpha \Delta w_{ji}(n-1) + \eta \delta(n) y_i(n) \qquad\qquad 6.3$$

where Δw_{ji} *(n)* is the correction applied to the weight $w_{ji}(n)$, which denotes the synaptic weight connecting the output of a neuron *i* to the input of a neuron *j* at iteration *n*. δ is the local gradient for a neuron. η is a constant that determines the rate of learning and α controls the feedback loop around $\Delta w_{ji}(n)$ [26].

6.4. Results and Discussion

6.4.1. Performance of the Modified Imaging Set-up

The set-up applied in chapter 5, was adequate to show the feasibility of time-resolved imaging of sensor arrays in microtiterplates, but lacks of poor illumination. As a result high indicator concentrations are required in order to compensate the week and heterogeneous light-field. Since the indicator/analyte interaction is a complex reaction and follows the mass-action law, indicator reactions in the lower µM-range are desired for the determination of heavy metal ions in concentration ranges set by standards and guidelines recommended by various institutions (see chapter 1.2). The set-up originally designed for evaluation of highly indicator loaded sensor foils [28] was modified to obtain excitation light of higher intensity. This was achieved by illuminating each well of a 96-well microtiterplate with a one LED, respectively.

Fluorescence is usually measured in a rectangular arrangement of excitation and emission light, which minimizes the amount of excitation light in the emission [29]. This is in contrast to the arrangement chosen here, where the light source and detector are inline. Therefore, excitation and emission filters with appropriate transmission characteristics are required, which exclude an overlap of the excitation and the emission. The optimum performance was obtained by the combination of the short-pass filters medium blue and BG12 together with a long-pass filter KV550. The spectral properties of the filtered LED-light as well as the transmission characteristics of the emission filter are shown in Figure 6.7.

The performance of the set-up was tested by imaging microtiterplates containing solutions of carboxyfluorescein buffered to pH 4 and pH 10. Carboxyfluorescein was chosen as the model fluorophore because (a) many ion probes are derivatives of this compound, (b) its quantum yield ($\Phi=0.92$) and (c) it is widely used. The excitation and emission spectra of carboxyfluorescein and PD beads are given in Figure 6.9. Both dyes can be excited using the LED/filter combination and the emission properties overlap the transmission spectrum of the long-pass emission filter. Figures 6.10A and 6.10B show the intensity pictures of solutions containing carboxyfluorescein in concentrations from 1 to 1000 nM buffered to pH 4 and pH 10 (no reference was added). The pictures were recorded with different resolutions of the CCD-chip (160x120 and 80x60 pixels). Figure 6.10A indicates a clear differentiation of a 10 nM carboxyfluorescein at pH 4 and pH 10 with negligible noise. Furthermore, the limit of detection (LOD) was found at a concentration of 1 nM as shown Figure 6.10B. Although the fluorescence was not excited and detected at the maxima, a detection in the lower nanomolar range is possible. This is remarkable because the fluorescence signal was obtained without

any amplification, which can be attributed to the high intensity of the excitation light. In case of using special designed emission bandpassfilters instead of the standard filter the signal could be even considerably increased (see Fig. 6.9).

The intensity distribution of one well in Figures 6.10A and 6.10B show inhomogeneities caused by the heterogeneous light-field of one single LED. Figure 6.10C displays the resulting gray-scale pictures after addition of the reference beads. The homogeneity of the gray distribution for each spot indicates the successful referencation of the inhomogeneities caused be the heterogeneous light field of the LED. The gray-scales of the obtained spots in Figure 6.10C indicate a clear differentiation of 10 nM carboxyfluorescein at pH 4 and pH 10. This is underlined by the pseudo-colour representation in Figure 6.10D. The differentiation of 1 nM carboxyfluorescein failed due bad signal to noise ratio.
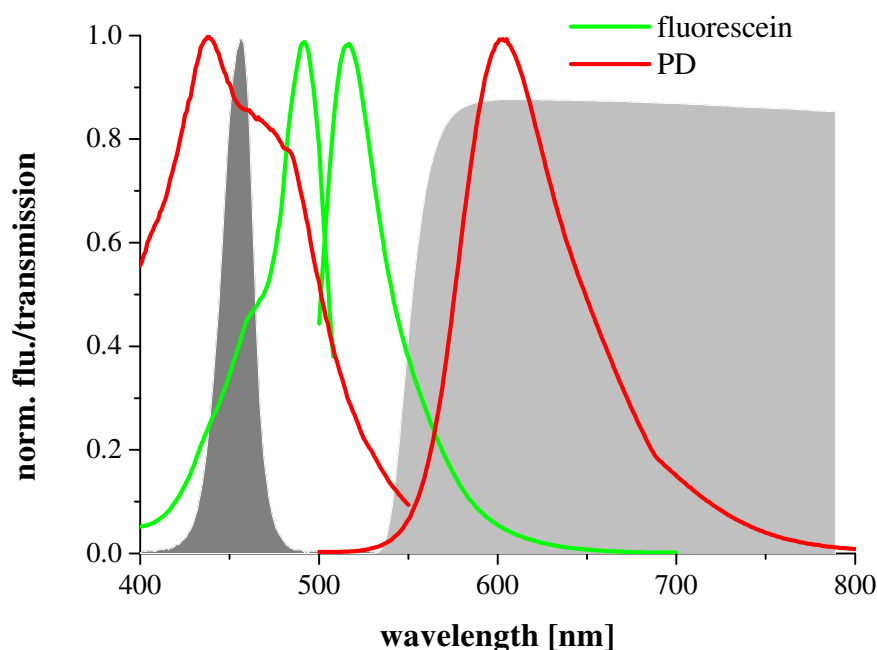
Fig. 6.9. Excitation and emission spectra of carboxyfluorescein solution buffered to pH 10 (green) and PD (red). The gray areas represents the optical properties of the imaging setup. The dark gray area gives the spectrum of the excitation light of a LED combined with a BG12 and dichroic medium blue filter. The light gray area displays the transmission characteristics of the long-pass filter (KV550) and simultaneously represents the emission signal detected by the CCD-camera.
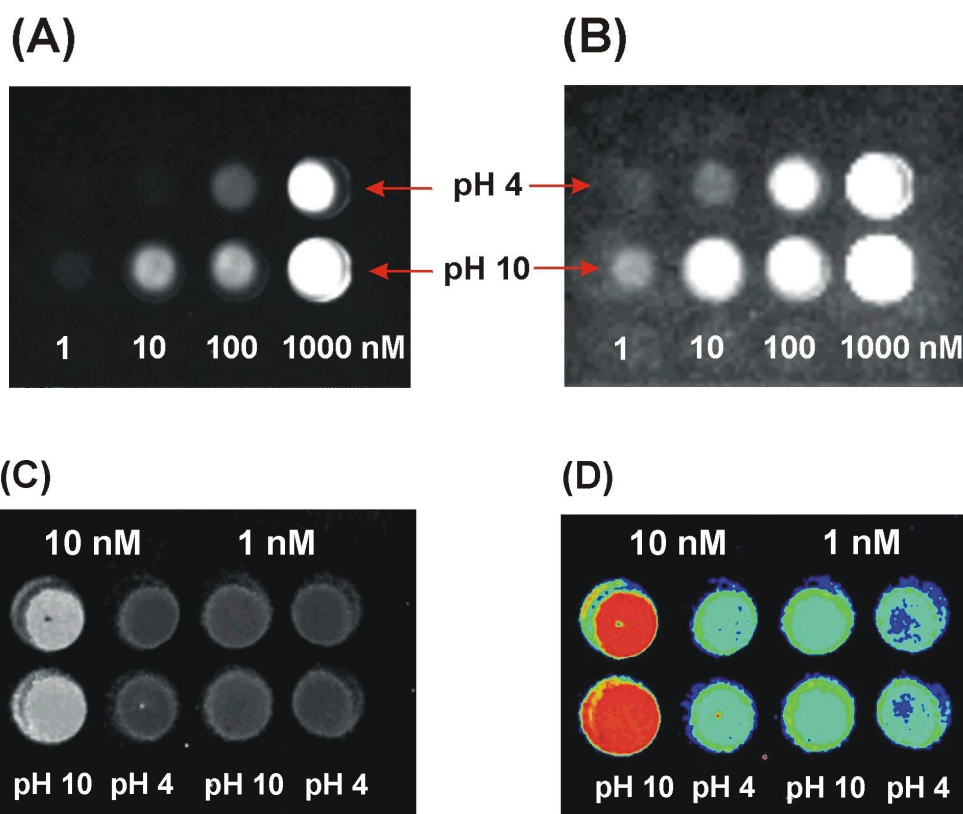
Fig. 6.10. *Images illustrating the performance. (A) Intensity picture of carboxyfluorescein solutions buffered to pH 4 and 10 contained in the wells of microtiterplates. Pictures were recorded with a resolution of 160x120 pixels, (B) Intensity picture at a resolution of 80x60 pixels. The signal obtained for 1 nM is the lowest signal to be detected (C) t-DLR referenced picture after adding the reference beads. (D) Pseudo-colour representation of picture (C).*

6.4.2. Choice of indicator

In contrast to common sensing schemes, where poor selectivity is a severe drawback, the cross-reactive approach makes use of indicators with unspecific interaction to the analyte. The main requirements to be fulfilled by the indicators for use in the cross-reactive array concept are the response to a minimum of two target ions and a response of high diversity. Furthermore, indicators were selected meeting the following criteria: (a) unselective response to the divalent cations calcium(II), copper(II), nickel(II), zinc(II) and calcium(II) in the µM-range, (b) indicator and reference luminophore are excitable at a single band of wavelength due a strong overlap of the excitation spectra (note that LEDs can be employed emitting light in the range from 400 to 470 nm), (c) decay time are in the nanosecond range, (d) high quantum yield, and (e) good water solubility.

FluoZin-1, BTC-5N, Calcein, Lucifer Yellow, Phen Green, Newport Green, Oregon Green BAPTA 5N and **Fluo-5N** were found to fulfill many of these requirements. The chemical structures are shown in Figure 6.11. All chosen indicators show excellent water-solubility and sufficient quantum yield. They can be excited with blue LEDs (λ_{max}= 470 nm) and then emit light with a maximum at >500 nm. Their fluorescence decay time is in the range of 2-6 s. The unselective but diversified response to the target ions is summarized in Table 6.1.
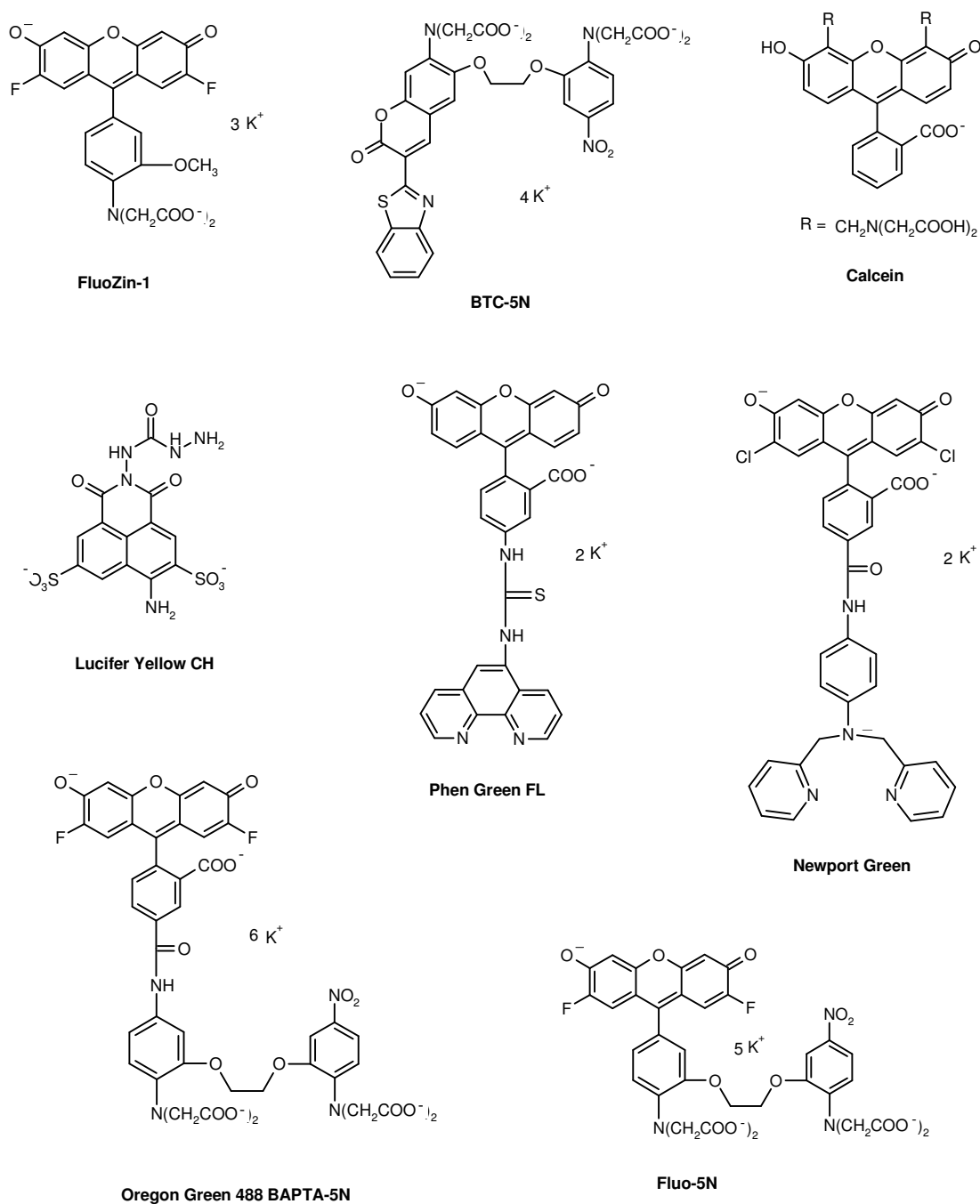
Fig. 6.11: Chemical structures of fluorescent probes used for the cross-reactive array

Table 6.1. *Response of indicators in presence of 100 µM ion solution. Blue indicates quenching and red enhancement of fluorescence.*

Indicator	Ca^{2+}	Cu^{2+}	Ni^{2+}	Zn^{2+}	Cd^{2+}
Fluo-Zin1			red	red	red
BTC-5N		blue		red	
Calcein		blue	blue		
Lucifer Yellow		blue	blue		
Phen Green		blue			blue
Newport Green			red	red	red
Oregongreen BAPTA-5N	red	blue			red
Fluo-5N	red	blue		red	

The response of the chosen indicators is illustrated by the different colors, which already implies a certain pattern. The fluorescence can be either enhanced or quenched depending on the signaling mechanism as well as the type of metal ion. Enhancement of fluorescence is obtained for probes employing photoinduced electron transfer (PET) (**Oregon Green BAPTA 5N, Newport Green**), charge transfer (CT) (**FluoZin-1**, **BTC-5N**, **Fluo-5N**) among others. The observed quenching of fluorescence of certain indicators by copper(II) and nickel(II) can be attributed to the open-shell electron configuration of these ions. Normalized excitation and emission spectra of the respective indicator in presence and absence of the target ions are shown in Figure 6.12.

(A) FluoZin-1
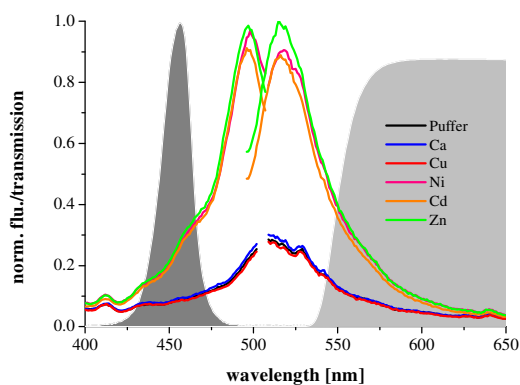
(B) BTC-5N
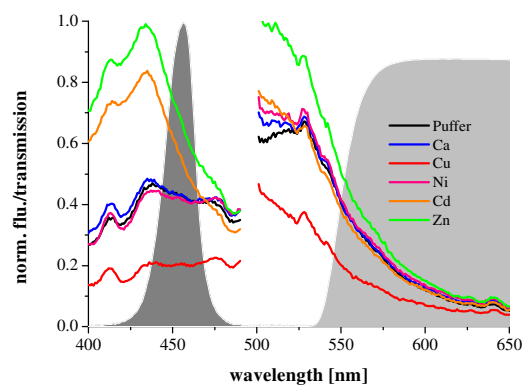
(C) Calcein
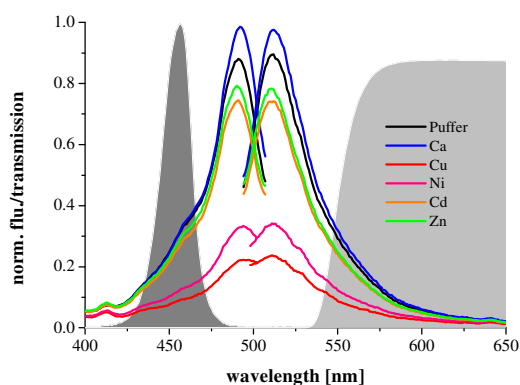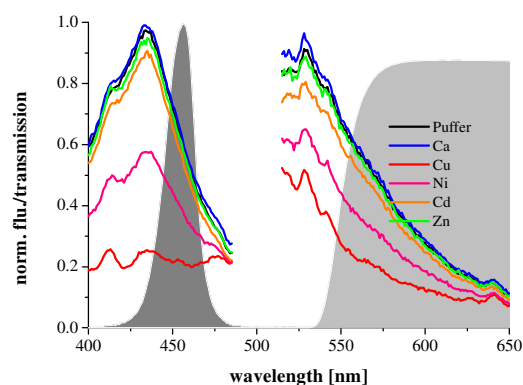
(D) Lucifer Yellow
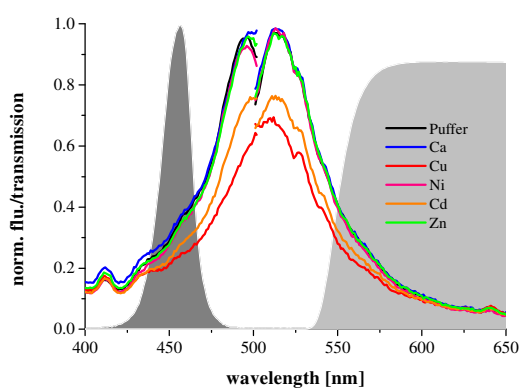
(E) Phen Green

(F) Newport Green
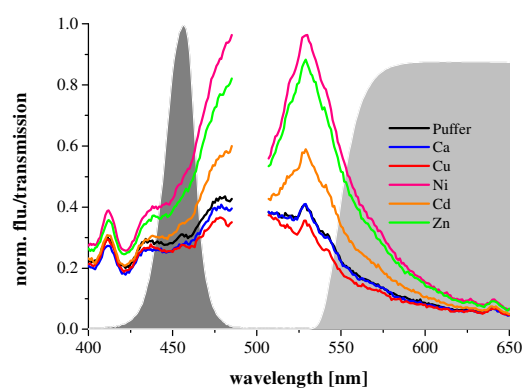
(G) Oregon Green BAPTA-5N
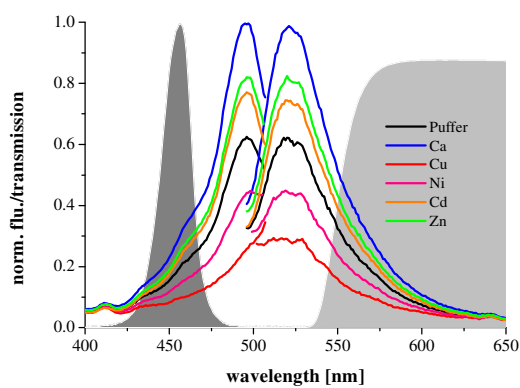
(H) Fluo-5N
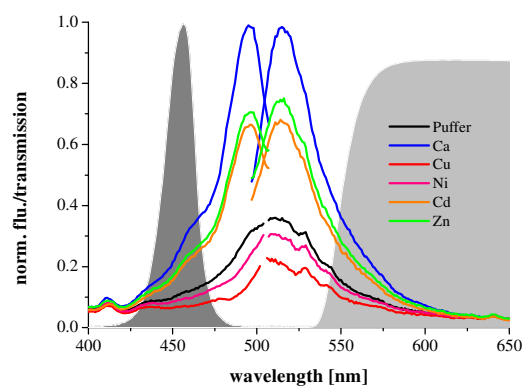
Fig. 6.12. Excitation and emission spectra of the (A) FluZin-1, (B) BTC-5N, (C) Calcein, (D) Lucifer Yellow, (E) Phen Green FL, (F) Newport Green, (G) Oregon Green BAPTA-5N, (H) Flu-5N in presence and absence of calcium(II), copper(II), nickel(II), zinc(II) and cadmium(II). Spectra were recorded at the excitation wavelength of 470 nm and the emission wavelength of 530 nm. The gray areas represent the optical properties of the imaging setup. The dark gray area gives the spectrum of the excitation light derived from a filtered LED. The light gray area displays the transmission characteristics of the long-pass filter (KV550) and simultaneously represents the emission signal detected by the CCD-camera.

6.4.3. Choice of Reference Dye

The criteria for the reference luminophore for the application in t-DLR imaging as well as the reason for the choice of PD beads were discussed in chapter 5.4.2. The spectral properties of PD beads given in Figure 6.8 indicate an overlapping with the spectrum of excitation light and the emission window.

6.4.4. Response Characteristics

After adding the indicator/reference dye solution, the wells were illuminated by LEDs and the entire microtiterplate was imaged with a CCD-camera. The interaction of the analyte ions and the indicators results in fluorescence signals which generate a characteristic pattern for different ion mixtures. Figure 6.12 displays the resulting grey-scale picture reflecting the intrinsically referenced luminescence intensity of the spots. In comparison to the microtiterplate shown in Figure 6.2 the spots show a homogeneous intensity distribution.

Sample No.	Ca^{2+} [µM]	Cu^{2+} [µM]	Ni^{2+} [µM]	Zn^{2+} [µM]	Cd^{2+} [µM]	Image
1	0	0	0	0	0	
2	1	1	1	1	1	
3	10	10	10	10	10	
4	100	100	100	100	100	
5	1	0	0	0	0	
6	0	1	0	0	0	
7	0	0	1	0	0	
8	0	0	0	1	0	
9	0	0	0	0	1	
10	10	0	0	0	0	
11	0	10	0	0	0	
12	0	0	10	0	0	

Fig. 6.12. Grey-scale pictures of a 96-mircotiterplate containing 12 cross-reactive arrays on exposure of the ion mixtures given on the left. One row represents one array consisting of 8 elements (spots). The uniformity of the gray distribution of the spots indicate that local intensity variations have been successfully referenced out by using the DLR method.

The obtained grey-scales reflect R-values (see eq. 5.1) obtained by the ratio of the two images recorded during the measurement cycle. Each spot in the images represents a signal in the response pattern of the array. For data evaluation, the values of the signal were obtained by extracting a circular area from the middle of each spot. This cut-out represents 34 single measurements obtained by the sensing elements of the CCD-chip. The average values for each spot were summarized in a matrix for the training of the ANN listed in Appendix C. Moreover, new images were generated in order to visualize the response of the array in presence of various ion mixtures. The pseudo-color picture of the signals (average values) of 12 different arrays is shown in Figure 6.13. The coloration of the spots depends on the signal intensity, resulting in a characteristic response pattern each ion mixture. Pseudo color picture of the response pattern for all investigated ion mixtures are given Figure 6.14.
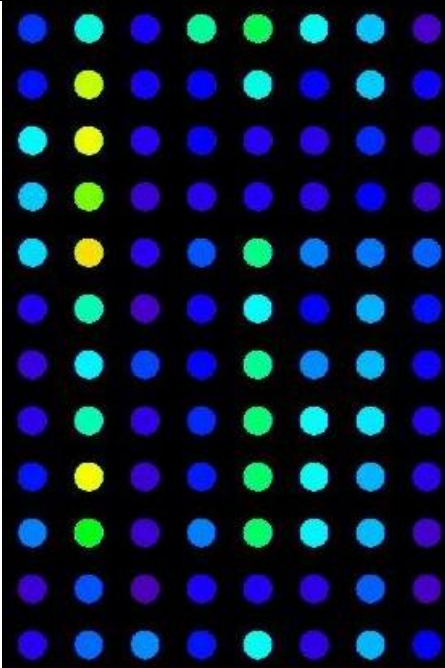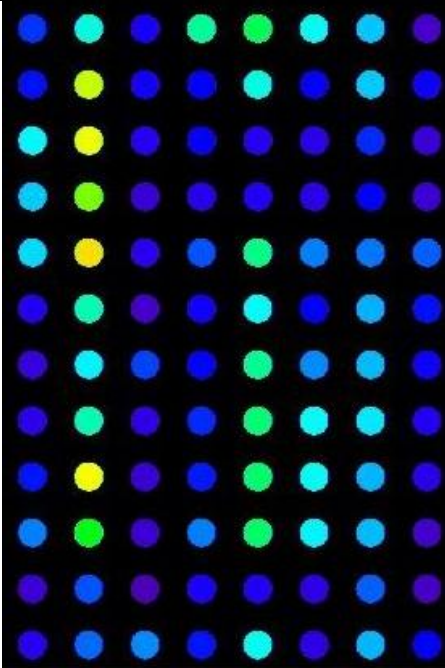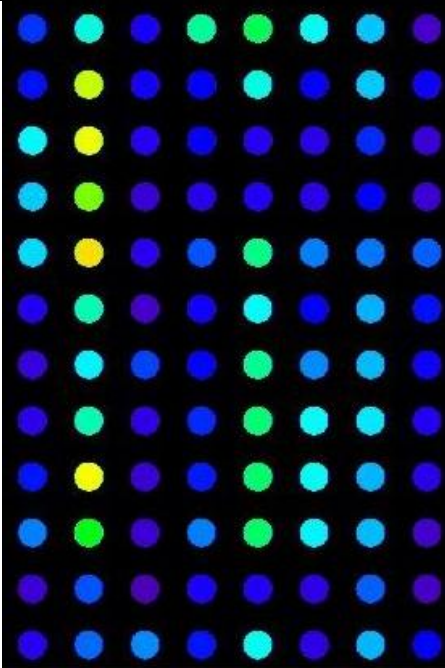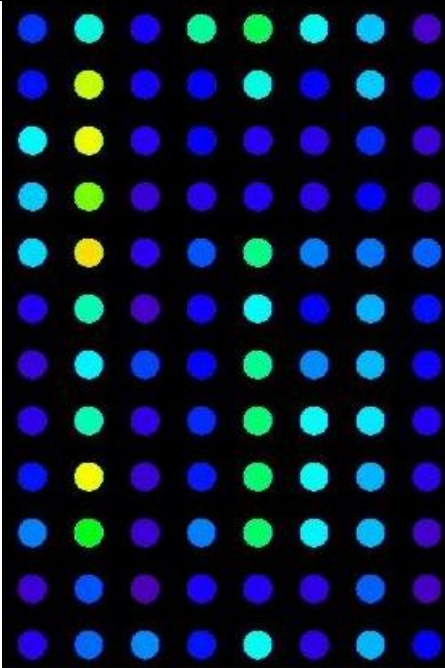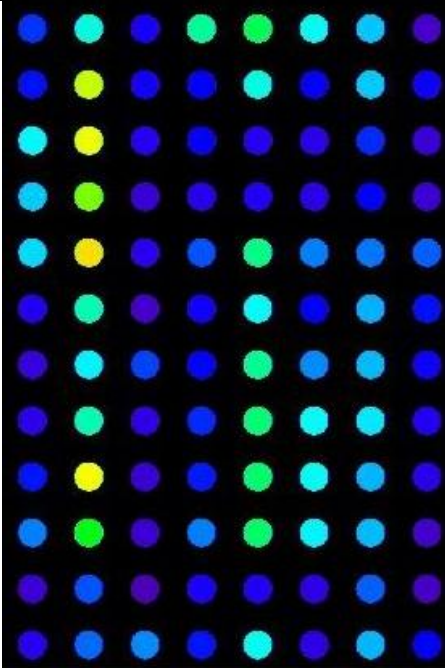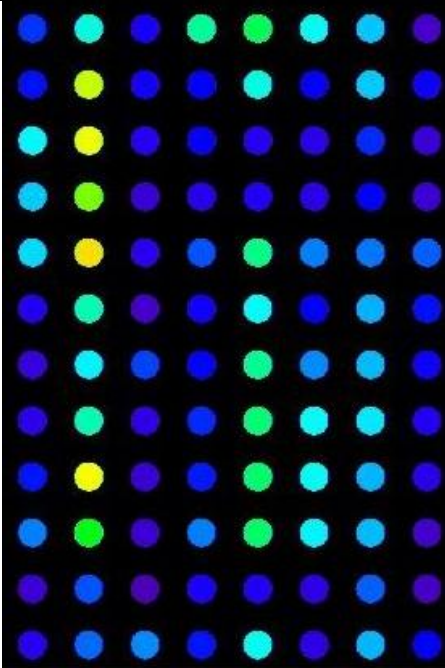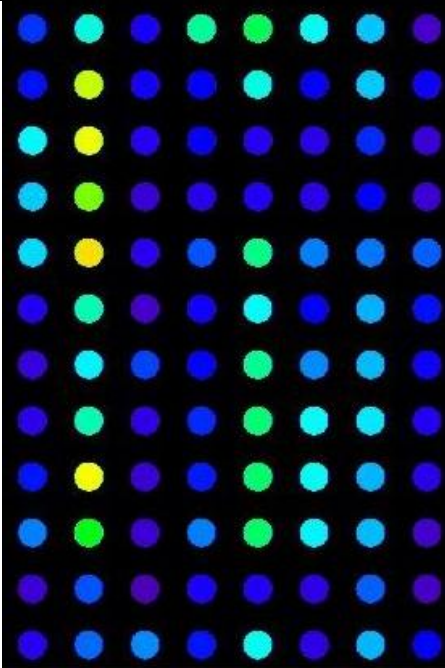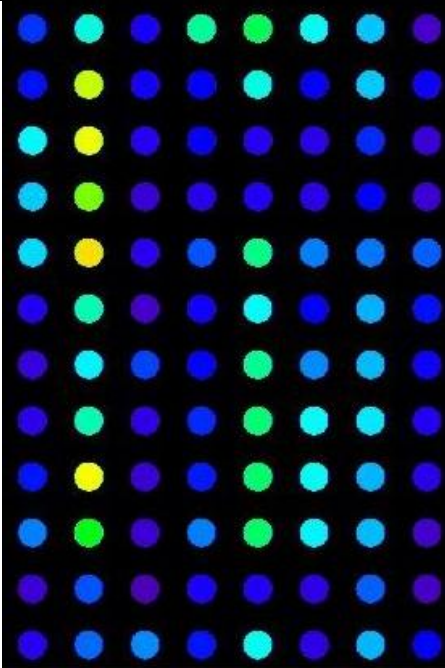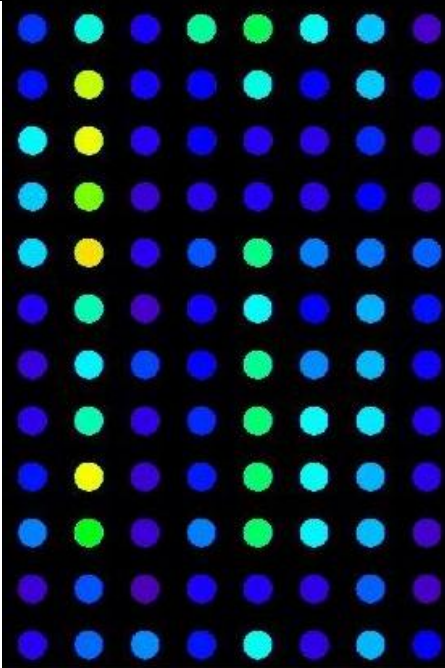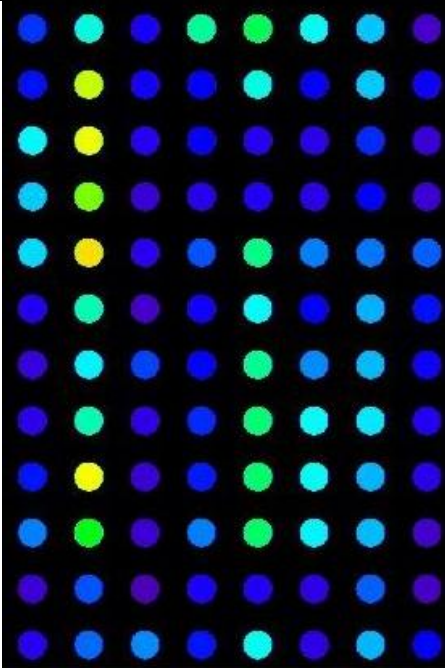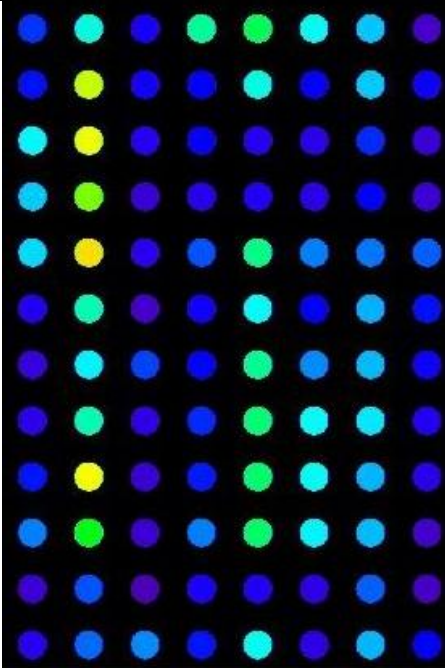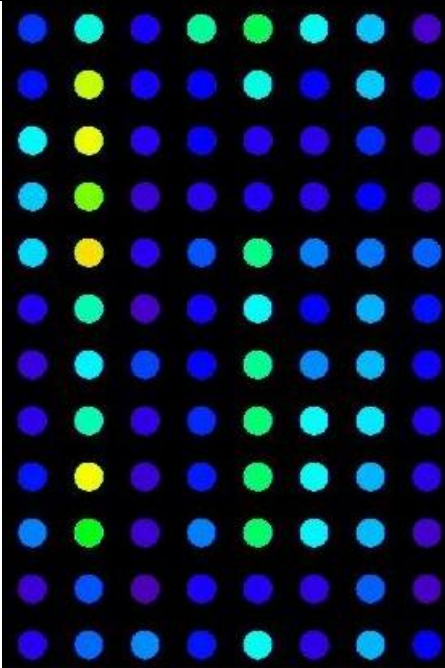
Sample no.	Ca^{2+} [µM]	Cu^{2+} [µM]	Ni^{2+} [µM]	Zn^{2+} [µM]	Cd^{2+} [µM]	Image
1	0	0	0	0	0	
2	1	1	1	1	1	
3	10	10	10	10	10	
4	100	100	100	100	100	
5	1	0	0	0	0	
6	0	1	0	0	0	
7	0	0	1	0	0	
8	0	0	0	1	0	
9	0	0	0	0	1	
10	10	0	0	0	0	
11	0	10	0	0	0	
12	0	0	10	0	0	

Fig. 6.13. *Pseudo-color picture of the characteristic response pattern of a 96-mircotiterplate containing 12 cross-reactive arrays on exposure of the ion mixtures given on the left. One row represents one array consisting of 8 elements (spots). The spots represent the average value of a extracted circular area of the spots in Figure 6.12.*

Ca	Cu	Ni	Zn	Cd
0	0	0	10	0
0	0	0	0	10
100	0	0	0	0
0	100	0	0	0
0	0	100	0	0
0	0	0	100	0
0	0	0	0	100
1	1	0	0	0
1	0	1	0	0
1	0	0	1	0
1	0	0	0	1
0	1	1	0	0
0	1	0	1	0
0	1	0	0	1
0	0	1	1	0
0	0	1	0	1
0	0	0	1	1
10	10	0	0	0
10	0	10	0	0
10	0	0	10	0
10	0	0	0	10
0	10	10	0	0
0	10	0	10	0
0	10	0	0	10
0	0	10	10	0
0	0	10	0	10
0	0	0	10	10
100	100	0	0	0
100	0	100	0	0
100	0	0	100	0
100	0	0	0	100
0	100	100	0	0
0	100	0	100	0
0	100	0	0	100
0	0	100	100	0
0	0	100	0	100
0	0	0	100	100
1	1	1	0	0
1	1	0	1	0
1	1	0	0	1
1	0	1	1	0
1	0	1	0	1
1	0	0	1	1
0	1	1	1	0
0	1	1	0	1
0	1	0	1	1
0	0	1	1	1
10	10	10	0	0

Ca	Cu	Ni	Zn	Cd
10	10	0	10	0
10	10	0	0	10
10	0	10	10	0
10	0	10	0	10
10	0	0	10	10
0	10	10	10	0
0	10	10	0	10
0	10	0	10	10
0	0	10	10	10
100	100	100	0	0
100	100	0	100	0
100	100	0	0	100
100	0	100	100	0
100	0	100	0	100
100	0	0	100	100
0	100	100	100	0
0	100	100	0	100
0	100	0	100	100
0	0	100	100	100
1	1	1	1	0
1	0	1	1	1
1	1	0	1	0
1	0	0	0	1
0	1	1	1	1
10	10	10	10	0
10	0	10	10	10
10	10	0	10	10
10	10	10	0	10
0	10	10	10	10
100	100	100	100	0
100	0	100	100	100
100	100	0	100	100
100	100	100	0	100
0	100	100	100	100
1	100	0	0	0
1	0	100	0	0
1	0	0	100	0
1	0	0	0	100
100	1	0	0	0
0	1	100	0	0
0	1	0	100	0
0	1	0	0	100
100	0	1	0	0
0	100	1	0	0
0	0	1	100	0
0	0	1	0	100
100	0	0	1	0
0	100	0	1	0

Ca	Cu	Ni	Zn	Cd		Ca	Cu	Ni	Zn	Cd	
0	0	100	1	0		100	0	10	1	0	
0	0	0	1	100		0	100	10	1	0	
100	0	0	0	1		0	0	10	1	100	
0	100	0	0	1		100	0	0	1	10	
0	0	100	0	1		0	100	0	1	10	
0	0	0	100	1		0	0	100	1	10	
1	10	100	0	0		10	100	0	0	1	
1	10	0	100	0		10	0	100	0	1	
1	10	0	0	100		10	0	0	100	1	
1	100	10	0	0		100	10	0	0	1	
1	0	10	100	0		0	10	100	0	1	
1	0	10	0	100		0	10	0	100	1	
1	100	0	10	0		100	0	10	0	1	
1	0	100	10	0		0	100	10	0	1	
1	0	0	10	100		0	0	10	100	1	
1	100	0	0	10		100	0	0	10	1	
1	0	100	0	10		0	100	0	10	1	
1	0	0	100	10		0	0	100	10	1	
10	1	100	0	0		1	10	0	0	0	
10	1	0	100	0		1	0	10	0	0	
10	1	0	0	100		1	0	0	10	0	
100	1	10	0	0		1	0	0	0	10	
0	1	10	100	0		10	1	0	0	0	
0	1	10	0	100		0	1	10	0	0	
100	1	0	10	0		0	1	0	10	0	
0	1	100	10	0		0	1	0	0	10	
0	1	0	10	100		10	0	1	0	0	
100	1	0	0	10		0	10	1	0	0	
0	1	100	0	10		0	0	1	10	0	
0	1	0	100	10		0	0	1	0	10	
10	100	1	0	0		10	0	0	1	0	
10	0	1	100	0		0	10	0	1	0	
10	0	1	0	100		0	0	10	1	0	
100	10	1	0	0		0	0	0	1	10	
0	10	1	100	0		10	0	0	0	1	
0	10	1	0	100		0	10	0	0	1	
100	0	1	10	0		0	0	10	0	1	
0	100	1	10	0		0	0	0	10	1	
0	0	1	10	100		0	0	0	0	0	
100	0	1	0	10		1	100	100	100	0	
0	100	1	0	10		1	100	100	0	100	
0	0	1	100	10		1	100	0	100	100	
10	100	0	1	0		1	0	100	100	100	
10	0	100	1	0		100	1	100	100	0	
10	0	0	1	100		100	1	0	100	100	
100	10	0	1	0		100	1	0	100	100	
0	10	100	1	0		0	1	100	100	100	
0	10	0	1	100		100	100	1	100	0	

Fig. 6.14. *Response pattern illustrated by pseudo-color pictures for all imaged ion mixtures. Concentrations (in µM) are given on the left of the pictures.*

A three-layer back propagation neural network was developed for identification of the ion mixtures. The results presented here are the first evaluation of the cross-reactive array concept and were intended as demonstration of the feasibility of the chosen indicators. For this purpose the response pattern of about 200 different ion mixtures was used for training the model. The solutions contained variations of calcium(II), copper(II), nickel(II), zinc(II) and cadmium(II) ions in concentration of 0, 1, 10, 100 µM. The model was performed with a 8-7-5 network architecture of 8 neurons in the input, 7 in the hidden and 5 in the output layer. After training the neural network, it was used for prediction of the ion concentration in the mixtures. It was not able to assign concentrations in a significant way but a trend for high ion concentrations can be predicted. Table 6.2. lists the given and predicted concentrations for certain ion mixtures. The assigned value for 100 µM is always the highest value with a large margin. Hence, the presence of an ion in a concentration of 100 µM can be predicted and demonstrates that the principle of a cross-reactive array is working for this presented approach. However, the network lacks of structure due to insufficient number of training data. Increasing this number to about 1000 will contribute to an improved classification ability of the model. Poor prediction is not assumed to random errors because solutions were prepared by an robotic dispensing system , the indicator and the reference dye were added from the same stock solution and the referenced data were used. Kinetic influences are not expected since the measurements were taken immediately after adding the indicator/reference and all wells are measured at the same instance by a digital picture.

Table 6.2. *Predicted and given concentrations of various ion mixtures. The highest values in each row allows the prediction of the presence of this ion in the mixture.*

given concentration [µM]					predicted concentrations				
Ca^{2+}	Cu^{2+}	Ni^{2+}	Zn^{2+}	Cd^{2+}	Ca^{2+}	Cu^{2+}	Ni^{2+}	Zn^{2+}	Cd^{2+}
100	0	0	0	0	**14**	0	0	1	0
0	**100**	0	0	0	7	**67**	17	5	0
0	0	**100**	0	0	5	3	**76**	12	0
0	0	0	**100**	0	11	0	1	**46**	0
0	0	0	0	**100**	15	1	2	20	**73**
1	0	**100**	0	0	7	6	**75**	14	0
1	0	0	**100**	0	22	1	0	**65**	0
1	0	0	0	**100**	19	0	0	22	**67**
100	1	0	0	0	**31**	0	0	15	1
0	1	**100**	0	0	6	1	**77**	17	0
0	1	0	**100**	0	19	0	0	**67**	0
0	1	0	0	**100**	18	2	2	30	**92**
100	0	1	0	0	**27**	0	0	14	0
0	**100**	1	0	0	13	**86**	26	16	3
0	0	1	**100**	0	19	3	3	**73**	0
0	0	1	0	**100**	19	1	1	25	**81**
100	0	0	1	0	**35**	0	0	19	0
0	**100**	0	1	0	15	**82**	17	19	3
0	0	**100**	1	0	6	2	**86**	16	0
0	0	0	1	**100**	17	1	2	29	**78**
100	0	0	0	1	**34**	0	0	21	0
0	**100**	0	0	1	15	**83**	15	18	1
0	0	**100**	0	1	6	2	**85**	14	0
0	0	0	**100**	1	16	1	2	**52**	4

6.5. Conclusion

The scheme introduced in chapter 5 was successfully improved by a powerful novel set-up which allows the determination of fluorophores in the nM-range without any amplification. The optimized scheme was applied to a cross-reactive array in microtiterplates based on 8 different unselective indicators for 5 cations. The array was arranged in microtiterplates which were entirely mapped with a CCD-camera. The resulting intrinsically referenced pictures imply a pattern or fingerprint, which was analyzed by a MLP. The trained model was able to predict a trend for solutions containing ions in concentrations of $100 \, \mu M$. This is promising regarding the small number of data used for training the network, which is the reason for the poor prediction ability. Furthermore, the analysis of the data separation in statistical independent components seem to be more promising with respect to the complex interaction of indicator and mixture of ions.

The modified set-up enables measuring fluorescence of indicators with detection limits comparable with a conventional microtiterplate reader. The advantages of the imaging set-up are the rapid measurement of a whole microtiterplate within a few microseconds and the collection of the entire data set in one picture. The presented method was shown to be superior to other imaging methods due to a successful elimination of inhomogeneities and a compared small instrumental effort.

6.6. References

[1]   K. Persaud, G. Dodd, *Analysis of discrimination mechanisms in the mammalian olfactory system using a model nose*, Nature, **299**, 352 (1982)

[2]   I. Lundström, R. Erlandsson, U. Frykman, E. Hedborg, A. Spetz, H. Sundgren, S. Welin, F. Winquist, *Artificial 'olfactory' images from a chemical sensor using a light-pulse technique*, Nature, **352**, 47 (1991)

[3]   J. Kauer, *Contributions of topography and parallel processing to odor coding in the vertebrate olfactory pathway*, Trends Neurosci., **14**, 79 (1991)

[4]   B. Malnic, J. Hirono, T. Sato, L. B. Buck, *Combinatorial receptor codes for odors*, Cell, **96**, 713 (1999).

[5]   D. Lancet, *Olfaction. The strong scent of success*, Nature, **351**, 275 (1991).

[6]   G. Shepherd, *Discrimination of Molecular Signals by the Olfactory Receptor Neuron*, Neuron, **13**, 771 (1994).

[7]   K. J. Albert, N. S. Lewis, C. L. Schauer, G. A. Sotzing, S. E. Stitzer, T. P . Vaid, D. R. Walt, *Cross-Reactive Chemical Sensor Arrays*, Chem. Rev., **100**, 2595 (2000)

[8]   S. R. Johnson, J. M. Sutter, H. L. Engelhardt, P. C. Jurs, J. White, J. S. Kauer, T. A. Dickinson, D. R. Walt, *Identification of Multiple Analytes Using an Optical Sensor Array and Pattern Recognition Neural Network,* Anal. Chem., **69,** 4641 (1997).

[9]   J. White, J. S. Kauer, T. A. Dickinson, D. R. Walt, *Rapid Analyte Recognition in a Device Based on Optical Sensors and the Olfactory System*, Anal. Chem., **68**, 2191 (1996).

[10]   K. Albert, D. R. Walt, *High-Speed Fluorescence Detection of Explosives-like Vapors*, Anal. Chem., **72**, 1947 (2000)

[11]   A. D'Amico, C. Di Natale, R. Paolesse, A. Macagnano, A. Mantini, *Metalloporphyrins as basic material for volatile sensitive sensors*, Sens. Actuators, **B65**, 209 (2000)

[12]   G. A. Bakken, G. W. Kaufmann, R. C. Jurs, K. J. Albert, S. S. Stitzel, *Pattern recognition analysis of optical senor array datao to detect nitroaromatic compound vapors*, Sens. Actuators, **B79**, 1 (2001)

[13]   N. A. Rakow, K. S. Suslick, *A colorimetric sensor array for odour visualization,* Nature, **406**, 710 (2000)

[14]   Y. Vlasov, A. V. Legin, A. Rudnitskaya, *Cross-sensitivity evaluation of chemical sensors for electronic tongue: determination of heavy metal ions*, Sens. Actuators, **B44**, 532 (1997).

[15] A. L. Kukla N. F. Starodub, N. K. Kanjuk, , Y. M Shirshov, *Multienzyme electrochemical sensor array for determination of heavy metal ions,* Sens. Actuators, **B57,** 213 (1999).

[16] Y. G. Vlasov, A. V. Legin, A. M. Rudnitskaya, A. D´Amico, C. Di Natale, *Electronic tongue – new analytical tool for liquid analysis on the basis of non-specific sensors and methods of pattern recognition*, Sens. Actuators, **B65**, 235 (2000).

[17] J. Kim, X, Wu, M. Herman, J. S. Dordick, *Enzymatically generated polyphenols as array-based metal-ion sensors*, Anal. Chim. Acta, **370**, 251 (1998).

[18] H. Prestel, A. Gahr, R. Niessner, *Detection of heavy metals in water by fluorescence spectroscopy: On the way to a suitable sensor system*, Fresenius J. Anal. Chem., **368**, 182 (2000).

[19] A. Goodey, J. J. Lavigne, S. M. Savoy, M. D. Rodriguez, T. Curey, A. Tsao, G. Simmons, J. Wright, S-J. Yoo, Y. Sohn, E. V. Anslyn, J. B. Shear, D. P Neikirk, J. T. McDevitt, *Development of Multianalyte Sensor Arrays Composed of Chemically Derivatized Polymeric Microspheres Localized in Micromachined Cavities*, J. Am. Chem. Soc., **123,** 2559 (2001)

[20] H. Lohninger, *Teach Me/Data Analysis*, Springer, Berlin (1999).

[21] R. E. Shaffer, S. L. Rose-Pehrsson, R. A. McGill, *A comparison study of chemical sensor array pattern recognition algorithms*, Anal. Chim. Acta, **384**, 305 (1999)

[22] R. P. Haughland, *Handbook of Fluorescent Probes and Research Products*, Molecular Probes, Eugene (2001).

[23] http://www.probes.com/handbook/figures/1573.html

[24] T. Mayr. G. Liebsch, O. S. Wolfbeis, *Time-resolved imaging applied to multi-ion sensor array in microtiterplates,* in abstract book of the 7th Conference on Methods and Application of Fluorescence, Poster number 132

[25] M. Otto, *Chemometrie: Statisitik und Computereinsatz in der Analytik*, VCH, Weinheim (1997).

[26] S. Haykin, *Neural Networks – A Comprehensive Foundation*, Macmillan Colloge Publishing Company, New York (1994).

[27] G. Liebsch, I. Klimant, B. Frank, G. Holst, O. S. Wolfbeis, *Luminescence Lifetime Imaging of Oxygen, pH, and Carbon Dioxide Distribution Using Optical Sensors*, Appl. Spec., **54**, 548 (2000).

[28] G. Liebsch, I. Klimant, C. Krause, O. S. Wolfbeis, *Fluorescent Imaging of pH with Optical Sensors Using Time Domain Dual Lifetime Referencing*, Anal. Chem., **73**, 4354 (2001).

[29] J. R. Lakowicz, *Principles of Fluorescence Spectroscopy – 2nd Edition*, Kluwer Academic/Plenum Publishers, New York (1999)

7. Summary

The thesis describes the development of optical sensors for the determination of heavy metal ions in aqueous samples. A sensing schemes for the selective determination of copper(II) based fluorescence intensity measurement was presented. This scheme was then optimized by a referencing method, which enables decay time measurements. Furthermore, a uniform scheme in a microtiterplate array format for the determination of several ions in parallel was introduced. This novel scheme employs time-resolved imaging as detection method.

Chapter 1 gives a short introduction concerning heavy metals followed by an overview of optical sensing for cations.

In Chapter 2, the fluorophore LY is shown to be a highly selective reagent for the determination of copper(II) in the ppb concentration range. The fluorescence of **LY** is statically quenched by copper(II) ions. A dynamic range of copper(II) determination from 0.06 mg/l (1 µM) to 6.3 mg/l (100 µM) with a limit of detection of 0.019 mg/l (0.3 µM) was obtained which is below recommended concentrations for drinking water by the EU and the WHO. The cross sensitivity to heavy metal ions was evaluated by the separate solution method and by competitive binding experiments. No interference from the alkali or alkaline earth metals or from the heavy metal ions zink(II), silver(I), cadmium(II), and lead(II) was found. The determination is not affected between pH 6 and 8. Finally, the quick and simple method was successfully applied to real samples and the accuracy was proved by reference methods.

In chapter 3 sensing membranes were obtained immobilizing Lucifer Yellow electrostatically to anion exchanger cellulose particles, which were subsequently embedded in a hydrophilic polymer. The sensing membrane allows the determination of copper(II) in the 0.01 µM (0.63 µg/l) to 100 µM (6300 µg/l) concentration range with an outstanding high selectivity, whereas mercury(II) was the only interferent. The application of the sensing membrane as single shot test was demonstrated in microtiterplates by copper(II) determination in tap water samples.

The sensing membrane was improved applying a scheme for internal referencation termed Dual Lifetime Referencing (DLR) in chapter 4. This sensing scheme makes use of the indicator **LY** and an inert reference luminophore (a ruthenium complex entrapped in polyacrylonitrile beads). The copper-dependent fluorescence intensity change of **LY** can be converted in either a frequency or time depending parameter. The advantages of the referencing method over intensity based measurements was demonstrated. Additionally the

scheme was successfully applied to 2-dimensional measurements in the time domain. Sensor integrated microtiterplates were imaged with a CCD-camera.

Chapter 5 deals with a novel type of sensor array in microtiterplates destined for water analyses that has high flexibility and is easily prepared. The uniform scheme delivers simple on/off patterns of complex ion mixtures. Thin films of dispersed fluorescent indicators for calcium(II), sodium(II), magnesium(II), mercury(II), sulfate, and chloride in a water-soluble polymer were arranged on the bottom of the wells of a microtiterplate. The analytical information was imaged with a CCD-camera within microseconds using the DLR-method. The fields of application are manifold. They include the analysis of environmental samples, drinking water and biological fluids.

In chapter 6 cross-reactive sensor arrays in microtiterplates for the quantitative analysis of ion mixtures containing calcium(II), copper(II), nickel(II), zink(II) and cadmium(II) in µM concentration range are presented. The luminescence of unselective indicators deliver characteristic patterns for each ion mixture. Each well of a microtiterplates was illuminated by one LED and the luminescence of the indicators were imaged with a CCD-camera. This novel set-up allows the determination of 10 nM carboxyfluorescein without any amplification of the signal. The pattern obtained from the cross-reactive array were evaluated by an artificial neural network.

8. Zusammenfassung

Diese Arbeit beschreibt die Entwicklung optischer Sensoren für die Bestimmung von Schwermetallionen in wässrigem Milieu. Ein Sensorprinzip für die selektive Bestimmung von Kupfer(II) basierend auf der Messung von Fluoreszenzintensitäten wird vorgestellt. Dieses wird anschließend durch eine Referenzierungsmethode optimiert. Ferner wird ein neues Sensorprinzip im Mikrotiterplattenformat für die gleichzeitige Bestimmung mehrerer Ionen mit Hilfe von bildgebenden Verfahren präsentiert.

Im ersten Kapitel wird die Problematik von Schwermetallen dargelegt und ein Überblick über die optische Sensorik für Kationen gegeben.

Im zweiten Kapitel wird die Charakterisierung von **LY** als hochselektives Reagenz die Bestimmung von Kupfer(II) im ppb-Konzentrationsbereich beschrieben. Die Fluoreszenz von **LY** wird statisch von Kupfer(II) gelöscht. Der dynamische Bereich für die Bestimmung von Kupfer(II) reicht von 0.06 mg/l (1 µM) bis 6.3 mg/l (100 µM), was unterhalb der Grenzwerte der WHO und EU liegt. Das Nachweisgrenze wurde mit 0.019 mg/l (0.3 µM) bestimmt. Die Querempfindlichkeit zu anderen Schwermetallen wurde mit Hilfe der „seperate solution method (SSM)" und mit Hilfe von kompetitiven Bindungsexperimenten untersucht. Die Alkali-, Erdalkalimetalionen und die Schwermetallionen Zink(II), Silber(I), Kadmium(II) und Blei(II) stören den Nachweis nicht. Die Bestimmung ist unabhängig im Bereich von pH 6-8. Schließlich wurde die schnelle und einfache Methode an Trinkwasserproben getestet und mit Referenzmethoden verglichen.

Im dritten Kapitel werden die Herstellung von Sensormembranen für Kupfer(II) beschrieben. **LY** wird elektrostatisch auf Aniontauscher Cellulose Partikel immobilisiert, die in ein hydrophiles Polymer eingebettet werden. Die erhaltenen Sensormembranen ermöglichen die Bestimmung von Kupfer(II) im Konzentrationsbereich von 0.63 µg/l (0.01 µM) bis 6300 µg/l (100 µM) mit einer außergewöhnlich hohen Selektivität. Eine Störung erfolgt nur durch Quecksilber(II). Ein Anwendung der Sensormembranen wurde in Mikrotiterplatten an Trinkwasserproben demonstriert.

Das Sensorprinzip wurde durch eine Referenzierungsmethode verbessert, die es erlaubt Fluoreszenzintensitäten in einen frequenz- oder zeitabhängigen Parameter zu konvertieren. Die Vorteile dieser Methode werden aufgezeigt. Zusätzlich wird das Prinzip auf 2-dimensionale Messungen in der Zeitdomäne angewendet. In Mikrotiterplatten integrierte Sensoren werden mit einer digitalen CCD-Kamera abgebildet.

In Kapitel 5 wird eine neuer Typ von Sensor Arrays in Mikrotiterplatten für die Wasseranalytik, vorgestellt. Diese Art Sensor Array ist leicht herzustellen und sehr flexibel. Das Prinzip liefert einfache Ein/Aus Muster komplexer Ionenmischungen. Hierzu werden dünne Filme aus wasserlöslichem Polymer in die Indikatoren gelöst sind, auf dem Boden der Näpfe von Mikrotiterplatten angeordnet. Die Lumineszenz wird mit einer CCD-Kamera und der DLR-Methode detektiert. Das System bietet mannigfaltige Anwendungsmöglichkeiten, z. B. im Bereich der Umwelt- oder Bioanalytik.

Im Kapitel 6 werden Sensor Arrays, die aus unselektiven Sensoren bestehen, beschrieben. Die Lumineszenzen von unselektiven Indikatoren liefern ein charakteristisches Muster von Ionenmischung aus Calcium(II), Kupfer(II), Nickel(II), Zink(II) und Cadmium(II). Hierzu wurde der Meßaufbau verbessert. Jeder Napf einer Mikotiterplatte wird durch eine LED beleuchtet und die Lumineszenzen der Indikatoren werden durch eine CCD-Kamera abgebildet. Dieser Aufbau erlaubt die Bestimmung von 10 nM Carboxyfluorescein ohne eine Verstärkung des Signals. Das erhaltene Muster des Arrays wird durch ein künstliches neuronales Netz ausgewertet.

9. Curriculum Vitae

Name:	Mayr	
Vorname:	Torsten	
Geburtsdatum:	06.05.1972	
Geburtsort:	Kaufbeuren	
Nationalität:	deutsch	
Schulbildung:	1978 - 1982	Beethovengrundschule Kaufbeuren
	1982 - 1992	Staatliches Gymnasium Kaufbeuren
Schulabschluß:	5/1992	Abitur
Zivildienst:	1992 - 1993	Bayerisches Rotes Kreuz, Dienstelle Kaufbeuren
Studium:	11/1993 - 3/1998	Chemie (Diplom) an der Universität Regensburg
	9/1996 – 2/1997	University of Aberdeen (Great Britain) (Erasmusstipendium)
	3/1998	Diplomprüfung
	6/1998 - 3/1999	Diplomarbeit am Institut für Analytische Chemie, Chemo- und Biosensorik, Universität Regensburg
		Thema: Neutral Carrier Based Fluorosensor for Silver(I) Ions
Studienabschluß:	3/1999	Diplom Chemiker
Promotion:	6/1999 - 5/2002	Doktorarbeit am Institut für analytische Chemie, Chemo- und Biosensorik, Universität Regensburg
		Stipendium der Deutschen Bundesstiftung Umwelt
		Thema: Optical Sensors for the Determination of Heavy Metal Ions
Sprachen:		Englisch (sehr gut)
		Französisch (Grundkenntnisse)
Hobbys und Interessen:		Eishockey, aktiv seit 1999 im erweiterten Vorstand, seit 2001 2. Vorstand des EHC Regensburg größter sportlicher Erfolg: Deutscher Juniorenmeister 1989 und 1991 mit dem ESV Kaufbeuren
		Reisen
		Rennradfahren

10. List of Publications and Presentations

Diploma Thesis

Neutral Carrier Based Fluorosensor forSilver(I) Ions, Institute for Analytical Chemistry, Chemo- and Biosensors, University of Regensburg (1999).

Papers

1. Christian Huber, Ingo Klimant, Christian Krause, Tobias Werner, Torsten Mayr, Otto S. Wolfbeis, ***Optical sensor for seawater salinity***, Fresenius J. Anal. Chem., **368**, 196 (1999).

2. Torsten Mayr, Dorota Wencel, Tobias Werner, ***Fluorimetric Copper(II) Determination in aqueous solution using Lucifer Yellow CH as selective metal reagent***, Fresenius J. Anal. Chem., **371**, 44 (2001).

3. Torsten Mayr, Tobias Werner, ***Highly-selective optical sensor for copper(II) ions based on fluorescence quenching of immobilised Lucifer Yellow***, Analyst, **127**, 248 (2002).

4. Torsten Mayr, Ingo Klimant, Tobias Werner, Otto S. Wolfbeis, ***Dual lifetime referenced optical sensor membrane for the determination of copper(II) ions***, Anal. Chim. Acta, in press.

5. Torsten Mayr, Gregor Liebsch, Ingo Klimant, Otto S. Wolfbeis, ***Multi-Ion Imaging Using Fluorescent Sensors in a Microtiterplate Array Format***, Analyst, **127**, 201 (2002).

6. Torsten Mayr, Gregor Liebsch, Ingo Klimant, Tobias Werner, Otto S. Wolfbeis, ***Time-resovled Imaging of Cross-Reactive Array Assays for Metal Ions Evaluated by an Artificial Neutral Network***, in preparation.

Cover image

Analyst, Volume 127 Number 2
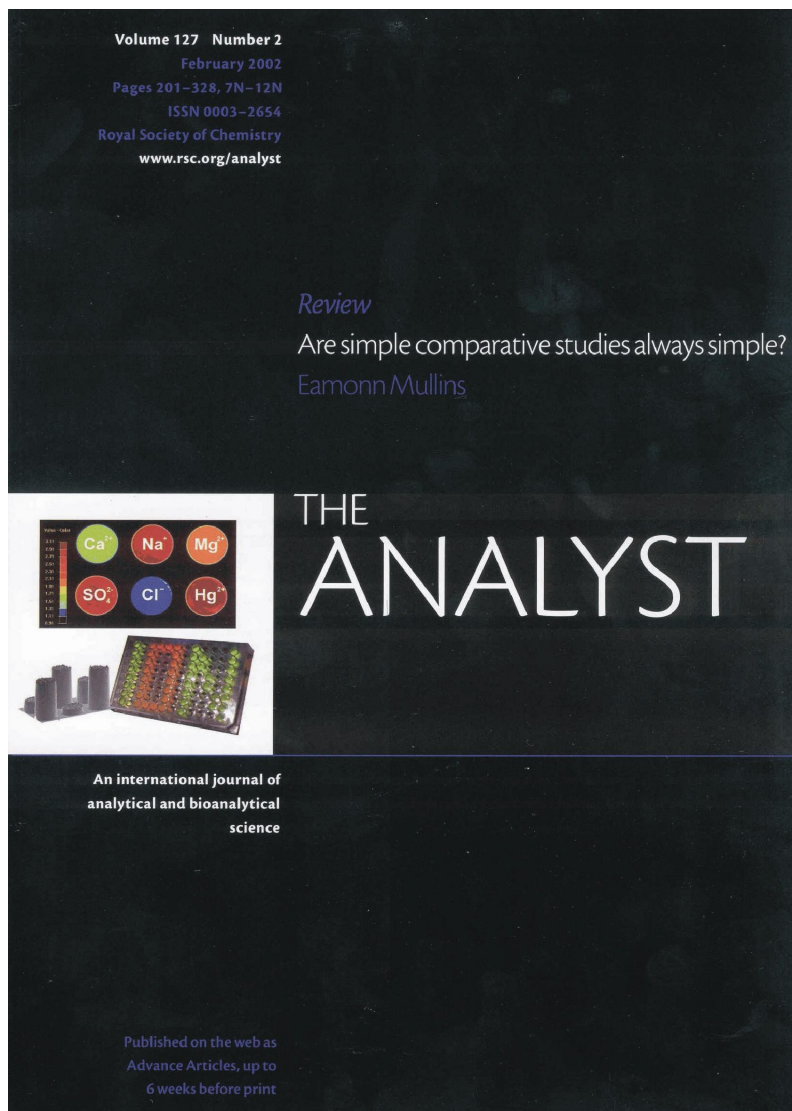
Posters

1. Torsten Mayr, Tobias Werner, Otto S. Wolfbeis, *Highly Selective Detection of Copper(II) Ion Using Immobilised Lucifer Yellow,* Europtrode V, Lyon, France (2000).

2. Torsten Mayr, Tobias Werner, Otto S. Wolfbeis, *Highly Selective Detection of Copper(II) Ion Using Immobilised Lucifer Yellow*, 1. Konferenz über Ionenanalytik, Berlin, Deutschland (2001)

3. Torsten Mayr, Gregor Liebsch, Tobias Werner, Otto S. Wolfbeis, *Time Resolved Imaging Applied to a Multi-Ion Sensor Array in Microtiterplates,* 7th Conference on Methods and Application of Fluorescence, Amsterdam, The Netherlands (2001)

Oral Presentations

1. Torsten Mayr, Tobias Werner, Otto S. Wolbeis, *Neutral Carrier Based Fluorosensor for Silver(I) Ions*, European Summer School "Sensors for Food Applications", Elba, Italy (1999)

2. Torsten Mayr, Tobias Werner, Otto S. Wolbeis, *Neutral Carrier Based Fluorosensor for Silver(I) Ions*, Advanced Study Course on Optical Chemical Sensors (ASCOS), Neusiedl, Austria (1999)

3. Torsten Mayr, *Lucifer Yellow - ein selektiver Fluoreszenzindikator für Kupfer(II)-Ionen,* Seminar for scholarship holders of the German Federal Environmental Foundation (DBU), Vilm Island, Germany (2000).

4. Torsten Mayr, *Optische Sensoren für Schwermetalle,* Seminar for scholarship holders of the German Federal Environmental Foundation (DBU), Helgoland Island, Germany (2001).

5. Torsten Mayr, Gregor Liebsch, Ingo Klimant, Otto S. Wolfbeis, *Multi-Ion Imaging Using Fluorescent Sensors in a Microtiterplate Array Format,* Europtrode VI, Manchester, Great Britain (2002)

Appendix:

A) Source code for filling microtiterplates with the Hamilton Microlab dispensing system

```
1   Filling the columns of 96 microtiterplate with the same ion mixtures, the ion mixtures are varied by
    import of the data from a Excellsheet
2
3       Initialise single needle arm
4       Initialise dispenser 1
5       Neue Position einstellen in titerplate2 bis 1 für Einzelnadelarm
6       Input value for row1 in range 0 to  2000 Default is 1
7       Input value for platecol in range 0 to  12 Default is 1
8       Open Excel : C:\arbeit\EXCEL\array.xls
9       loops=13-platecol
10      platecol=(platecol-1)*8+1
11
12  Loop loops
13
14
15          Read from Excel : data
16          vol1=8*bvol+5
17          Aspirate 10 + vol1 ul from container_buffer with syringe  1 , speed  300 steps per second
18          Set new position in titerplate2 to platecol for single needle arm
19          Loop 8
20                  Dispense  bvol ul to  titerplate2 with syringe  1 , speed  500 steps per second
21          End of loop
22           Wash needle with syringe  1, 5 mm above bottom in Waschen, 1000 ul 2 times, lift 20 mm
23
24
25          Loop 5
26
27              col1=_sysloop[2]+1
28              Read from Excel : data
29
30              If ion1 <> 1 jump to Endif
31                  var2=_sysloop[2]
32                  Set new position in Rack01 to var2 for single needle arm
33                  Aspirate 5 + 95 ul from Rack01 with syringe  2 , speed  300 steps per second
34                  Dispense  10 ul to  Rack3 with syringe  2 , speed  500 steps per second
35                      Set new position in titerplate2 to platecol for single needle arm
36                  Loop 8
37                      Dispense  10 ul to  titerplate2 with syringe  2 , speed  500 steps     per
                        second
38                  End of loop
39              Wash needle with syringe  2, 5 mm above bottom in Waschen, 100 ul 2 times, lift 20
                mm
40              Endif
41
42              If ion1 <> 10 jump to Endif
43                  var2=_sysloop[2]+5
44                  Set new position in Rack01 to var2 for single needle arm
45                  Aspirate 5 + 95 ul from Rack01 with syringe  2 , speed  300 steps per second
46                  Dispense  10 ul to  Rack3 with syringe  2 , speed  500 steps per second
47                      Set new position in titerplate2 to platecol for single needle arm
48                  Loop 8
```

49	Dispense 10 ul to titerplate2 with syringe 2 , speed 500 steps per second
50	End of loop
51	Wash needle with syringe 2, 5 mm above bottom in Waschen, 100 ul 2 times, lift 20 mm
52	Endif
53	
54	If ion1 <> 100 jump to Endif
55	var2=_sysloop[2]+10
56	Set new position in Rack01 to var2 for single needle arm
57	Aspirate 5 + 95 ul from Rack01 with syringe 2 , speed 300 steps per second
58	Dispense 10 ul to Rack3 with syringe 2 , speed 500 steps per second
59	Set new position in titerplate2 to platecol for single needle arm
60	Loop 8
61	Dispense 10 ul to titerplate2 with syringe 2 , speed 500 steps per second
62	End of loop
63	Wash needle with syringe 2, 5 mm above bottom in Waschen, 100 ul 2 times, lift 20 mm
64	Endif
65	
66	End of loop
67	platecol=platecol+8
68	row1=row1+1
69	
70	End of loop
71	
72	End of method

B) Layout of the excell-worksheet for filling microtiterplates

Ca [µM]	Cu [µM]	Ni [µM]	Zn [µM]	Cd [µM]
0	0	0	0	0
1	1	1	1	1
10	10	10	10	10
100	100	100	100	100
1	0	0	0	0
0	1	0	0	0
0	0	1	0	0
0	0	0	1	0
0	0	0	0	1
10	0	0	0	0
0	10	0	0	0
0	0	10	0	0

C) Data used for training the artificial neural network

Ca²⁺ [µM]	Cu²⁺ [µM]	Ni²⁺ [µM]	Zn²⁺ [µM]	Cd²⁺ [µM]	A	B	C	D	E	F	G	H
0	0	0	0	0	2.2968	3.1162	2.0431	3.3698	3.5849	3.0744	2.8088	1.8251
1	1	1	1	1	2.1698	4.5778	2.0706	2.1197	3.0842	2.1116	2.8246	2.0898
10	10	10	10	10	2.9856	4.6983	1.9873	2.099	1.9934	1.9513	2.258	1.8915
100	100	100	100	100	2.843	4.3127	1.89	1.9731	2.0103	1.946	2.1276	1.8659
1	0	0	0	0	2.8646	4.8638	1.9413	2.4103	3.4008	2.5672	2.5452	2.46
0	1	0	0	0	2.0144	3.2863	1.8396	2.0746	3.0252	2.1314	2.7438	2.159
0	0	1	0	0	1.9134	2.9623	2.3626	2.1525	3.379	2.6209	2.7826	2.0706
0	0	0	1	0	1.952	3.2872	1.9318	2.2684	3.4814	3.0388	2.9237	2.002
0	0	0	0	1	2.1858	4.7266	1.8857	2.2125	3.524	3.0479	2.7502	1.9492
10	0	0	0	0	2.5662	3.7982	1.8649	2.5555	3.5333	2.9748	2.7692	1.8402
0	10	0	0	0	1.8802	2.4012	1.7487	2.0232	2.0131	1.9275	2.4573	1.7946
0	0	10	0	0	1.9708	2.4889	2.6262	2.1948	3.0693	1.9398	2.7612	2.1213
0	0	0	10	0	2.3597	3.6722	2.2512	2.192	3.4324	2.6892	3.6895	2.6706
0	0	0	0	10	2.9889	5.037	2.0022	2.1723	3.5321	2.645	2.5359	2.7207
100	0	0	0	0	2.8324	4.9691	2.0086	2.3138	3.579	2.8905	2.7684	2.1456
0	100	0	0	0	1.9162	2.3996	1.8018	1.9104	2.0011	1.9918	2.0858	1.7841
0	0	100	0	0	1.8384	2.2848	2.7969	2.2263	2.0708	1.9403	2.5179	2.2941
0	0	0	100	0	2.2745	3.6358	2.1301	2.0407	3.0089	2.3235	3.302	2.9343
0	0	0	0	100	2.9962	4.6557	2.138	2.0088	3.2569	2.6282	2.3921	3.2703
1	1	0	0	0	2.9078	4.6489	1.7814	2.1178	3.0462	2.182	2.4266	2.3696
1	0	1	0	0	2.1458	3.7717	2.3012	2.1818	3.4115	2.6901	2.8497	2.1302
1	0	0	1	0	2.0574	3.5644	1.9367	2.2586	3.5102	2.9674	2.9402	1.9666
1	0	0	0	1	2.2347	5.0551	1.8897	2.2854	3.613	2.9832	2.7891	1.9769
0	1	1	0	0	2.0289	2.754	1.9688	2.1566	3.1915	2.2646	2.8186	1.9709
0	1	0	1	0	2.2688	3.0378	2.0085	2.2063	3.2172	2.2979	3.0652	1.9346
0	1	0	0	1	2.1837	4.7496	1.8604	2.1065	3.1155	2.2061	2.7058	1.9362
0	0	1	1	0	2.0352	3.2917	2.4136	2.3215	3.6236	2.7807	2.9389	2.1024
0	0	1	0	1	2.4044	4.9488	2.5225	2.3155	3.7002	2.9344	2.8161	2.1623
0	0	0	1	1	2.2792	4.9766	1.9272	2.3456	3.5797	3.1327	2.9686	2.0998
10	10	0	0	0	1.9718	2.6748	1.748	1.9661	1.981	1.9288	2.3472	1.9566
10	0	10	0	0	1.9035	2.4927	2.7705	2.1329	2.8372	1.9954	2.7475	2.2742
10	0	0	10	0	2.1481	3.5062	2.0993	2.1489	3.3801	2.601	3.5275	2.6816
10	0	0	0	10	2.9737	5.1791	1.958	2.1013	3.4908	2.8074	2.5251	2.7827
0	10	10	0	0	2.3821	4.2174	1.8914	2.004	1.9398	1.9741	2.4158	1.8248
0	10	0	10	0	2.0415	3.0937	1.7754	2.0573	2.0549	2.0294	3.1823	1.8288
0	10	0	0	10	2.9294	4.8673	1.7098	2.0329	1.9827	2.0087	2.3945	1.8549
0	0	10	10	0	3.1192	5.059	2.5057	2.282	3.2134	2.2101	3.2243	2.7008
0	0	10	0	10	3.089	5.1988	2.4302	2.1616	3.4337	2.2077	2.4638	2.9104
0	0	0	10	10	3.3396	5.1532	2.1692	2.2816	3.6427	2.8281	2.4495	2.9725
100	100	0	0	0	2.3034	2.8181	1.8996	2.0212	2.1336	2.0495	2.2271	1.8711
100	0	100	0	0	2.1301	2.7041	2.1079	2.169	2.1167	2.0061	2.4933	2.3115
100	0	0	100	0	2.4251	3.7279	2.0245	2.0199	3.1283	2.4102	3.0051	3.0843
100	0	0	0	100	3.0502	4.3641	2.0733	2.0045	3.2734	2.6645	2.2449	3.2679
0	100	100	0	0	2.3972	3.0057	1.8136	1.9323	1.8965	1.9883	2.0602	1.8623
0	100	0	100	0	2.0299	2.429	1.7958	1.8716	1.8779	1.9642	2.643	1.8193
0	100	0	0	100	2.9053	4.3998	1.8149	1.938	1.8872	2.0031	2.0973	1.8283
0	0	100	100	0	2.8596	4.6182	2.3079	2.076	2.4392	2.1251	2.6945	2.7104
0	0	100	0	100	3.1989	5.0468	2.4547	2.1613	2.6687	2.0645	2.3044	3.0702

0	0	0	100	100	3.5529	4.4778	2.1838	2.0957	3.2905	2.5684	2.3506	3.1625
1	1	1	0	0	2.9203	4.0402	1.9085	2.0949	3.0193	2.0786	2.5285	2.3823
1	1	0	1	0	2.3936	3.8945	1.8039	2.1642	3.0362	2.051	2.965	2.0001
1	1	0	0	1	2.5434	4.1632	1.8599	2.1393	3.0987	2.0721	2.7959	1.9943
1	0	1	1	0	2.1607	3.5313	2.0689	2.2953	3.459	2.6399	3.0448	2.2246
1	0	1	0	1	2.416	4.0653	2.1276	2.1393	3.4463	2.6026	2.7819	2.3585
1	0	0	1	1	2.4582	4.0583	1.9181	2.1628	3.4636	2.5874	2.9665	2.2345
0	1	1	1	0	2.0802	3.1784	1.8465	2.0956	3.0532	2.1097	2.9599	2.1022
0	1	1	0	1	2.282	4.0503	1.9082	2.0828	3.0173	2.0266	2.7711	2.0509
0	1	0	1	1	2.3435	4.0787	1.7538	2.0784	3.0434	2.1116	2.9147	1.9995
0	0	1	1	1	2.4878	4.1751	2.1475	2.2466	3.566	2.6946	3.0309	2.329
10	10	10	0	0	2.2662	3.1362	1.7917	2.0221	1.9705	1.928	2.4624	1.8782
10	10	0	10	0	2.4234	3.1955	1.9267	2.0552	1.9687	1.91	3.2997	1.9372
10	10	0	0	10	2.9924	4.1688	1.8031	2.0105	1.9884	1.9504	2.3992	1.899
10	0	10	10	0	2.6955	4.112	2.4646	2.228	3.2206	2.2302	3.1982	2.61
10	0	10	0	10	3.0211	4.3201	2.5618	2.2112	3.4303	2.303	2.5886	2.9578
10	0	0	10	10	3.2219	4.2923	2.0551	2.274	3.5849	2.8415	2.6481	3.0436
0	10	10	10	0	2.6067	3.7846	1.8712	2.0063	1.9277	1.9153	2.6967	2.0715
0	10	10	0	10	2.9268	4.0107	1.8605	1.9607	1.8883	1.8868	2.3323	1.9499
0	10	0	10	10	2.9753	3.9924	1.7205	2.0254	1.8969	1.9201	2.3409	1.9355
0	0	10	10	10	3.1118	4.2608	2.4239	2.1467	3.2446	2.3807	2.5826	2.9164
100	100	100	0	0	2.3011	2.553	1.7767	1.9148	1.8273	1.916	2.1283	1.8289
100	100	0	100	0	1.963	2.2766	1.7495	1.986	1.9516	1.8807	2.8928	1.8696
100	100	0	0	100	3.0778	3.7945	1.7204	1.9627	1.9114	1.972	2.2518	1.8899
100	0	100	100	0	3.0472	4.1116	2.5644	2.0822	2.1674	2.1847	2.7329	2.3595
100	0	100	0	100	3.0019	4.1859	2.6335	2.088	2.4059	2.0428	2.3295	3.0606
100	0	0	100	100	3.3054	4.2583	2.2173	2.139	3.3893	2.6241	2.3369	3.0772
0	100	100	100	0	2.2925	2.664	1.8308	1.9135	1.9456	1.9338	2.381	1.8612
0	100	100	0	100	2.8041	3.517	1.7337	1.9479	1.821	1.8869	2.1781	1.8942
0	100	0	100	100	2.8475	3.5427	1.7722	1.858	1.8429	1.8859	2.0826	2.0606
0	0	100	100	100	3.1011	4.0554	2.5298	1.9803	2.3285	2.1471	2.307	3.023
1	1	1	1	0	2.8797	4.0829	1.8625	2.0685	2.8167	2.0603	2.4658	2.3235
1	0	1	1	1	2.4973	4.1481	2.0967	2.1552	3.2902	2.5055	2.9897	2.2742
1	1	0	1	0	2.1496	3.6069	1.8149	2.1167	3.0145	2.1411	3.0442	1.9443
1	0	0	0	1	2.3529	4.1886	1.8592	2.2467	3.5598	2.7542	2.8666	2.0558
0	1	1	1	1	2.4556	4.2246	1.8739	2.1435	3.0551	2.1223	3.01	2.1059
10	10	10	10	0	2.2585	2.7864	2.0121	2.0699	1.9517	2.0289	3.2412	1.9692
10	0	10	10	10	3.1173	4.2804	2.4606	2.1305	3.1067	2.1629	2.464	2.8488
10	10	0	10	10	3.0443	3.9784	1.8278	2.0905	2.0032	1.9896	2.36	1.8951
10	10	10	0	10	2.9402	4.0399	1.8721	2.0976	2.0935	2.0559	2.4187	1.8956
0	10	10	10	10	2.9353	3.9598	1.7674	2.2034	1.9548	1.9837	2.4372	1.9877
100	100	100	100	0	2.2751	2.4344	1.8499	1.9063	1.813	1.9837	2.4782	2.1104
100	0	100	100	100	3.1767	4.0834	2.5822	2.0276	2.3595	2.1579	2.3706	3.1076
100	100	0	100	100	2.9164	3.4639	1.7145	1.9425	1.8447	2.0286	2.081	1.9145
100	100	100	0	100	2.8337	3.5804	1.7564	1.9076	1.7752	1.9798	2.1735	1.8445
0	100	100	100	100	2.9513	3.6007	1.779	1.9192	1.8147	2.0018	2.1482	1.8989
1	100	0	0	0	2.4539	2.7064	1.7575	1.938	1.9096	1.9793	2.1849	1.8228
1	0	100	0	0	2.1908	3.0004	2.4709	2.1718	2.0286	2.0438	2.5491	2.218
1	0	0	100	0	2.8748	3.8895	2.261	2.236	3.1576	2.319	3.6918	2.9492
1	0	0	0	100	3.213	4.5439	2.1462	2.1803	3.5736	2.5699	2.4238	3.3503
100	1	0	0	0	3.1343	4.2283	1.8881	2.2721	3.2287	2.3271	2.5889	2.372
0	1	100	0	0	2.2079	3.6968	2.686	2.3021	2.7143	2.1478	2.7852	2.9263
0	1	0	100	0	2.5373	3.502	2.0243	2.2905	3.0385	2.3111	3.4695	2.99
0	1	0	0	100	3.1942	4.3002	1.9136	2.1287	3.0438	2.1898	2.3828	3.212

100	0	1	0	0	3.0332	4.1675	2.3363	2.2242	3.5387	2.7899	2.5907	2.7872
0	100	1	0	0	2.1189	2.2688	1.7337	1.9858	1.8285	2.0433	2.0877	1.8468
0	0	1	100	0	2.3508	3.3465	1.9425	2.0783	2.4877	2.1498	3.4906	2.5776
0	0	1	0	100	3.2349	4.4859	2.0709	2.1615	3.2981	2.406	2.4321	3.2216
100	0	0	1	0	3.0199	4.288	1.9511	2.3626	3.7375	2.8524	2.6561	2.7045
0	100	0	1	0	2.207	2.4232	1.7297	2.0175	1.8894	2.1016	2.1795	1.8555
0	0	100	1	0	2.3314	3.0402	2.9151	2.2753	2.3811	2.0287	2.7429	2.6331
0	0	0	1	100	3.0285	4.1828	2.0369	2.1123	3.2033	2.2654	2.4214	3.2122
100	0	0	0	1	3.027	3.948	1.9547	2.2883	3.4796	2.6343	2.5624	2.6059
0	100	0	0	1	2.1712	2.1835	1.8195	2.0034	1.9913	2.0958	2.2107	1.8501
0	0	100	0	1	2.2953	3.7835	2.5924	2.3017	2.3391	2.074	2.6547	2.6506
0	0	0	100	1	2.641	3.7368	2.1254	2.1089	3.0197	2.2355	3.0793	2.9611
1	10	100	0	0	1.9534	2.778	2.2282	1.9914	1.8482	2.0095	2.6813	2.2199
1	10	0	100	0	2.1051	2.79	1.789	2.0243	1.9088	2.0444	3.146	2.211
1	10	0	0	100	2.8821	3.8756	1.7554	1.9965	1.8614	2.0039	2.3593	2.0776
1	100	10	0	0	2.3794	2.7516	1.7489	1.9065	1.7899	2.0092	2.1218	1.8036
1	0	10	100	0	2.299	3.3074	2.0525	2.1545	2.457	2.1114	3.4333	2.6159
1	0	10	0	100	3.0988	4.1168	2.2783	2.1729	3.1799	2.2093	2.497	3.1942
1	100	0	10	0	2.5289	2.8063	1.9075	1.9975	1.902	2.0649	2.2723	1.9337
1	0	100	10	0	2.1241	3.3245	2.6974	2.2059	2.3944	2.1066	3.3713	2.6967
1	0	0	10	100	3.1289	4.1212	2.176	2.2707	3.357	2.3362	2.4736	3.2547
1	100	0	0	10	2.6613	3.2588	1.8449	2.0177	2.0696	2.184	2.2296	1.8423
1	0	100	0	10	2.8595	3.8353	2.6016	2.225	2.3445	2.1009	2.5695	2.7332
1	0	0	100	10	3.2048	3.984	2.1694	2.138	3.2763	2.3781	2.5937	3.2047
10	1	100	0	0	2.4886	3.7805	2.7948	2.2028	2.4112	2.0948	2.8235	2.9962
10	1	0	100	0	2.4728	3.3365	2.031	2.1811	2.8794	2.2558	3.3585	2.9542
10	1	0	0	100	3.0249	4.1729	1.8676	2.0869	2.9672	2.1166	2.5096	3.0517
100	1	10	0	0	2.9498	4.0957	2.4176	2.196	3.0119	2.1697	2.5678	2.5653
0	1	10	100	0	2.5226	3.5608	2.1495	2.2113	3.0836	2.2458	3.3797	2.9872
0	1	10	0	100	3.1326	4.2586	2.1592	2.2049	2.8286	2.2029	2.5423	3.0967
100	1	0	10	0	3.8162	4.6302	2.3218	2.4009	3.2407	2.3326	2.7552	2.8528
0	1	100	10	0	2.6948	4.1716	2.8495	2.3333	2.6818	2.2468	3.273	3.0947
0	1	0	10	100	3.3749	4.2392	2.2341	2.4095	3.3044	2.3333	2.4934	3.2001
100	1	0	0	10	3.0812	4.2459	2.0664	2.3687	3.5419	2.4182	2.6934	2.7934
0	1	100	0	10	3.1467	4.0367	2.7308	2.6116	2.6775	2.1469	2.7163	3.1134
0	1	0	100	10	3.3385	4.2173	2.2213	2.1603	3.0536	2.3483	2.5971	3.4324
10	100	1	0	0	2.2093	2.4626	1.9103	1.9498	1.8702	2.1456	2.2612	2.0447
10	0	1	100	0	2.4724	3.3774	2.0598	2.1948	2.5736	2.2586	3.3266	2.7905
10	0	1	0	100	3.124	4.299	2.1502	2.2063	3.2503	2.4118	2.6144	3.3309
100	10	1	0	0	3.0049	4.1074	1.8859	2.1568	2.0167	2.1724	2.4468	1.9374
0	10	1	100	0	2.4221	3.318	1.9157	2.1499	2.1441	2.1647	3.4654	2.3664
0	10	1	0	100	3.2775	4.1937	1.8582	2.1985	2.0694	2.1973	2.4734	2.2591
100	0	1	10	0	3.3861	4.1595	1.9424	2.1253	3.3782	2.3194	2.528	2.3515
0	100	1	10	0	1.9942	2.264	1.7622	1.9021	2.0857	2.0764	2.0903	1.8016
0	0	1	10	100	3.0069	4.0338	1.8147	2.074	2.9586	2.1586	2.2608	2.58
100	0	1	0	10	2.9075	4.0601	1.8815	2.1306	3.432	2.5256	2.4743	2.6723
0	100	1	0	10	2.5299	2.9693	1.6832	1.9364	2.0713	2.0575	2.0769	1.7938
0	0	1	100	10	2.999	3.9076	1.8078	1.9739	2.7373	2.1749	2.3342	2.6245
10	100	0	1	0	2.0343	2.2553	1.7305	1.8246	1.9631	2.018	1.939	1.8338
10	0	100	1	0	1.9847	2.7284	1.8269	1.979	2.1746	2.068	2.5483	2.3308
10	0	0	1	100	2.9932	4.1087	1.7538	2.0081	3.2372	2.2585	2.3231	2.9563
100	10	0	1	0	2.8704	3.7759	1.7376	2.0508	1.9946	2.0968	2.2736	1.7608
0	10	100	1	0	2.0798	3.0179	1.7981	2.0429	2.1031	2.0853	2.3257	1.9574
0	10	0	1	100	2.94	3.839	1.7289	1.9742	2.0522	2.1206	2.1832	1.9514

100	0	10	1	0	2.4302	3.4731	1.7949	2.0417	2.0023	2.1266	3.2659	2.3459
0	100	10	1	0	2.5339	3.5709	2.1264	2.1533	2.0315	2.1928	2.5888	2.2805
0	0	10	1	100	2.4664	3.5241	1.7283	1.9997	2.0282	2.142	2.7054	1.9236
100	0	0	1	10	2.5362	3.7563	2.023	2.1109	3.4036	2.6005	3.1298	3.0368
0	100	0	1	10	2.535	4.2452	2.4722	2.2716	2.3559	2.2235	2.7489	2.8455
0	0	100	1	10	2.1935	2.567	1.6737	1.9986	1.8844	2.3264	2.1431	1.8636
10	100	0	0	1	2.8672	3.9865	2.1149	2.0757	2.6858	2.2301	2.5386	2.9009
10	0	100	0	1	2.6901	3.141	1.7174	1.9527	2.0073	2.153	2.1978	1.9811
10	0	0	100	1	2.8406	3.7201	1.7683	2.1077	3.4524	2.7078	2.6045	2.882
100	10	0	0	1	2.8761	3.9006	1.994	2.1522	2.924	2.3358	2.5299	3.0646
0	10	100	0	1	1.9439	2.2272	1.8222	1.9755	1.9053	2.2722	2.3019	2.0361
0	10	0	100	1	2.8804	4.0094	2.4549	2.2142	3.4696	2.5214	3.1068	3.2543
100	0	10	0	1	2.6785	4.3184	2.569	2.2377	3.3977	2.2502	2.9842	2.6239
0	100	10	0	1	2.0344	2.4537	1.7957	1.9341	1.8988	2.1111	2.0703	1.8619
0	0	10	100	1	2.5547	3.7027	2.1686	2.2256	2.8971	2.2242	3.1458	2.811
100	0	0	10	1	2.4652	4.0035	2.0289	2.2188	3.5581	2.4897	3.2063	2.6373
0	100	0	10	1	2.017	2.3164	1.6851	2.0045	1.9095	2.0836	2.2576	1.8886
0	0	100	10	1	2.3225	3.8448	2.5744	2.1444	2.5196	2.0706	2.9521	2.8992
1	10	0	0	0	1.8413	2.4339	1.7561	1.973	1.9351	2.0875	2.4831	1.8629
1	0	10	0	0	1.8954	2.3888	2.2979	2.1529	3.0003	2.1275	2.6837	2.2169
1	0	0	10	0	2.0744	3.1276	1.9799	2.1785	3.4805	2.4796	3.6161	2.5776
1	0	0	0	10	2.9854	4.2098	1.8922	2.188	3.631	2.6966	2.4697	2.6728
10	1	0	0	0	2.3769	3.9815	1.7916	2.1733	3.281	2.3202	2.7832	2.1164
0	1	10	0	0	2.0366	2.9416	2.2702	2.2485	3.118	2.2164	2.7325	2.3211
0	1	0	10	0	2.4327	3.6239	2.0758	2.126	2.9424	2.5353	3.5616	2.3696
0	1	0	0	10	2.8778	4.5978	1.8366	2.0493	3.1431	2.2729	2.4726	2.3484
10	0	1	0	0	2.4925	4.4357	2.4952	2.2411	3.6036	2.6863	2.7359	2.2602
0	10	1	0	0	1.9151	2.7371	1.8383	2.0105	2.0751	2.0822	2.3865	1.8128
0	0	1	10	0	2.1148	3.3593	2.0239	2.149	3.2851	2.6862	3.515	2.4738
0	0	1	0	10	2.9188	4.6959	2.2327	2.1065	3.464	2.771	2.442	2.6957
10	0	0	1	0	2.364	4.5448	1.9758	2.1176	3.4947	2.9357	2.8798	2.2879
0	10	0	1	0	1.9515	2.7184	1.7535	1.9938	1.9146	2.007	2.4901	1.8078
0	0	10	1	0	1.9254	2.9826	2.5831	2.1257	3.1714	2.152	2.9732	2.3827
0	0	0	1	10	2.9795	4.7623	1.9858	2.0994	3.568	2.9323	2.486	2.6467
10	0	0	0	1	2.5925	4.6605	1.8984	2.213	3.5911	2.8893	2.7232	2.287
0	10	0	0	1	2.4202	4.1554	1.73	2.0326	1.9918	2.0602	2.3999	1.8052
0	0	10	0	1	1.8573	2.4359	2.0828	1.8828	1.9575	1.7476	3.0039	2.4597
0	0	0	10	1	3.1038	2.3716	2.5443	2.6416	2.1282	2.6602	4.7254	3.1787
0	0	0	0	0	3.0427	2.3535	2.6685	3.0452	2.0851	2.1225	4.8471	3.2114
1	100	100	100	0	3.0552	2.4112	2.6478	2.9485	2.0299	2.0923	4.7694	3.1519
1	100	100	0	100	2.9665	2.68	2.5347	2.479	2.0941	2.6065	4.4389	2.9375
1	100	0	100	100	3.0946	2.3238	2.523	2.4239	1.9927	2.7276	4.6657	3.0617
1	0	100	100	100	2.0421	2.1242	2.013	1.8552	1.861	1.7737	3.9897	2.8203
100	1	100	100	0	1.8658	2.159	2.0442	1.8716	1.9733	1.7335	3.9257	2.7821
100	1	0	100	100	1.8746	2.6585	2.0505	1.9708	1.946	1.8447	2.3919	1.9423
100	1	0	100	100	1.9453	2.8863	3.1261	3.7421	2.4982	1.9398	3.2992	2.0689
0	1	100	100	100	2.7628	3.2129	2.9133	3.6641	2.1898	2.1686	4.7102	2.644
100	100	1	100	0	2.5965	2.7477	2.1689	3.3625	2.2264	2.9276	4.9314	2.6484

Danksagung

Besonderer Dank gebührt **Prof. Dr. Otto S. Wolfbeis** für die Vergabe des interessanten Themas und der tatkräftigen Unterstützung während der Arbeit.

Ebenso bedanke ich mich herzlich bei **Dr. Tobias Werner** für die gute Betreuung der Arbeit, die ständige Unterstützung, die zahlreichen wissenschaftlichen Diskussionen und die steten Aufmunterungen.

Weiterhin bedanke ich mich bei:

Prof. Dr. Ingo Klimant für die guten Tips und Anregungen, die besonders in den letzten Teil der Arbeit einflossen.

Dr. Gregor Liebsch für die Einarbeitung in das Imaging, die Programmierarbeiten für meine Anwendungen und natürlich für die Diskussionen über Wissenschaft, Politik, Sport und das Leben.

Athanas Apostolidis für seine Hilfe mit dem Pipettierroboter, welcher ihm schon oft den letzten Nerv gekostet hat, und die Unterstützung bei diversen Problemen, die im wissenschaftlichen Leben so anfallen. Weiterhin bedanke ich mich für die gute Nachbarschaft.

Dr. Christian Krause für die Bereitstellung der neuesten Generation von Beads aus der Polymerforschungsabteilung von Optosense. Absolut HighChem!

Hannelore Brunner, für Ihre gewissenhafte Hilfe und das angenehme Arbeitsklima.

Edeltraud Schmid für Ihre organisatorische Unterstützung, insbesondere bei den Abrechnungen für mein Projektkonto.

Dr. Christian Huber für seine Hilfe, seinen Tee und die gemeinsame Laborzeit.

den restlichen Mitgliedern unseres Instituts, im besonderen, *Bernhard Weidgans, Michael Meier, Pawel Chojnacki, Meng Wu, Zhi Won Lin, Sarina Arain, Jens Kürner, Claudia Schröder, Gisela Hierlmeier, Michaela Gruber, Axel Dürkopp, Bernard Oswald* für die gute Zusammenarbeit.